ABSTRACT

Title of Dissertation: PREPARATION AND CHARACTERIZATION OF CARBOHYDRATE-FUNCTIONALIZED NANOMATERIALS FOR USE AS CELLULAR PROBES AND TARGETED DELIVERY VEHICLES

Juhee Park, Doctor of Philosophy, 2008

Dissertation directed by: Professor Philip DeShong
Department of Chemistry and Biochemistry

Carbohydrates are the most abundant biomolecules found in living organisms. In addition to their roles such as fuel storage and structural components, carbohydrates encode molecular recognition information. Carbohydrates presented on the cell surface interact with cell surface receptors. These carbohydrate-receptor interactions are involved in a variety of biological processes including intercellular adhesion, microbial attachment, and signal transduction. Research in the DeShong laboratory has been focused on the development of cellular probes and targeted delivery vehicles utilizing carbohydrate-cell surface receptor interactions. The work reported herein details (1) the synthesis of glycoconjugates to functionalize the surface of gold, silica, nanoparticles, and surfactant vesicles, and (2) the preparation and characterization of carbohydrate-functionalized gold nanospheres and surfactant vesicles.

A variety of N-linked glycoconjugates tethered to thiols, siloxanes, and hydrocarbons were synthesized via modified Staudinger methodology with a high

stereoselectivity. The stereochemistry at the anomeric center (α vs. β) was readily controlled by choosing the appropriate reaction conditions. Typically, the α-stereochemistry arose from the reaction of ester derivatives with isoxazolines generated *in-situ* via epimerization of β-phosphorimines at high temperature. The ability to control tether length has been demonstrated.

Carbohydrate-functionalized gold nanospheres were prepared by two methods: (1) *in-situ* reduction of gold salt in the presence of thiolated glycoconjugates to provide ca. 2 nm particles and (2) a stepwise method where thiolated glycoconjugates were self-assembled on the surface of pre-formed, citrate-capped gold nanospheres to provide nanospheres with larger diameters (15 - 73 nm).

Carbohydrate-functionalized surfactant vesicles were prepared by mixing a cationic surfactant cetyltrimethylammonium tosylate (CTAT) and an anionic surfactant sodium dodecylbenzenesulfonate (SDBS) in the presence of lipidated glycoconjugates. The resulting surfactant vesicles were stable, in mean diameter of ca. 140 nm, and showed significant amounts of glycoconjugate incorporation.

The bioactivity of carbohydrates on the surface of gold nanospheres and surfactant vesicles was investigated through agglutination assays using carbohydrate-binding lectins concanavalin A and peanut agglutinin. These agglutination results indicated that both gold nanospheres and surfactant vesicles display multiple presentations of carbohydrates on their surfaces that can be used for binding of receptors.

The suitability of the resulting glycosylated nanomaterials for use as cellular probes and targeted delivery vehicles is being investigated.

PREPARATION AND CHARACTERIZATION OF CARBOHYDRATE-FUNCTIONALIZED NANOMATERIALS FOR USE AS CELLULAR PROBES AND TARGETED DELIVERY VEHICLES

By

Juhee Park

Dissertation submitted to the Faculty of the Graduate School of the
University of Maryland, College Park in partial fulfillment
of the requirements for the degree of
Doctor of Philosophy
2008

Advisory Committee:

Professor Philip DeShong, Chair

Prefessor Ibrahim Ades

Professor Jeffery Davis

Professor Michael Doyle

Professor Sang Bok Lee

DEDICATION

To my wife, Hyeju

ACKNOWLEDGEMENTS

First of all, my sincere gratitude goes to my advisor and mentor, Phil. It is absolutely certain that I am not standing as a chemist today without him. Thanks for opening my eyes toward an exciting chemistry, keeping me focused, and guiding me into the right direction. I am deeply grateful to Dr. Ahn for showing me the way to keep studying chemistry. I am thankful to all the committee members and Dr. English for their advisor and support.

I am thankful to all the former and current members of the DeShong group, and to all of my colleagues including Yiu-Fai and Yinde in the department. Personally, I am thankful to all of my church members. All of you have made my life in Maryland enjoyable.

I bow with earnest respect and appreciation to my parents, and my parents-in-law for their love and support. I am thankful to my brother and my sister for their support.

I wish to thank my wife Hyeju for her prayer, support, encouragement, and everlasting love for me. My daughter Iseul and my son David who are the source of happiness for my life deserve many thanks.

Last but not least, I thank God for His Love. *"The LORD is my shepherd, I shall not be in want." Psalms 23:1*

TABLE OF CONTENTS

LIST OF TABLES

Chapter 2

Chapter 3

Chapter 4

Appendix

LIST OF FIGURES

Chapter 1

Chapter 2

Chapter 3

Chapter 4

Appendix

LIST OF SCHEMES

Chapter 2

Chapter 3

Chapter 4

Appendix

LIST OF ABBREVIATIONS

AFM	atomic force microscopy
ATR	attenuated total reflection
AuNSs	gold nanospheres
calcd	calculated
Con A	concanavalin A
CTAT	cetyltrimethylammonium tosylate
d	day(s)
DIEA	diisopropylethylamine
DLS	dynamic light scattering
DMF	*N*,*N*-dimethylformamide
EI	electron ionization
equiv	equivalent(s)
Et	ethyl
Et_2O	diethyl ether
FAB	fast atom bombardment
h	hour(s)
Hz	Hertz
IR	infrared
J	coupling constant
M	molarity
M^+	molecular ion
m/z	mass-to-charge ratio

Me	methyl
MHz	megahertz
min	minute
mL	milliliter
MS	mass spectrometry
MALDI-FOF	matrix assisted laser desorption/ionization-time of flight
nm	nanometer
NMR	nuclear magnetic resonance
OAc	acetate
PNA	peanut agglutinin
PEG	poly(ethylene glycol)
Ph	phenyl
Rf	retardation factor
RT	room temperature
SAM	Self-assembled monolayer
SDBS	sodium dodecylbenzenesulfonate
SEC	size exclusion chromatography
SPR	surface plasmon resonance
TEM	transmission electron microscopy
TLC	thin layer chromatography
UV	ultraviolet
XPS	X-ray photoelectron spectroscopy

Chapter 1: Introduction

Biological Importance of Carbohydrates

Carbohydrates (*i.e.*, saccharides) are the most abundant biomolecules found in living organisms. The roles of carbohydrates in living cells are as fuel storage elements (starch and glycogen) and structural components (cellulose, chitin, and peptidoglycans).[1] In addition, carbohydrates encode molecular recognition information. Carbohydrates presented on the cell surfaces are covalently attached either to proteins or lipids to form glycoconjuates (glycoproteins and glycolipids). Receptors (proteins) presented on other cell surfaces recognize specific carbohydrate moieties on the glycoconjugates. These carbohydrate-receptor interactions are involved in a wide range of biological processes including intercellular adhesion, microbial attachment, and signal transduction (Figure 1).[1,2]

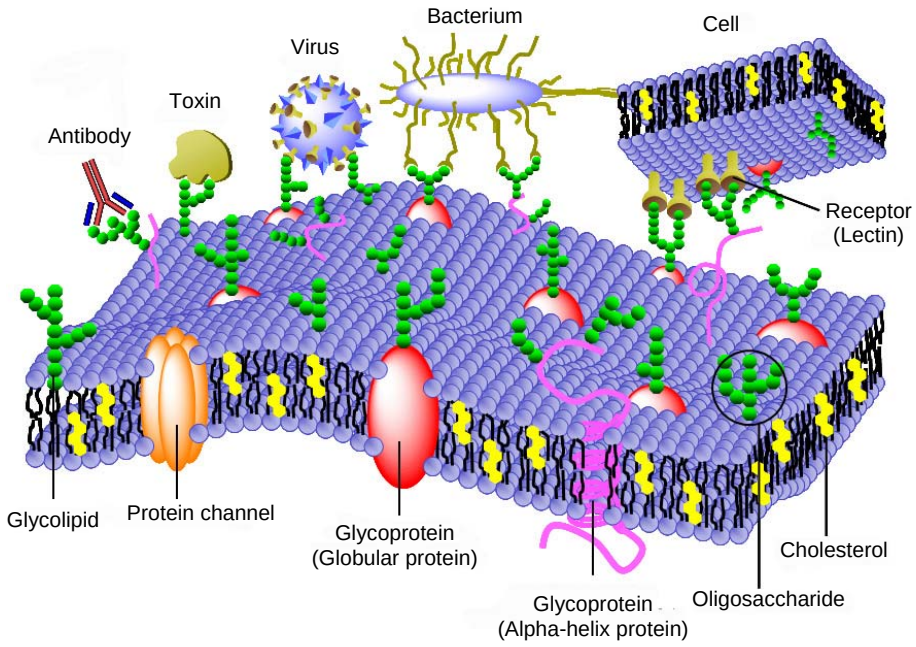

Figure 1. Schematic illustration of carbohydrate-receptor interactions on cell surfaces.

Carbohydrates have been of great significance for human health due to their central roles in pathogen infection, cancer metastasis, and mediation of immune response. Furthermore, aberrant glycosylation has been detected in diseases such as autoimmune diseases and cancer.[2,3] For example, *Vibrio cholerae* (cholera) toxin, *Clostridium tetani* (tetanus) toxin, influenza virus, polyoma virus, *Helicobacter pylori* bacterium, and malaria parasite target terminal sialic acid residues of glycoconjugates presented on human cell surfaces in the earliest phases of infection (Figure 2).[3-5]

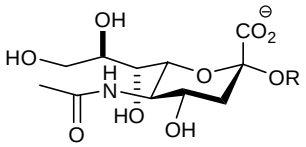

N-Acetylneuraminic acid (NeuAc)
R = various α-glycosidic linked carbohydrate chains

Figure 2. Structure of N-acetylneuraminic acid which is the most common form of sialic acid found in mammalian glycoconjugates.

The human immunodeficiency virus (HIV-1) utilizes carbohydrate-receptor interactions to facilitate infection of T cells.[6] During transmission, HIV encounters dendritic cells located in the mucosae (including the oral, vaginal, and intestinal mucosa), and the viral envelope glycoprotein gp120 targets a receptor known as dendritic cell-specific intercellular adhesion molecule-3 grabbing nonintegrin (DC-SIGN) expressed on the surface of dedritic cells. The interaction of the DC-SIGN receptor with mannose-rich oligosaccharides on the viral surface gp120 is required for the binding of HIV to dendritic cells. Thus, dendritic cells carry captured HIV to lymph nodes, where HIV migrates to the CD4 receptor on T cell surfaces through the cell-cell junctions known as infectious synapses to initiate infection of T cells, which causes AIDS (Figure 3).[6,7]

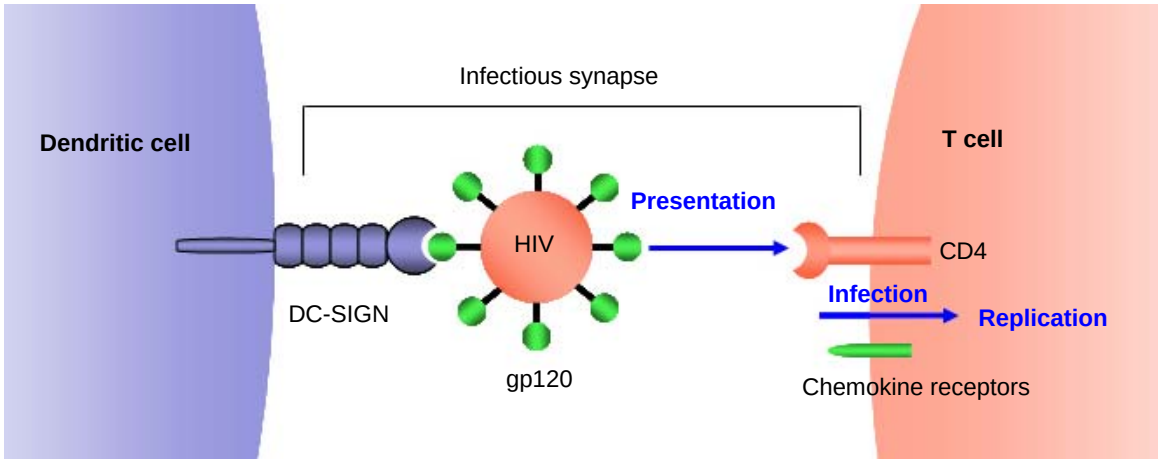

Figure 3. Schematic illustration of dendritic cell-mediated HIV infection.

In the human defense system, five distinct classes of immunoglobulins (IgA, IgD, IgE, IgG, and IgM) have been identified, and these are highly glycosylated with considerable diversity in the number, type, and location (Figure 4).[8] The oligosaccharides attached to immunoglobulins (Igs) play crucial roles both on the structure and biological functions of Igs.[8-10] For example, IgA and IgD are the only Igs that have oligosaccharides in the hinge regions (Figure 4). Since the hinge regions in IgA and IgD are more extended than those in the other Igs, they are susceptible to proteolytic cleavage. The oligosaccharides located on the hinge regions in IgA and IgD protect the hinge regions from proteases secreted by pathogens.[8] Oligosaccharides on Igs directly or indirectly participate in binding events with a variety of receptors to initiate effector systems which are on the pathways to eliminate targeted antigens. Directly, oligosaccharides provide recognition epitopes to the receptors. Indirectly, oligosaccharides maintain a specific conformation of crystalizable fragment (Fc) for optimal binding with Fc receptors.[8] The distribution of oligosaccharides in a given state of Igs is well controlled and reproducible. However, alternations in glycosylation of Igs cause diseases such as rheumatoid arthritis

(RA), IgA nephropathy, and congenital disorders of glycosylation (CDGs).[8-10]

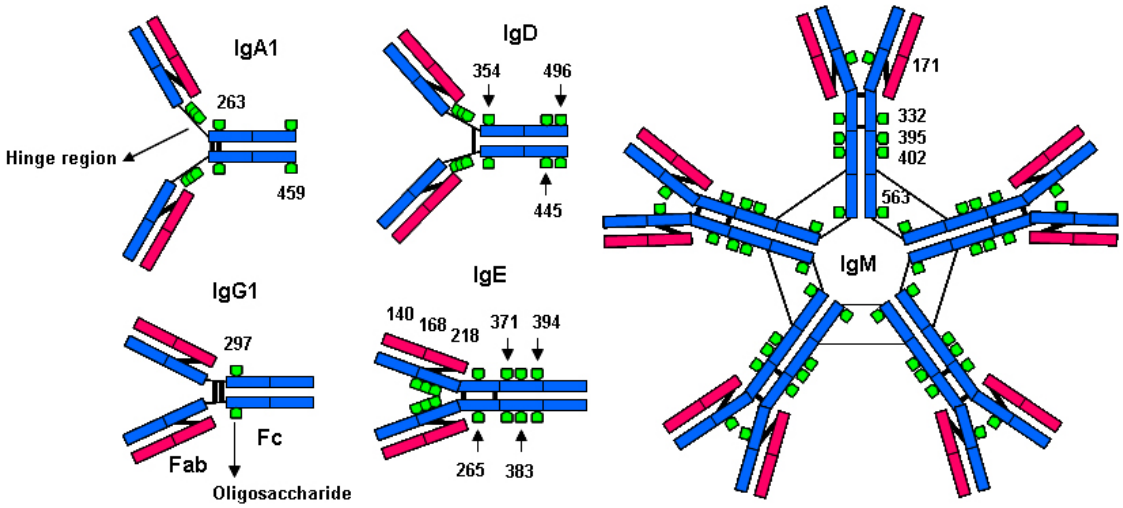

Figure 4. Diagrammatic representation of immunoglobulins (Igs) showing light chains (purple), heavy chains (blue), interchain disulfide bridges (black), and carbohydrates (green). Each number corresponds to the sites of glycosylation in Igs. Redrawn from ref. 8.

Leukocyte extravasation is another process in which carbohydrates play a key role. Leukocyte extravasation is the migration of leukocytes from the circulatory system toward the site of tissue damage or infection in order to initiate inflammatory response. During the multistep extravasation process (Figure 5), leukocytes circulating in the bloodstream interact in a sequential fashion with cell adhesion molecules expressed on the vascular endothelium, resulting in weak adhesion and rolling, firm attachment, and transendothelial migration of leukocytes into the target tissue (Figure 5).[11,12] In order to have an acute inflammatory response, the recruitment of leukocytes to the sites of injury is essential. The first stage, involved in the specific recruitment and rolling of leukocytes, is mediated by the multiple interactions between carbohydrates (sialyl Lewis a or sialyl Lewis x) and receptors (E-selectin and/or P-selectin) (Figure 5).[3,11,12]

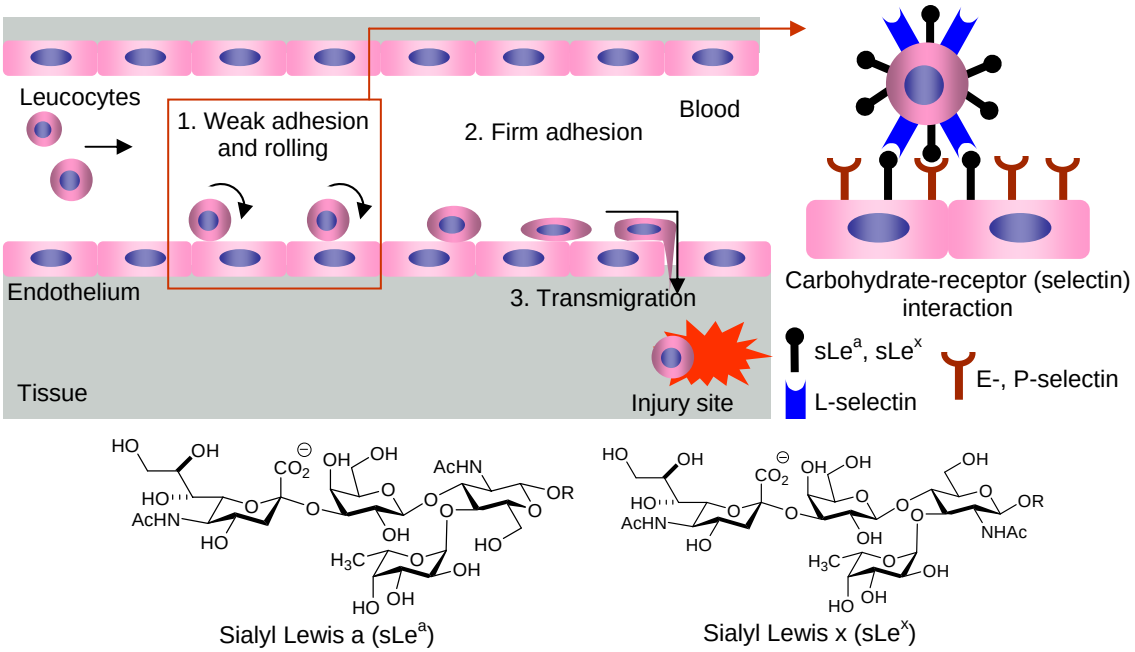

Figure 5. Schematic illustration of leukocyte extravasation from the blood stream into the target tissues. The weak adhesion and rolling steps of leucocytes with different receptors are specified, and the structures of carbohydrates responsible for the adhesion are shown.

Altered glycosylation is a universal feature of cancer cells.[3] Changes in glycosylation include under- and overexpression of naturally-occurring carbohydrates. For example, carbohydrates expressed on cancer cells are often increased in size and branching. The increased branching produces additional sites for terminal sialic acid residues, which leads to an increase in sialylation.[13] Examples of carbohydrate epitopes commonly found on cancer cells are shown in Figure 6.[13]

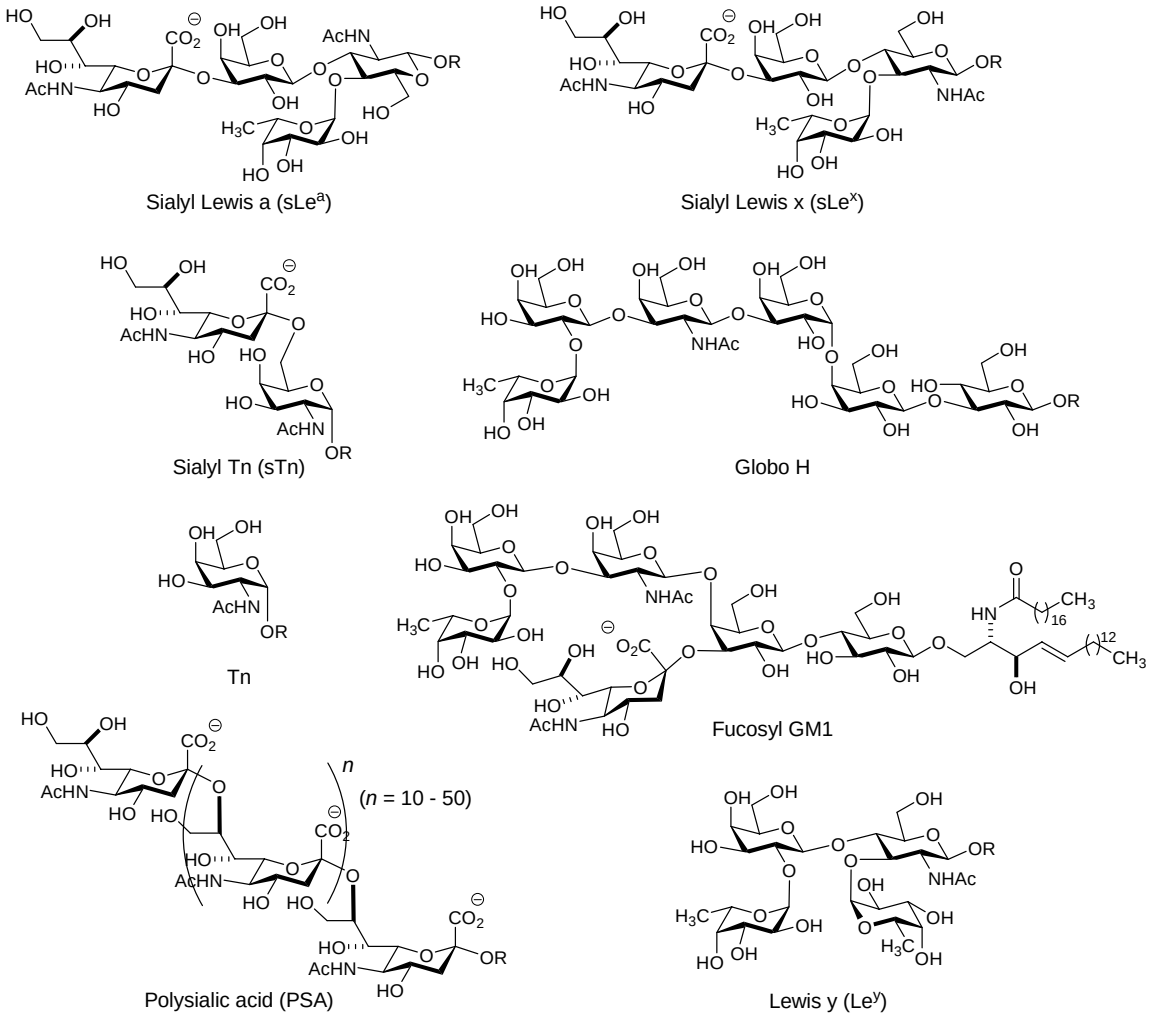

Figure 6. Cancer-associated oligosaccharide epitopes.

In addition, cancer cells utilize altered carbohydrates to regulate many different stages of cancer progression, including proliferation, invasion, angiogenesis and metastasis.[14] For instant, metastasis responsible for the death of most cancer patients is a multi-step process where cancer cells intravasate from their primary site to the blood stream (dissociation and invasion), disseminate through the bloodstream, extravasate to the targeted organs, and form metastases. These processes are similar to those of leukocyte-endothelial interaction in inflammation (Figure 5).[11] During the intravasation,

sialylated oligosaccharides (*e.g.*, sTn in Figure 6) overexpressed on cancer cells promote dissociation of cancer cells. Once the cancer cells enter the bloodstream, they form an aggregation with host cells such as platelets and leukocytes to facilitate dissemination and migrate to the metastatic organ by binding to the endothelium.[14] The formation of an aggregate and binding to the endothelium are mediated by the interactions between altered carbohydrates (*i.e.*, sLe^a and sLe^x in Figure 6) on the cancer cells and selectins expressed on activated platelets (P-selectin), leukocytes (L-selectin) and endothelial cells (E-selectin).[14]

The examples described above represent a fraction of the biological systems that demonstrate the importance of carbohydrates. It is clear that carbohydrates are associated with many aspects of human health and diseases, which means that they are also critical in developing a new generation of therapeutics and diagnostics. Understanding the structure and function of carbohydrates in cellular events (carbohydrate-receptor interaction), monitoring and controlling glycosylation processes (altered glycosylation), and cracking the sugar code in effective and efficient manner are major challenges for glycobiology.

Glycotechnology: Carbohydrate Meets Modern Technologies

Carbohydrates have intrigued biologists for decades because of their tremendous importance in complex cellular events. Therefore, glycobiology dealing with the structure and function of carbohydrates has become one of the most widely studied areas in biochemistry and cell biology. Rapid advances in glycobiology, however, have been hindered by the lack of research tools and the complexity of oligosaccharides. Due to their nature of linkage diversity, oligosaccharides have an inherent structural complexity.[2,3] For example, each monosaccharide can have linkage up to five positions with either α or β stereochemistry. This means that there are more than 15 million possible combinations to form tetrasaccharides from the eight common monosacchrides.[15] The identification of the oligosaccharide sequence on a specific glycoconjugate is further complicated because several of the eight common monosaccharides have identical masses. Technically, it is very difficult to isolate sufficient quantities of chemically defined oligosaccharides and glycoconjugates from natural sources because of their heterogeneity and low concentration. Simple and effective synthetic approaches are, therefore, essential to solve many problems in glycobiology.

Two general synthetic strategies are used for the preparation of oligosacchrides: enzymatic synthesis and chemical synthesis (Figure 7).[16] In enzymatic synthesis (Figure 7a), the formation of glycosidic bonds is catalyzed by enzymes, typically, glycosyltransferases or glycosidases. Although their availability, cost, and ability to assemble novel saccharides are major limitations, a great advantage utilizing enzymes is

that absolute regio- and stereochemistry can be controlled, which is the central challenge in carbohydrate chemistry.

In chemical synthesis (Figure 7b), a nucleophilic acceptor reacts with an electrophilic intermediate created by the activation of glycosyl donor, resulting in the formation of either α- or β-anomer. In order to obtain the desired configuration of a glycosidic linkage, it is necessary to control regio- and stereochemistry in chemical synthesis. Current chemical methods to achieve regiochemical and stereochemical control in glycosidic bond formation require tremendous manipulation of protecting groups, time consuming transformations, and laborious synthetic processes, which decrease the overall synthetic efficiency.

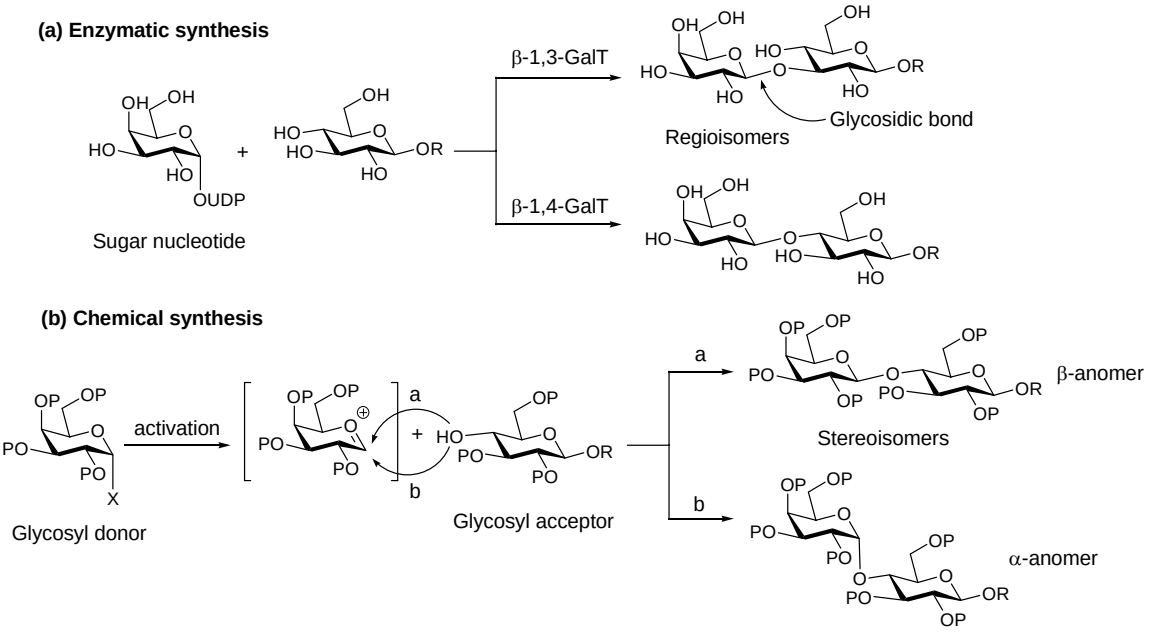

Figure 7. Two general approaches for the preparation of oligosaccharides.

Recent advances in chemical synthesis of oligosaccharides and the development of solid phase enzymatic synthesis have provided access to obtaining pure, chemically

defined oligosaccharides.[15,17] Solid phase enzymatic synthesis has been achieved by the immobilization of ether the acceptor carbohydrate or the enzyme to the solid support (Figure 8). When the acceptor carbohydrates are bound to the solid supports (Figure 8a), the required enzymes and their corresponding nucleotide sugars react consecutively to produce complex oligosaccharides.[18] Alternatively, the growing carbohydrates attached to a water-soluble polymer react consecutively with nucleotide sugars and enzymes immobilized on solid supports (Figure 8b).[19] In each step, the carbohydrates produced are readily purified by gel filtration due to the size of polymer.

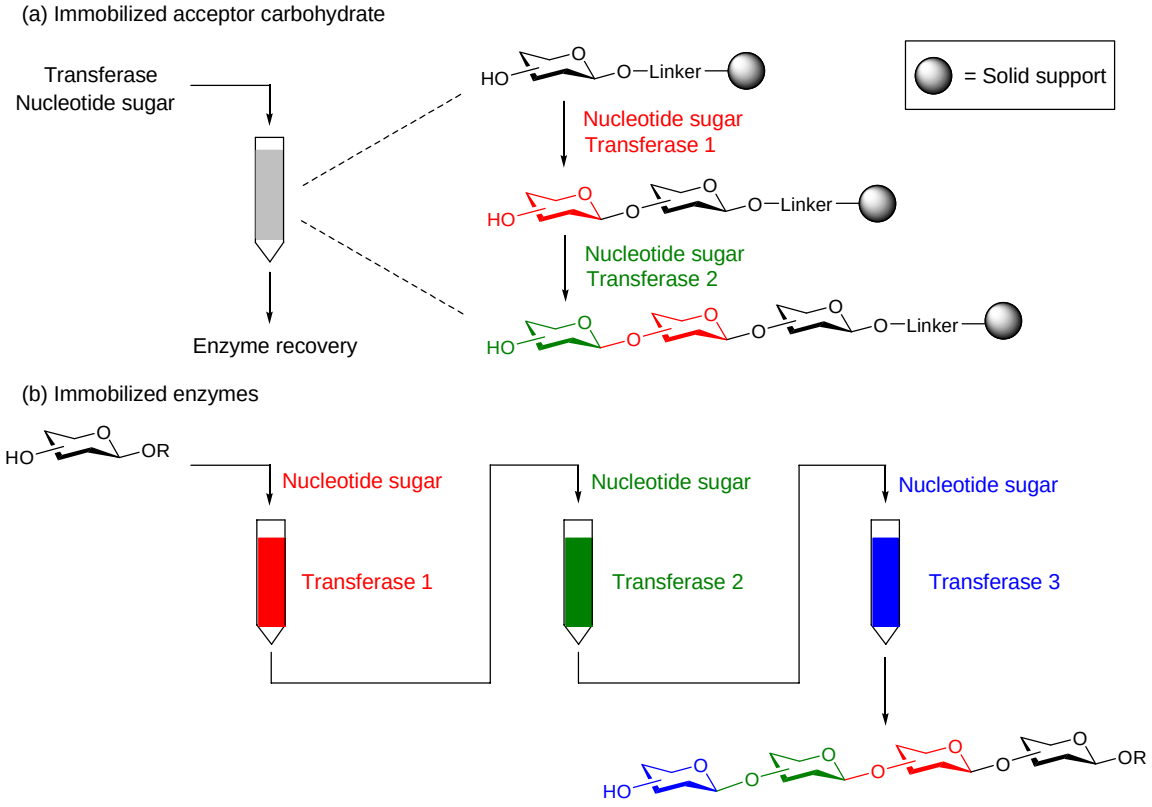

Figure 8. Schematic illustration of solid phase enzymatic synthesis of oligosaccharides.

The strategy of programmable solution phase, one-pot synthesis (Figure 9a) is based on the relative reactivity of different protected carbohydrate 'building blocks'.[20] A

computer program known as ‘OptiMer’ contains the database regarding relative reactivity values of hundreds of building blocks. OptiMer uses this database to analyze a target oligosaccharide, selects the best combinations of build blocks, and determines the order in which they should be added during oligosaccharide assembly. This approach has been used with success in the synthesis of a large number of oligosaccharides, including Globo-H (Figure 6),[21] fucosyl GM1 (Figure 6),[22] and heparin-like oligosaccharides.[23]

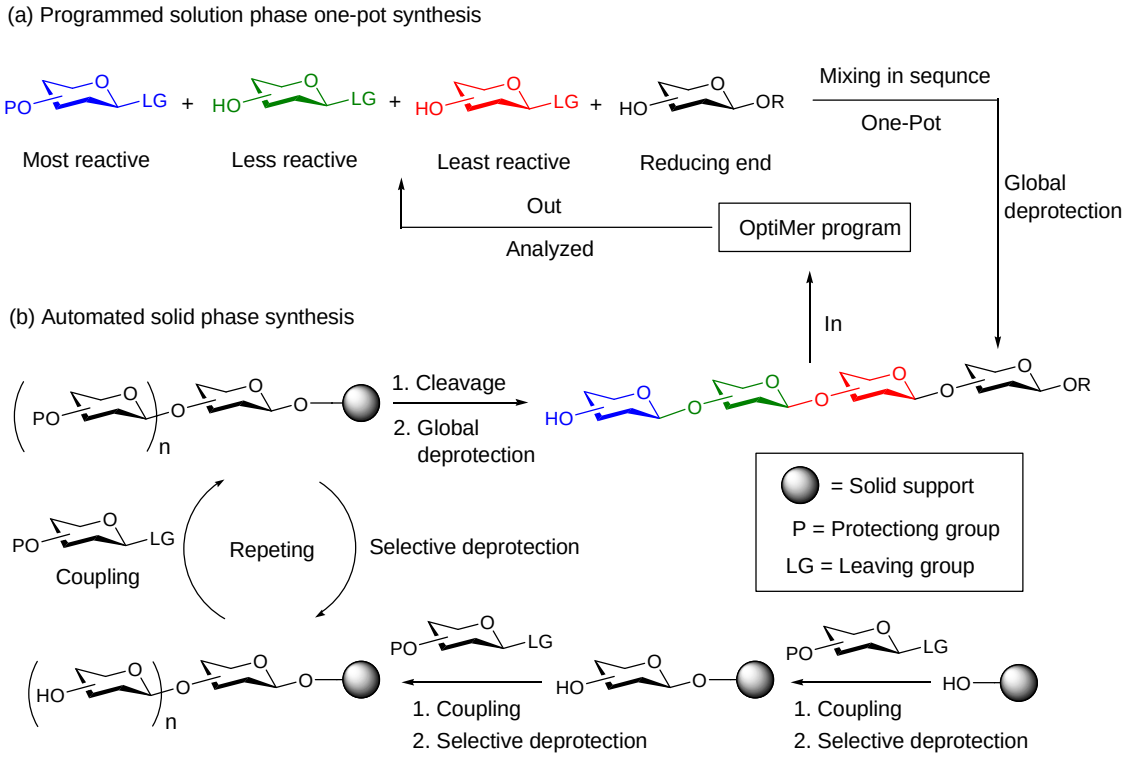

Figure 9. Recent advances in chemical synthesis of oligosaccharides.

The automation of solid phase oligosaccharide synthesis (Figure 9b) has been achieved by the modification of existing automated peptide technology.[24] Like a general procedure of solid phase synthesis of oligosaccharides, the first carbohydrate building block is bound to the solid support by coupling reaction. Selective deprotection reveals a new acceptor hydroxyl group, and the cycle of coupling and selective deprotection is

repeated as many times as needed. Finally, cleavage and global deprotection produce the desire oligosaccharide. This process has been fully automated and has been utilized for the preparation of oligosaccharides of interest.[25] Linear heptamannoside (seven mannose linked in a linear fashion), for example, was prepared by this automated synthesizer in 20 hours with 42 % overall yield. As a comparison, manual synthesis of linear heptamannoside on solid support took 14 days with 9 % overall yield.[24]

The interaction between a carbohydrate and the individual binding site in a protein is typically weak. However, binding strength and specificity are often increased through polyvalent interactions characterized by simultaneous binding of multiple carbohydrates presented on the cell surfaces to oligomeric carbohydrate-binding proteins.[26] Therefore, carbohydrate immobilized onto a solid surface, which presents multiple copies of carbohydrate, could be particularly suitable for studying carbohydrate-protein interactions.

At present some of the fascinating tools for studying carbohydrate-protein interactions are illustrated in Figure 10.[17,27-29] Carbohydrate-based vaccines consisting of a carbohydrate antigen and an immunogenic protein (Figure 10a) have been developed against bacteria, parasites, viruses, and human cancers.[17] The cell surface of pathogens and human cancers often display distinct carbohydrates. Those carbohydrate markers are either isolated[30] or synthesized[31] and then attached to the proteins by a number of viable linking chemistries[32] to generate immune responses.

Analogous to DNA and protein arrays, carbohydrate microarrays (Figure 10b) have been used for the high-throughput evaluation of carbohydrate binding to a variety of macromolecules, as well as entire cells.[17,27,28,33] Mono- and multivalent interactions

between self-assembled monolayer of carbohydrates (Figure 10b) and proteins have been proved by means of surface plasmon resonance (SPR) spectroscopy.[34,35]

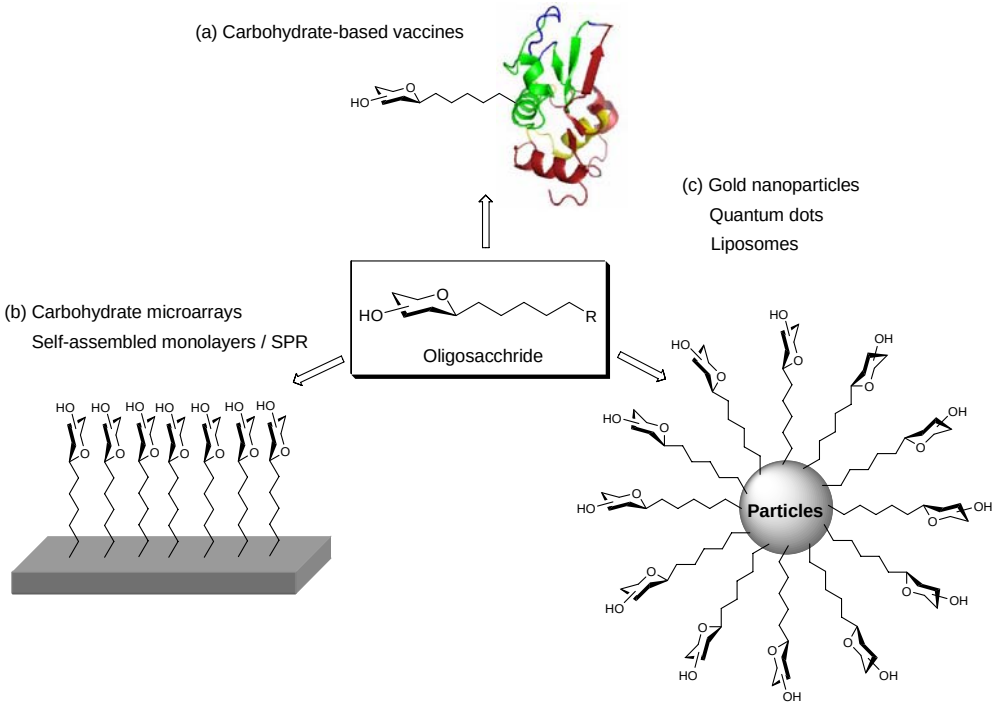

Figure 10. Glycotechnology: tools for glycobiology.

Carbohydrate functionalized nanoparticles (Figure 10c) have lately gained a great attraction as cellular probes and drug delivery vehicles.[27,29,36] Gold nanoparticles and quantum dots functionalized with carbohydrates have unique properties which include size-related electronic, magnetic, and optical responses. The dense presentation of the carbohydrates on the globular surface can mimic the situation encountered on cell surfaces that allows for multivalent interactions of relatively weak binding carbohydrates. These materials have been utilized as tools for the study of carbohydrate-carbohydrate interactions, carbohydrate-protein interactions, as biolabels, in toxin detection, and in

biomedicine.[27,29] The preparation and applications of gold nanoparticles functionalized with carbohydrates will be discussed in Chapter 3.

Liposomes have been employed as pharmaceutical carriers due to their huge inside cavity in which pharmaceuticals can be entrapped and released.[37,38] A major drawback of liposomal formulations, however, is the inherent instability, expense and difficulty of preparation associated with liposomes. In Chapter 4, the preparation and characterization of surfactant-based vesicles as alternatives to conventional liposomes is reported. It is hoped that these carbohydrate-functionalized vesicles will have applications in both basic and applied glycobiology.

Research Goals

Research in the DeShong group has been focused on the development of cellular probes and targeted delivery vehicles utilizing carbohydrate-cell surface receptor interactions. Toward this goal, three distinct sub-goals were included: first, simple and effective methodologies for the synthesis of a variety of N-linked glycoconjugates to functionalize solid surfaces were to be achieved, and the results of these studies are discussed in Chapter 2. Once the glycoconjugates were prepared, the second phase was to prepare carbohydrate-functionalized gold nanospheres and surfactant vesicles. Finally, the bioactivity of carbohydrates on the surface of gold nanospheres and surfactant vesicles was to be investigated. The results of studies with gold nanoparticles and surfactant vesicles are discussed in Chapter 3 and Chapter 4, respectively.

Chapter 2: Stereoselective Synthesis of N-Linked Glycoconjugates for the Functionalization of Solid Surfaces

INDRODUCTION

As the dense presentation of carbohydrates on the cell surfaces allows for multivalent interactions of relatively weak binding carbohydrates, correctly immobilized carbohydrates on the solid surface can provide both excellent selectivity and quantitative performance toward the binding of proteins that mimic natural systems. Therefore, effective synthetic methods and efficient functionalization techniques that control the density and orientation of carbohydrates on a solid surface are prerequisites to understand the structure and the function of carbohydrates in biological systems.

Structural Features of Glycoconjugates Found on the Cell Surface

Oligosaccharides are synthesized by glycosyltransferases and trimmed by glycosylases in step-wise fashion primarily in the endoplasmic reticulum and Golgi apparatus.[3] Most of the oligosaccharides presented on the cell surface are attached either to proteins or to lipids (Figure 11).

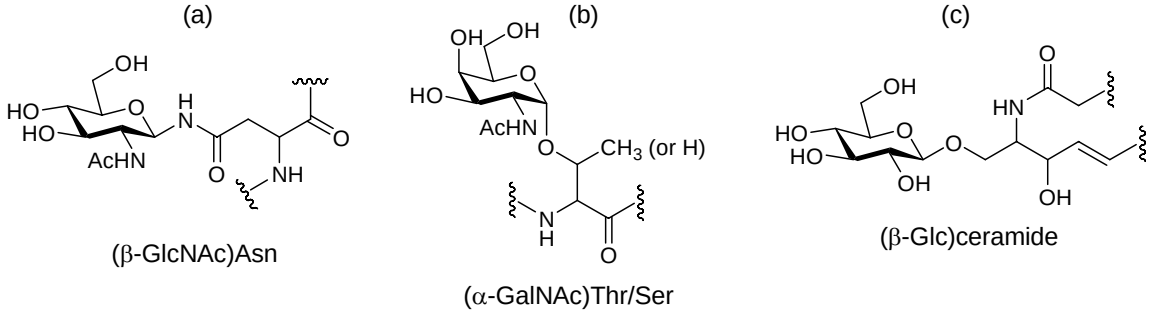

Figure 11. Structural features of glycoconjugates found on the cell surface. (a) N-linked glycoprotein, (b) O-linked glycoprotein, and (c) O-linked glycolipid.

Glycoproteins in which the carbohydrate is attached to proteins are classified into two principle groups according to the linkage between the carbohydrate and the amino acid residue: N-linked glycoproteins and O-linked glycoproteins. In most N-linked glycoproteins, an initial N-acetylglucosamine (GlcNAc) is attached to the nitrogen of an asparagine (Asn) residue on the protein and the linkage is typically β-configuration (Figure 11a).[2] In most O-linked glycoproteains, an initial N-acetylgalactosamine (GalNAc) is attached to the oxygen of a serine or a threonine residue on the protein and the linkage is typically α-configuration (Figure 11b).[2] Glycolipids in which the carbohydrate is linked to the oxygen of head groups of lipids are usually used to describe the glycosphingolipids (GSL). There are two main subgroups of glycosphingolipids, which can be differentiated by whether the first carbohydrate attached to ceramide is galactose or glucose with β-configuration (Figure 11c).[3]

These structural features of glycoconjugates have been utilized for the construction of specific linkages (N-linkages or O-linkages) to immobilize carbohydrates on the solid surface.

Strategies for the Functionalization of Solid Surfaces with Carbohydrates

To date, a variety of strategies for the immobilization of carbohydrates on the surface have been developed.[39-41] The general scheme is outlined in Figure 12. The required carbohydrates (simple carbohydrates, oligosaccharides, and polysaccharides) are obtained from chemical, enzymatic synthesis or a natural source after being detached from glycoconjugates. Sequential chemical manipulations enable the obtained carbohydrates to be immobilized on the surface. By the construction of tethers containing

functional groups, carbohydrates are immobilized on the surface by either direct attachments (Figure 12a and 12b) with adsorptive groups or indirect attachments with reactive groups to form a noncovalent linkage (Figure 12c) or a covalent linkage (Figure 12d).

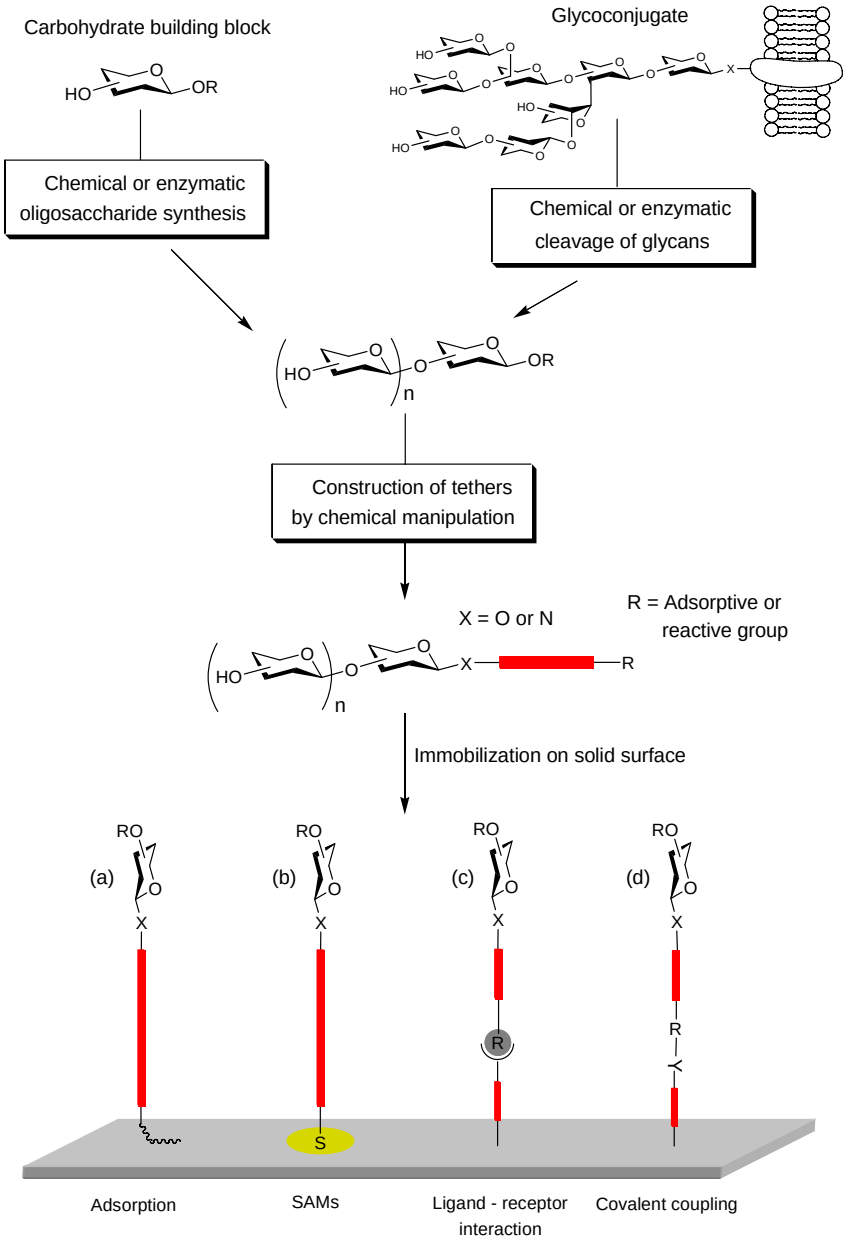

Figure 12. Strategies for the functionalization of solid surfaces with carbohydrates. (a) adsorption to the surface, (b) self-assembled on gold, (c) noncovalent coupling using a ligand-receptor interactions, and (d) attached surface by covalent coupling.

As representative methods to build up the specific tethers, the Fischer-Helferich, Koenigs-Knorr, and trichloroacetimidate method have been used for O-glycosylation. For N-glycosylation, a reductive amination with various amine derivatives has been utilized.

As proper solid surfaces, glass slides are the most extensively used, but gold and nitrocellulose membrane are also utilized.

Methods for the Construction of Specific Linkages

Via O-glycosidation

The Fischer-Helferich method, reported a century ago, is still the simplest glycosylation procedure that provides O-linked glycosides (Scheme 1a).[42]

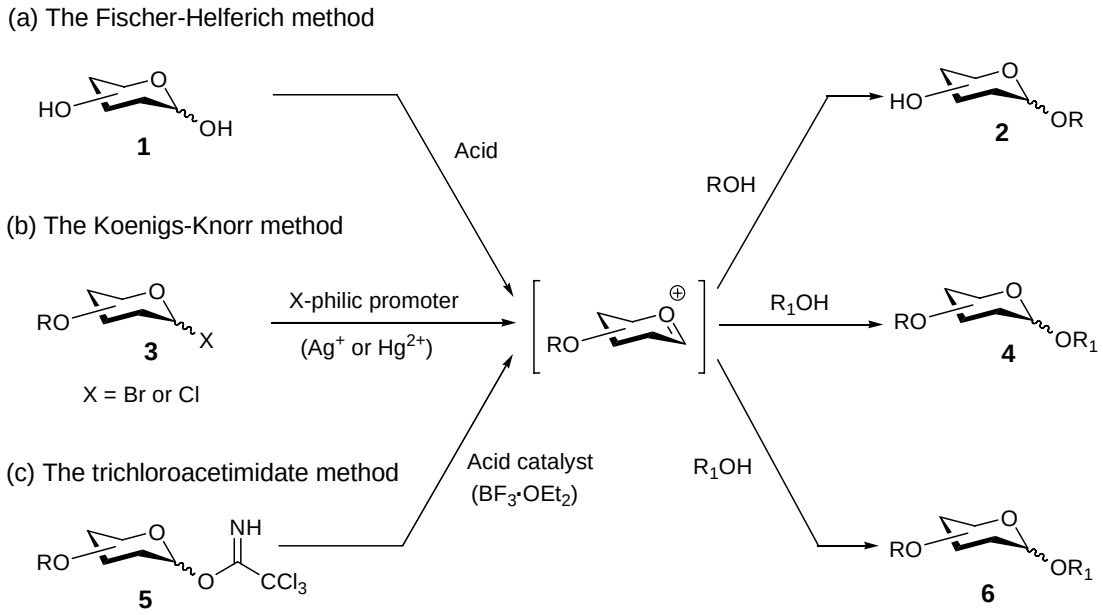

Scheme 1. Methods for the construction of O-linkage.

It consists of an acid-catalyzed activation of anomeric oxygen, followed by addition of an alcohol to provide a mixture of α- and β-anomeric glycosides **2**. Generally, longer reaction time results in the anomerization to the thermodynamically more stable

α-adduct due to the anomeric effect. However, as a result of its reversibility, this method has hardly gained any significance.

In the Koenigs-Knorr method introduced also a century ago, an anomeric hydroxyl group is exchanged by bromide or chloride, which provides a good leaving group (Scheme 1b).[42,43] It involves the activation of a glycosyl bromide or chloride **3** by halophilic promoter, typically heavy metal salts, and sequential addition of an alcohol derivative to produce O-linked glycosides **4** in an irreversible manner. The resulting anomeric stereochemistry including most glycosidation reactions is controlled by the nature of the C2 substituent (Scheme 2).[42,43]

Scheme 2

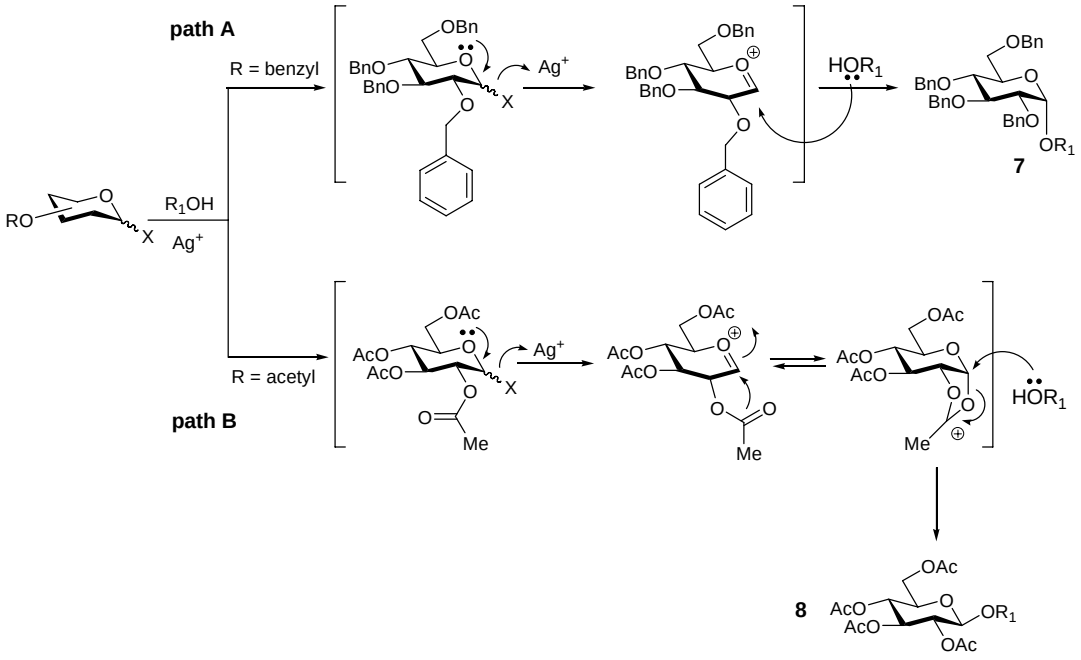

When the C2 oxygen is protected with an alkyl or benzyl group (path A), the α-anomer **7** is preferentially formed because of the anomeric effect. When the C2 oxygen is protected with participating groups such as an acetyl or benzoyl (path B), the stereochemical outcome is opposite to that of the C2 protecting groups and the β-anomer **8** is formed.[44]

This method is a very valuable technique for the synthesis of glycoconjugates and has been extensively developed. However, several disadvantages of this method are that the glycosyl halides **3** exhibit low thermal stability and are sensitive to hydrolysis. Therefore, it is often generated only *in situ*. Also this method requires at least an equimolar amount of the heavy metal salt as promoter. This is problematic for large-scale preparation due to safety concerns and disposal of waste materials.

The trichloroacetimidate method developed by Schmidt is a very powerful method to control the stereochemistry at anomeric center (Scheme 1c and 3).[42] The glycosyl trichloroacetimidates **5** can be selectively prepared by the addition of the anomeric hydroxyl group to trichloroacetonitrile in the presence of a base such as NaH or K_2CO_3 under kinetically (β-anomer in Scheme 3) or thermodynamically (α-anomer in Scheme 3) controlled conditions.[45] The imidates **5** produced are stable, isolable, and require only catalytic amounts of Lewis acids such as TMSOTf or $BF_3{\cdot}OEt_2$ to activate. Unless a C2-participating group is present, the glycosidation usually proceeds with inversion of configuration by S_N2-type addition of an alcohol derivative (Scheme 3).[44]

Scheme 3

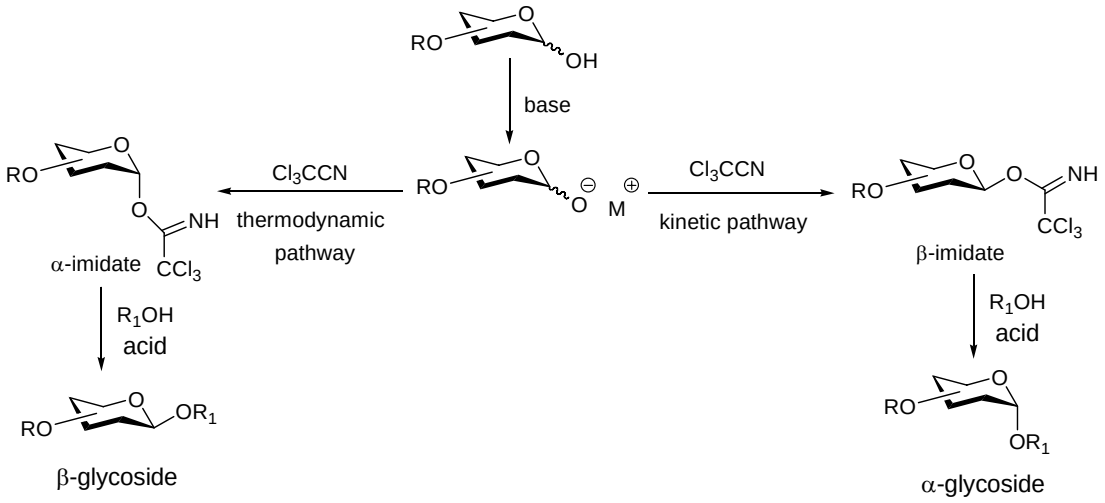

Via N-Glycosidation

The preparation of N-linked glycoconjugates has been achieved by amination (Scheme 4), whereby the reducing end of the carbohydrates is reacted with an amino group. When amine derivatives are utilized (Scheme 4a), imines **9** are produced. Since the formation of imines **9** is reversible, it is required to reduce the imines **9** with reducing agents to form a physiologically stable amine bond **10**. However, the ring opening of the reducing end residue **10** occasionally affects the biological function of carbohydrates.[46,47]

(a) Reductive amination with amines

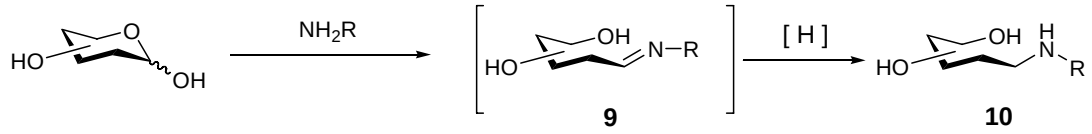

(b) Amination with hydrazides

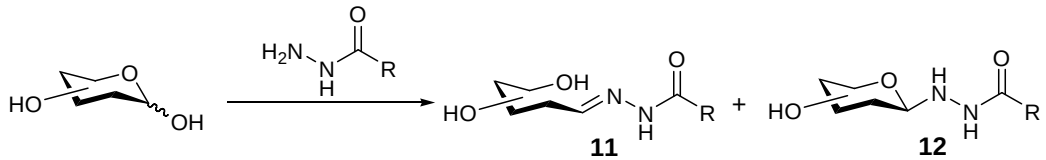

(c) Reductive amination with aminooxy groups

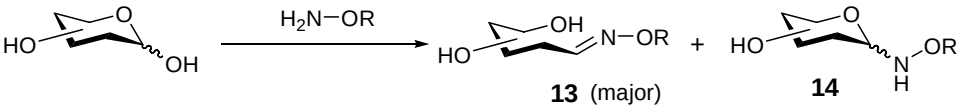

(d) Amination by Kochetkov method

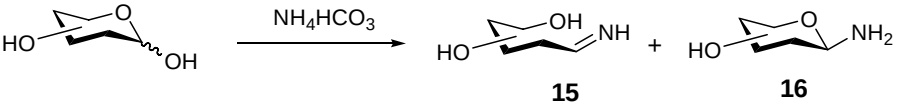

Scheme 4. Methods for the construction of N-linkage.

As an alternative to amine groups, when hydrazides are employed (Scheme 4b), the β-N-linked glycosylhydrazides **12** are predominantly produced in the absence of reducing agents.[48,49] The glycosylhydrazide linkage is very stable under neutral to basic conditions. However, the linkage is easily hydrolyzed under acidic condition.[50]

Highly nucleophilic aminooxy groups can be condensed with the reducing end aldehydes of carbohydrates to form acyclic oximes **13** with minor amounts of cyclic forms **14** (Scheme 4c).[46,51,52] The resulting oxime linkages are stable under a wide range of pH.

A much improved approach involves the introduction of primary amines at the reducing terminus of carbohydrates by the Kochetkov method.[53,54] The terminal hydroxyl group is converted to an amino group upon treatment with aqueous ammonium bicarbonate (Scheme 4d). The predominantly produced β-linked glycosylamines **16** have been used as intermediates for further elaboration that leads to selectively defined glycoconjugates.[55,56]

Methods for the Immobilization of Carbohydrates

Two general strategies have been used for immobilizing simple and complex carbohydrates. The first strategy is based on the direct attachment in which chemically modified or free carbohydrates are immobilized on the surface. The surface can be derivatized or underivatized. The second strategy is based on the indirect attachment in which chemically conjugated carbohydrate are immobilized on the derivatized surface by ligand-receptor interactions or to form covalent linkages.

Direct Immobilization of Carbohydrates

I. Nonspecific Immobilization of Chemically Unmodified Carbohydrates

Chemically unmodified carbohydrates are nonspecifically and directly adsorbed on solid surfaces. As an example of this method, Wang and co-workers demonstrated that a variety of unmodified microbial polysaccharides can be immobilized on nitrocellulose-coated glass slides through nonspecific adsorption (Figure 13).[57] The immobilization efficiency of carbohydrates was significantly influenced by their molecular weight. The large polysaccharides of 3.3 - 2000 kDa were efficiently adsorbed on the surface, but smaller ones were less retained on the surface after extensive washing.[57]

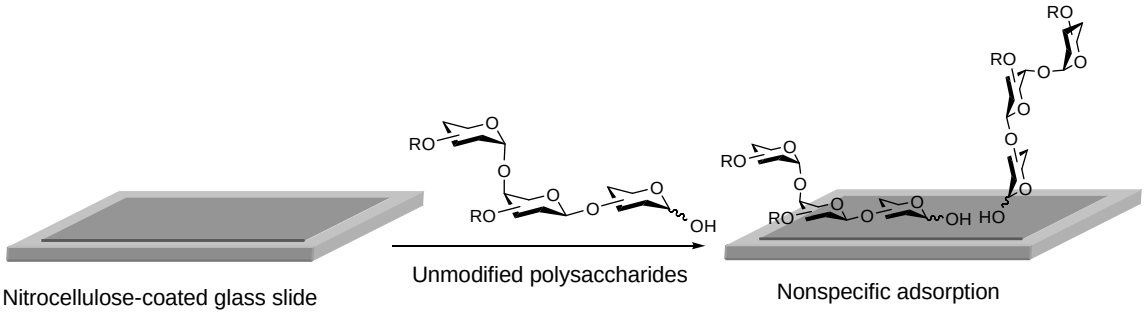

Figure 13. Nonspecific adsorption of chemically unmodified carbohydrates on nitrocelluose-coated glass slides.

This is the most straightforward method for the immobilization of carbohydrates because it needs neither a modified surface nor chemical-linking techniques. However, the use of this method is limited by the fact that carbohydrates simply adsorb to the surface in nonspecific manner and display various orientations, many of which are unlikely to be relevant to the natural presentation of carbohydrates on the cell surface.

II. Site-Specific Immobilization of Chemically Conjugated Carbohydrates

The chemical conjugation of carbohydrates with tethers allows site-specific immobilization on a solid surface. For example, carbohydrates linked to lipids were shown to adsorb on nitrocellulose-coated glass slides by mainly hydrophobic interactions (Figure 14).[58] The oligosaccharides **18** were obtained by chemical or enzymatic cleavage from biological sources **17**, and then conjugated with amino lipid **19** by reductive amination to form neoglycolipids **20** (Figure 14).

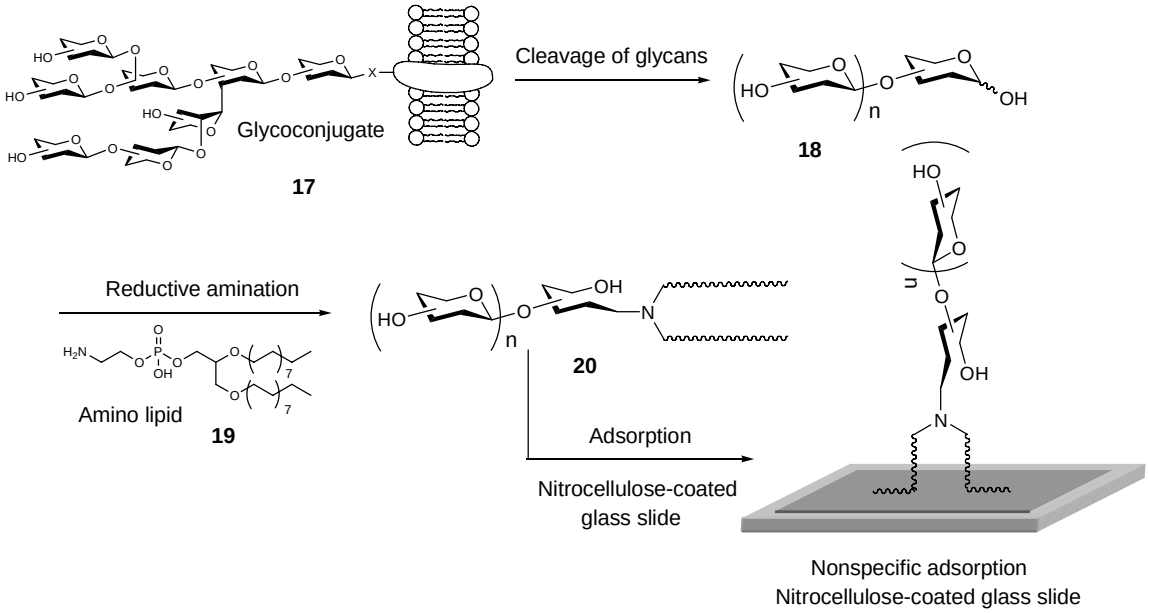

Figure 14. Site-specific adsorption of lipid-conjugated carbohydrates on nitrocellulose-coated glass slides.

The immobilization efficiency of the neoglycolipids **20** on nitrocellulose was found to be independent of the size of carbohydrates. However, the generation of neoglycolipids **20** by reductive amination resulted in the open-chain form of the reducing terminal residue, which may affect the biological activities of oligosaccharides if it is part of the recognition motif. Therefore, they recently prepared neoglycolipids by oxime ligation as an alternative to reductive amination. From the NMR studies, they provided evidence that

a significant proportion of the oxime-linked core monosaccharide is in the ring-closed form, and this form selectively interacts with a carbohydrate-binding protein.[46]

Wang and co-workers studied the retention ability of lipid-linked galactoses on the hydrophobic polystyrene surface, depending on the nature of lipids.[59] They prepared a variety of galactoses linked to lipids ranging from aliphatic to aromatic hydrocarbons in different lengths. When the lipid component was a saturated hydrocarbon between 13 and 15 carbons in length, the galactose showed complete retention after extensive aqueous washing, which suggested that the chain length of lipids is a critical factor in determining the stability of glycolipids on the hydrophobic surface.

Monosaccharides linked to a single fluorous tail (C_8F_{17}) were recently shown to adsorb avidly to glass slides coated with fluoroalkylsilane[60,61] because of the affinity arising from the nature of fluorine-fluorine interactions.[62] Fluorous-tagged monosaccharides were even shown to resist washing with detergent-containing buffer.

It was known that alkanethiolates form self-assembled monolayers (SAMs) on gold with well-defined structures and the properties of the monolayer depend on the functional groups that are exposed at the surface.[63]

Self-assembled monolayers (SAMs) derived from biological molecules on gold have been shown to be useful multivalent systems for studying cell adhesion.[64] In order to fabricate SAMs of carbohydrates on gold, carbohydrates are linked to tethers containing thiol groups by chemical manipulation.[65-67] For example, Penades and co-workers prepared SAMs presenting the disaccharide maltose (Figure 15).[67] The perbenzoylated maltose **21** was conjugated with the corresponding linker **22** under trichloroacetimidate conditions in the presence of a participating neighboring group at the

C2-position to generate β-O-linked maltose conjugate **23**. Deprotection of benzoyl groups in basic media gave disulfide-tethered glycoconjugate **24**, which was self-assembled on gold surfaces. The structural features of the SAMs were characterized by high resolution atomic force microscopy and X-ray photoelectron spectroscopy.

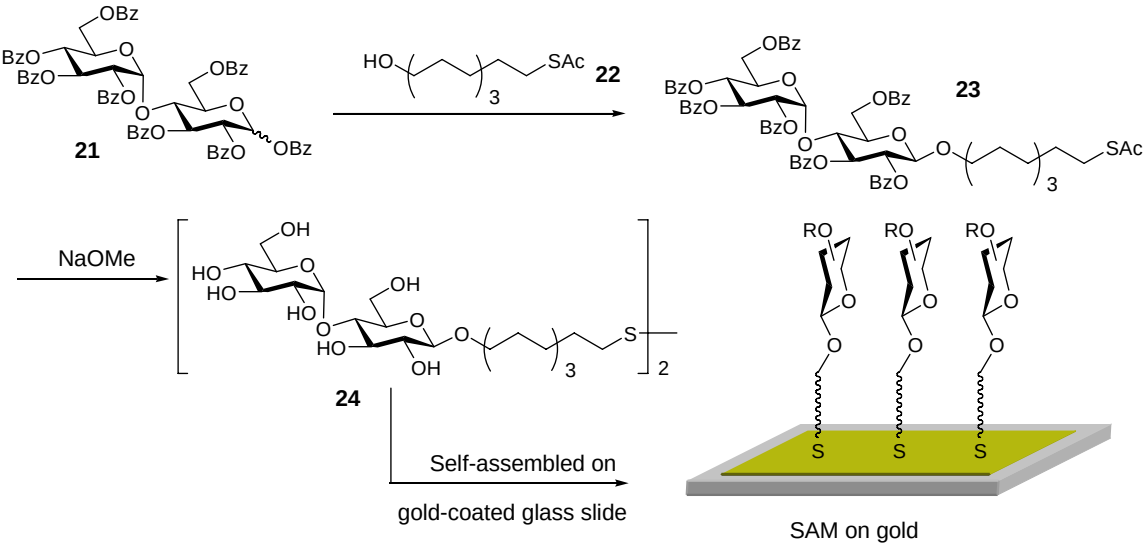

Figure 15. Site-specific immobilization of thiol-terminated maltoses on gold-coated glass slides.

III. Site-specific Immobilization of Chemically Unmodified Carbohydrates on Derivatized Surface

Chemically unmodified carbohydrates have been attached to hydrazide-,[47,68] aminooxy-,[47,69] or diazirine[70]-functionalized surfaces. Advantages of this method are that free carbohydrates are attached to the surface irrespective of their size. Also, it is not necessary to introduce a multiple chemical synthesis and individual purification steps to prepare carbohydrate conjugates. Although a couple of chemical steps are needed to fabricate the active surfaces, purification steps are simple just like solid-phase synthesis.

Zhi and co-workers site-specifically attached heparin oligosaccharides **27** to SAMs of hydrazides on gold (Figure 16).[68]

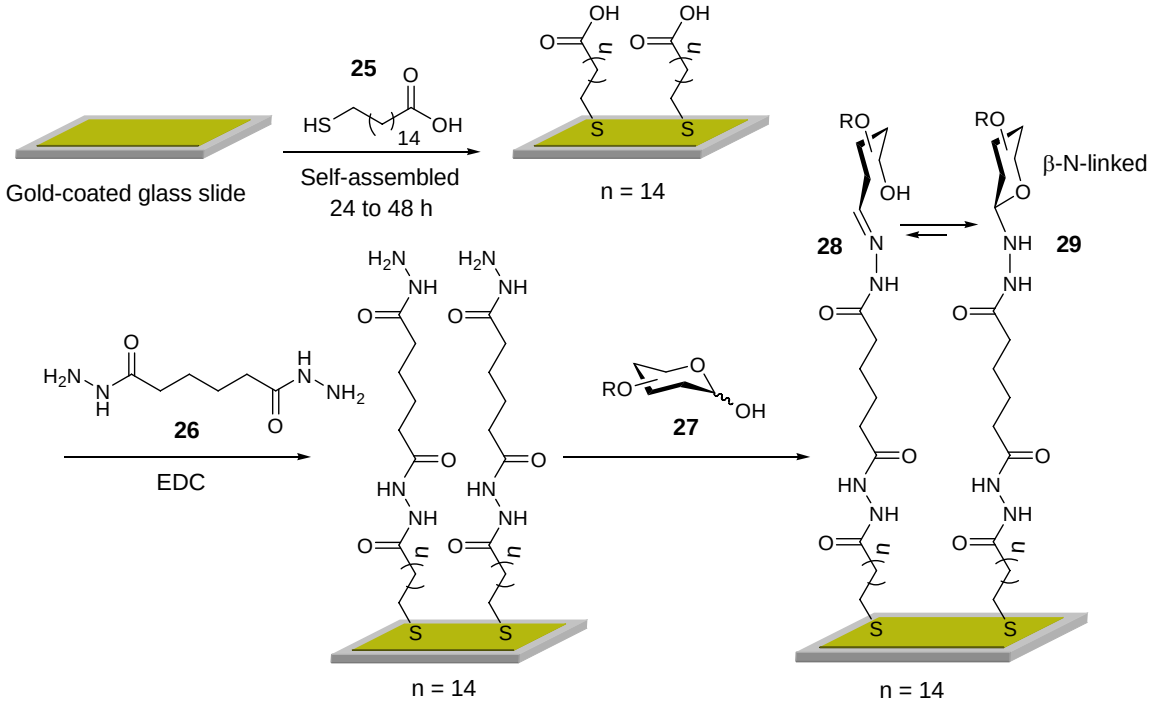

Figure 16. Site-specific immobilization of unmodified oligosaccharides on hydrazide-derivatized SAMs on gold.

First, mercaptohexadecanoic acid **25** was self-assembled on gold-coated glass slides. Then, the acid groups on the surface were reacted with adipic anhydride **26** to afford the corresponding hydrazide surfaces. Reducing end heparin oligosaccharides **27** were efficiently coupled to the hydrazide surfaces to initially form the acyclic hydrazone **28**, followed by conversion to the β-cyclic adduct **29**.

Diazirines have been widely used to investigate the structure and function of nucleic acids, proteins, and various macromolecular complexes.[71,72] The advantages utilizing diazirines as a photoaffinity labeling reagent are that they possess excellent chemical stability and rapid photolysis at wavelengths (350-360 nm) beyond the

absorbance region of most biomolecules, which circumvents the problem of irradiation damage of biomolecules. Upon photolysis, they generate highly reactive carbenes, which readily crosslink to various functional groups including the inert aliphatic C-H bonds.[72]

The feasibility of unmodified carbohydrate immobilization using diazirines was demonstrated by Sigrist and co-workers (Figure 17).[70] Photolabile aryltrifluoromethyl diazirine-functionalized glass slides **30** were irradiated at the wavelength of 365 nm for 4 min in the presence of polysaccharides **31**. The generated active carbene species **32** rapidly reacted with free polysaccharides **31** to form covalent bonds. The whole photoimmobilization process is very fast and occurs in a single step. However, a drawback of this approach is that free glycans were nonspecifically immobilized on the surface without specific orientation due to the nonspecific nature of the carbene reaction.

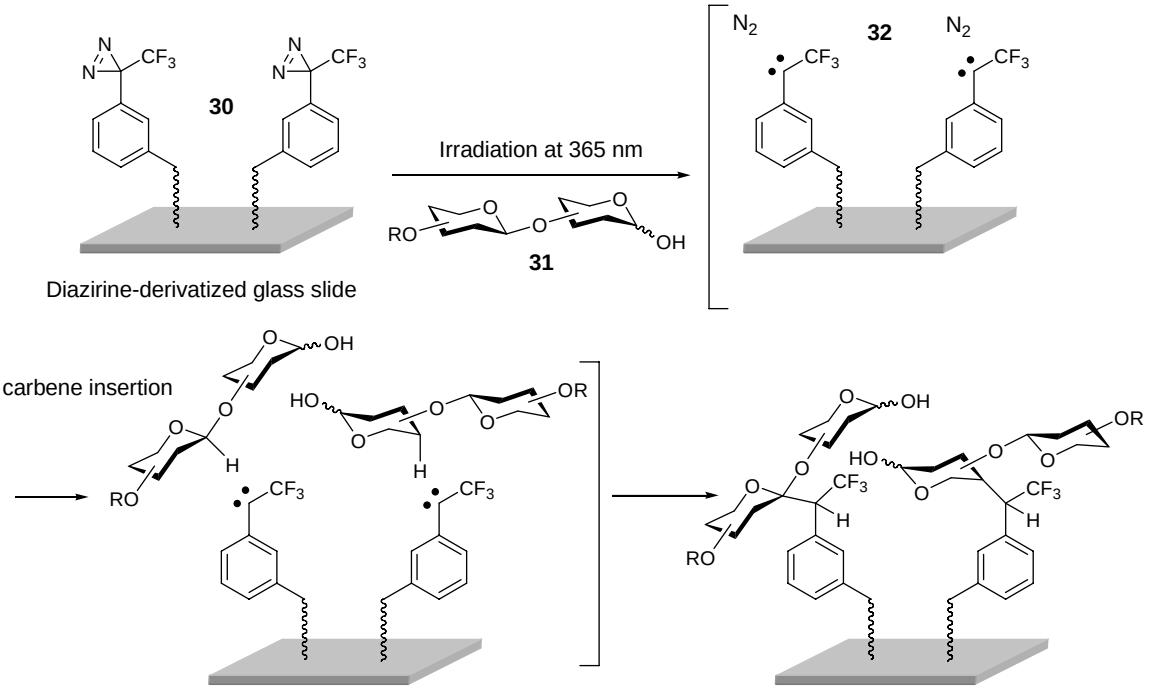

Figure 17. Photo-induced immobilization of free oligosaccharides on diazirine-derivatized glass slides.

Indirect Immobilization of Carbohydrates

This strategy requires both a modified surface and chemical-linking techniques. Carbohydrates linked to specific functional groups selectively react with a complementary-activated surface to form a non-covalent attachment (Figure 12c) or covalent attachment (Figure 12d). Non-covalent attachment depends on the binding of biotinylated carbohydrates to streptavidin-functionalized surfaces. This method has been successfully employed for the presentation of carbohydrates on a surface.[73,74]

A great effort has been placed on the covalent attachment. Although preparation of functionalized carbohydrates requires multiple chemical sequences and is time-consuming, simple carbohydrates and oligosaccharides are efficiently immobilized on the surface in a site-specific manner, resulting in the enhancement of protein binding.

Shin and co-workers reported the method to immobilize carbohydrates on a solid surface by covalent attachment of maleimide-terminated carbohydrates to thiol-derivatized glass slides (Figure 18).[75,76] They prepared a variety of mono- and disaccharides in the form of glycosylamines (**33**, **34**, and **35)** with controlling stereochemistry at the anomeric center. The condensation of the corresponding carbohydrates with allyl alcohol under Fischer-Helferich conditions or Koenigs-Knorr conditions provided α-O-linked **33** or β-O-linked glycoside **34**, respectively. The resulting glycosides were reacted with cysteamine to give α-O-linked **33** or β-O-linked glycosylamines **34**, respectively. The one-pot amination by Kochetkov method afforded β-N-linked glycosylamines **35**. Finally, glycosylamines were coupled to the bifunctional cross-linker to produce maleimide-terminated glycoconjugates (**36**, **37**, and **38**), which were then covalently immobilized on the thiol-derivatized glass surfaces by hetero-

Michael addition of thiol groups on the surfaces to the maleimide moieties of the glycoconjugates. The binding study with proteins demonstrated that both the anomeric configuration (α- or β-) and the nature of the anomeric linkage (O-linked or N-linked) of the glycoconjugates on the surface affect their binding affinities to the proteins.

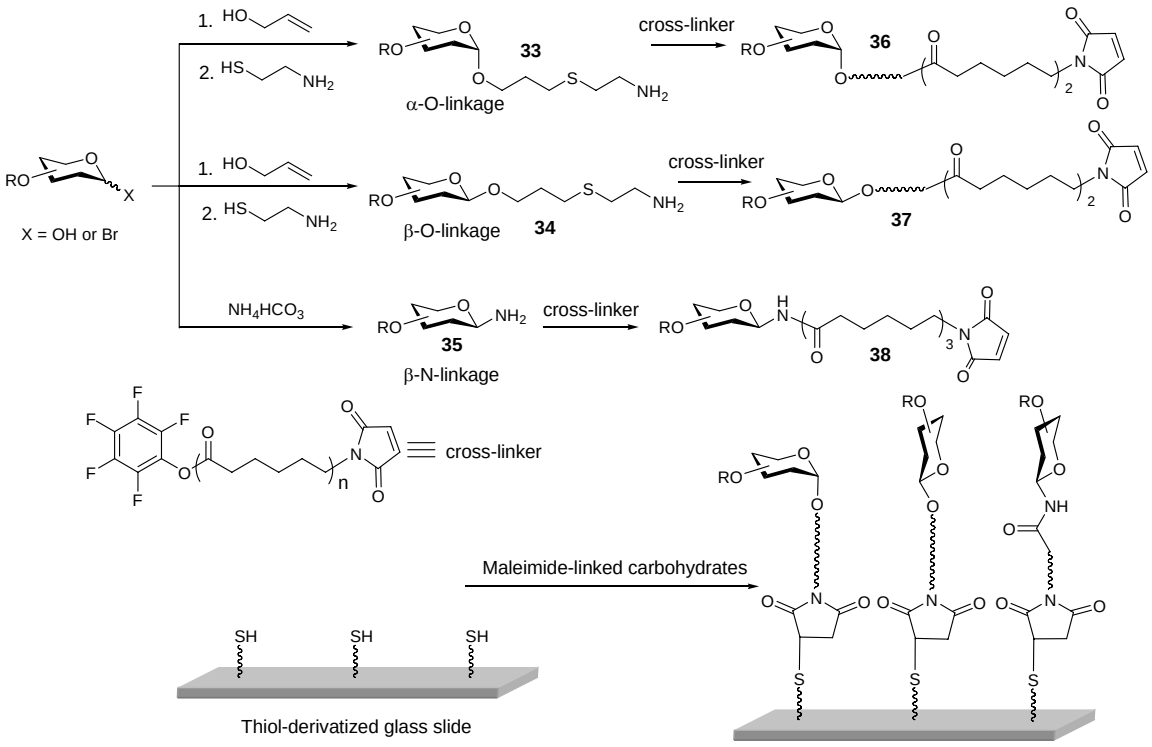

Figure 18. Immobilization of maleimide-linked carbohydrates on thiol-derivatized glass slides.

Alternatively, thiol-linked carbohydrates were immobilized on maleimide-functionalized SAMs on gold.[77,78]

Houseman and Mrksich described the approach that relies on the Diels-Alder reaction-mediated immobilization of cyclopentadiene-linked carbohydrates to the self-assembled monolayers presenting benzoquinone groups (Figure 19).[79] Monosaccharides **42** linked to cyclopentadiene were stereoselectively prepared by the condensation of the corresponding peracetylated glycosyl bromides **39** with aminopentanol under Koenigs-

Knorr conditions, followed by deprotection to give glycosyl amines **40**. Conjugation of glycosyl amines **40** with linker **41** provided cyclopentadiene-conjugated carbohydrates **42**. The monolayers were prepared by the immersion of gold-coated glass slides into a mixture of two alkanethiols, one of which has a hydroquinone group exposed. By adjusting the relative concentration of the two alkanethiols, they controlled the density of carbohydrates on the surface. Hydroquinone-containing SAMs were oxidized to corresponding benzoquinone derivatives to which cyclopentadiene-conjugated carbohydrates **42** are covalently attached through the Diels-Alder cycloaddition reaction.

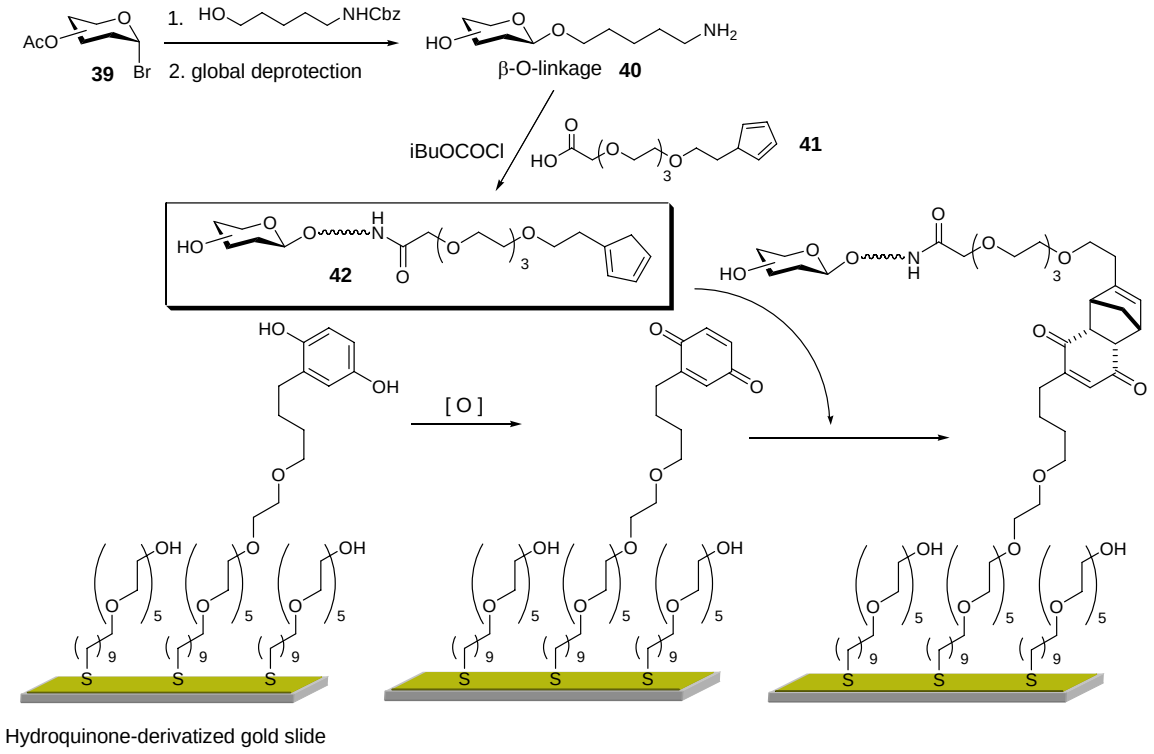

Figure 19. Immobilization of cyclopentadiene-conjugated carbohydrates on SAMs of benzoquinone via a Diels-Alder reaction.

The advantages of this method are that the density of immobilized carbohydrates can be controlled by adjusting the relative concentration of the two alkanethiols. Also, the

surfaces presenting penta(ethylene glycol) moieties are inert into the nonspecific adsorption of proteins.

The Cu(I)-catalyzed Huisgen 1,3-dipolar cycloaddition, termed “click chemistry” has been employed to immobilize carbohydrates on solid surfaces such as microtiter plates,[80] glass slides,[81] and gold.[82] The formation of triazole by the reaction of azide and alkyne is irreversible and usually quantitative. In addition, the reaction is extremely mild and indifferent to solvent and pH.

Wang and co-workers explored a Huisgen 1,3-dipolar cycloaddition reaction as a general strategy for the immobilization of carbohydrates on gold surface (Figure 20).[82] Mono-, di- and trisacchrides **44** linked to an azide were stereoselectively prepared by the condensation of corresponding peracetylated trichloroacetimidates **43** with azidotriethylene glycols, followed by the deprotection. Alkyne disulfide **45** synthesized was self-assembled on gold surface, and then azido carbohydrates **44** were covalently attached by the Cu(I)-catalyzed regiospecific 1,3-dipolar cycloaddition reaction.

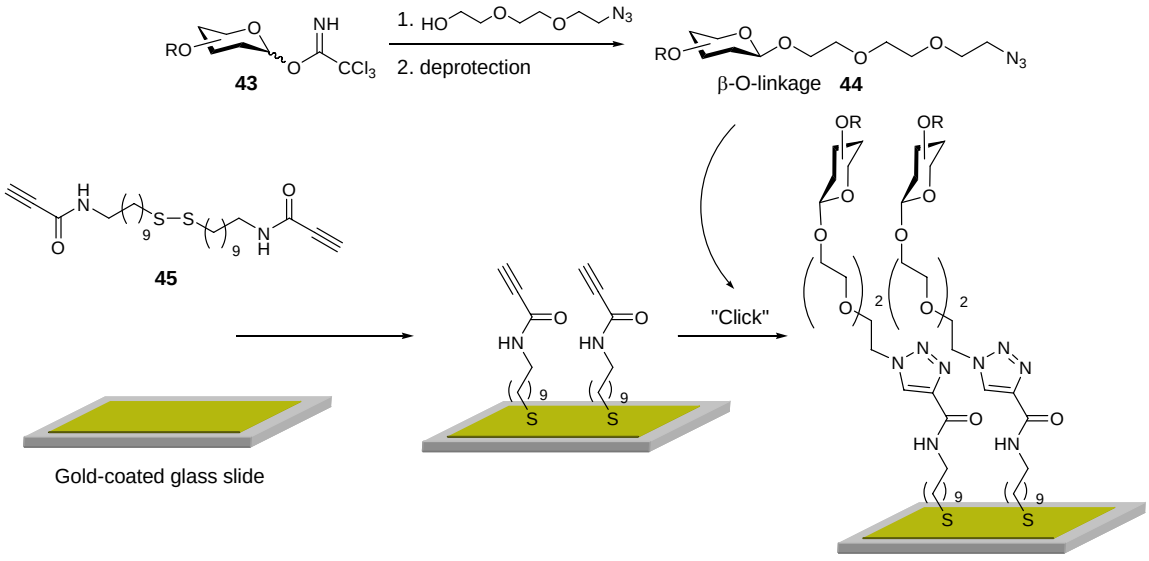

Figure 20. Immobilization of azide-terminated carbohydrates on SAMs of alkyne using a Huisgen 1,3-dipolar cycloaddition.

With so many alternatives for the immobilization of carbohydrates, it is difficult to conclude that one method is superior to all others. However, the methods for site-specific immobilization of carbohydrates would be better than nonspecific attachment, since carbohydrate immobilized on the surface are presented in homogeneous and oriented fashion so that all carbohydrates have equal activity toward carbohydrate binding proteins. Furthermore, the preservation of the correct ring form of the terminal carbohydrate residue and the stereochemical control of anomeric center are obviously important for the binding of proteins. Accordingly, a general synthetic approach that can control the stereochemistry of the anomeric center is required. The trichloroacetimidate method introduced by Schmidt two decades ago has been extensively developed and is a powerful method to control the stereochemistry at the anomeric center with preserving the cyclic form. However, this method is mainly limited to the O-linkage. In spite of significant progress over the few decades, controlling the stereochemistry of N-linkages still presents a significant challenge, especially for the amide linkages.

Damkaci and DeShong[83,84] have developed a methodology for the stereoselective synthesis of N-linked glycosyl amides **49** and **51** (Scheme 5) by the modification of Staudinger reaction.[85]

Scheme 5

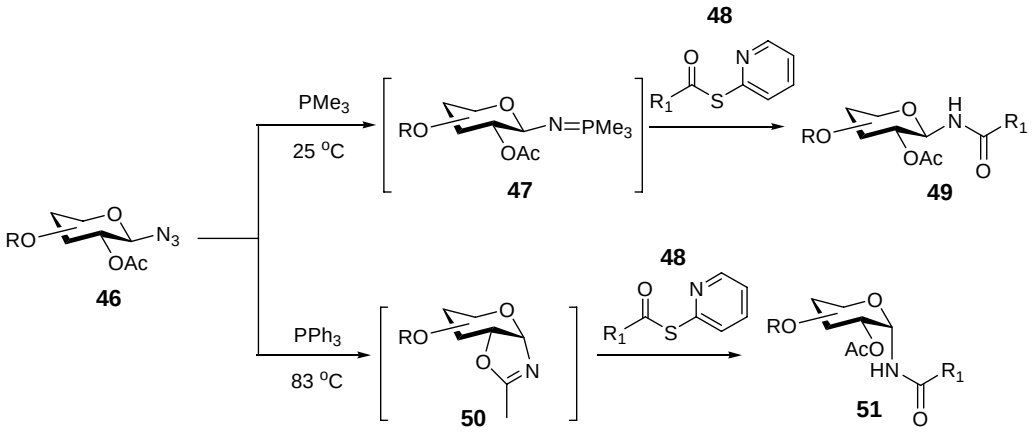

In this process, the stereochemistry of amide linkages is easily controlled by the reaction conditions. For example, β-stereochemistry arises from the reaction of β-glycosyl azide **46** with trimethyl phosphine to generate β-phosphorimine **47**, followed by the coupling with thiopyridyl ester **48**. On the other hand, α-stereochemistry results from the formation of isoxazoline intermediate **50** (Scheme 6). At high temperature, the β-phosphorimine **52** initially produced by the reaction of β-glycosyl azide **46** with triphenylphosphine is equilibrated to the α-phosphorimine **53**, which then cyclized to form isoxazoline **50**.[83]

Scheme 6

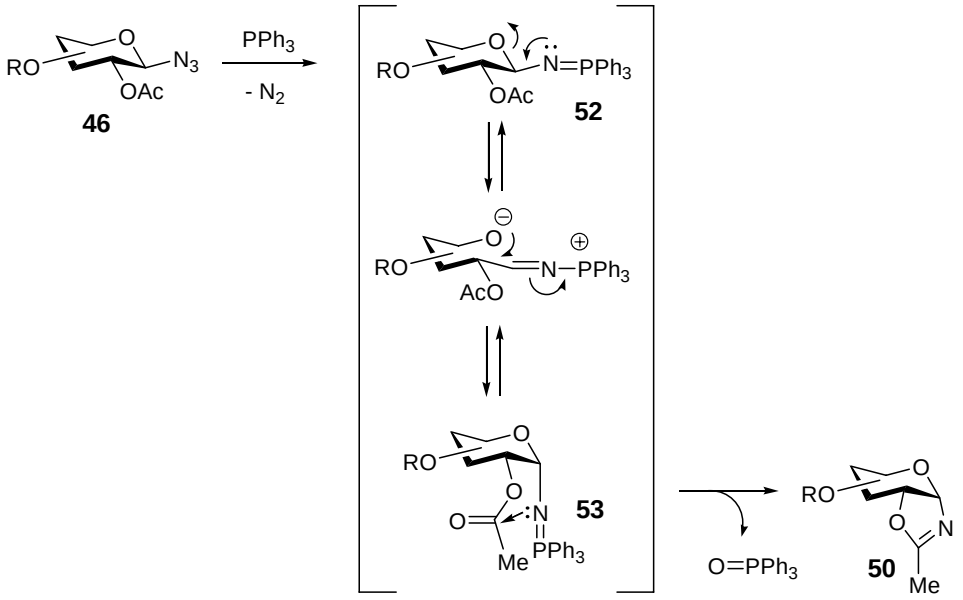

This coupling reaction is very useful because by choosing the appropriate reaction conditions a variety of N-linked glycoconjugate containing different tethers can be prepared in a stereoselective manner.

The goal of this study was to synthesize N-linked glycoconjugates that are tethered to thiols **54** for the functionalization of gold surfaces, to siloxanes **55** for the functionalization of silica surfaces, and to alkyl chains **56** for the functionalization of

surfactant vesicles by hydrophobic insertion into the outer bilayer of the vesicle, utilizing this methodology (Scheme 7). For these studies, the preparation of a range of building blocks **46** is prerequisite.

Scheme 7

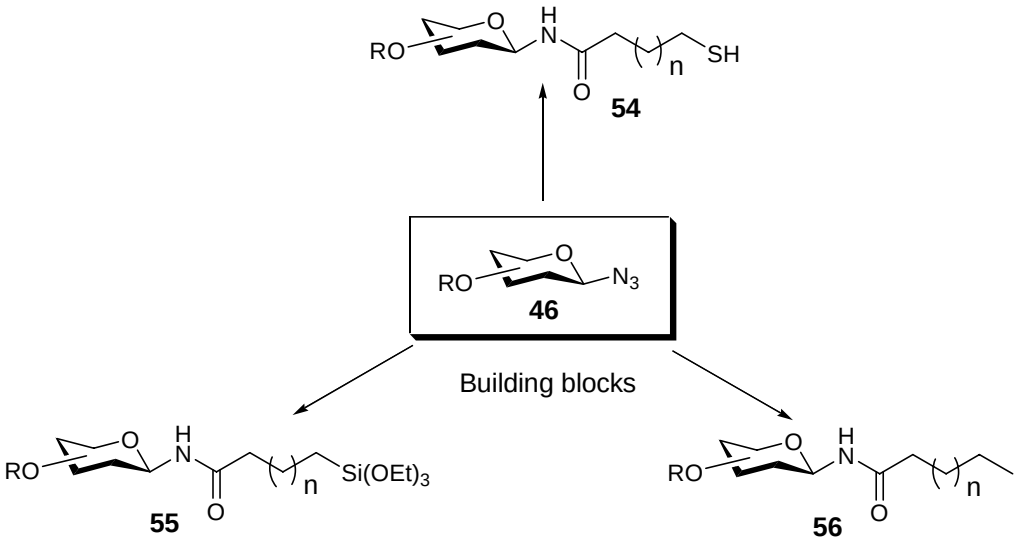

RESULTS AND DISCUSSION

A range of building blocks were prepared by the reaction of glycosyl peracetates with trimethylsilyl azide in the presence of tin tetrachloride. The results are summarized in Table 1.

Table 1. Synthesis of glycosyl azides.[a]

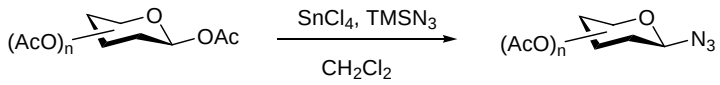

entry	substrate[b]		product		yield[c] (%)
1	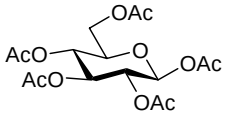	**57**	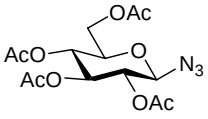	**63**	95
2	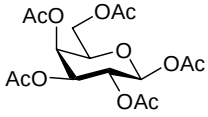	**58**	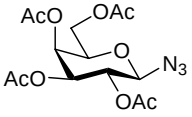	**64**	83
3	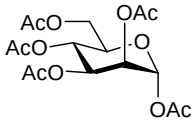	**59**	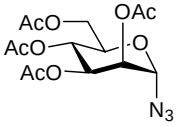	**65**	97
4	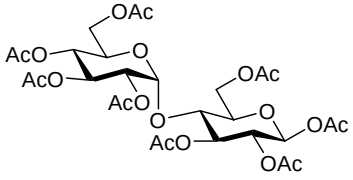	**60**	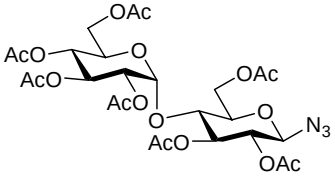	**66**	92
5	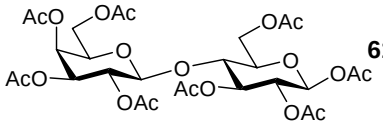	**61**	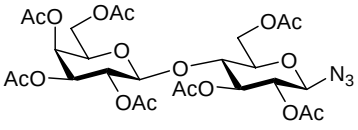	**67**	89
6	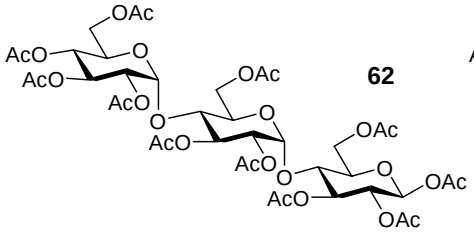	**62**	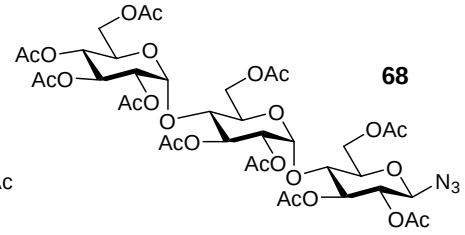	**68**	93

[a] Reactions were performed at room temperature for 24 h. [b] For detailed acetylation procedures for the substrates, see experimental section. The configuration of major anomer was as shown. [c] Isolated yields.

All the glycosyl azides were smoothly transformed from corresponding peracetates in moderate to excellent yields with β-configuration except for mannose azide **65** (Table 1, entry 3). The stereoselectivities, including mannose azide **65**, of this glycosylation reaction are explained by the 1,2 trans rule with neighboring group participation at C2 oxygen, as discussed early.[42]

Having synthesized a variety of building blocks, the feasibility of the coupling reaction to construct N-linked glycoconjugates in stereoselective manner was investigated.

Synthesis of Glycoconjugates Anchored to Thiols

For the direct and site-specific immobilization of carbohydrates on gold surface, naturally occurring thioctic acid **69** (lipoic acid) was selected as a coupling partner for a number of reasons: the presence of two sulfur atoms in thioctic acid provides a strong attachment to gold surfaces, and thioctic acid-anchored biomolecules prevent nonspecific protein binding.[86,87]

In order to construct β-linkage, trimethylphosphine was added into the solution containing glycosyl azides at room temperature to β-phosphorimines according to a typical Staudinger reaction.[85] Before anomerization occurs, the *in situ* formed β-phosphorimines were coupled with D/L-thioctic aicd **69** to produce exclusively β-N-linked glycoconjugates in moderate yields. The results are summarized in Table 2.

Table 2. Synthesis of β-N-linked glycoconjugates tethered to thioctic acid.[a]

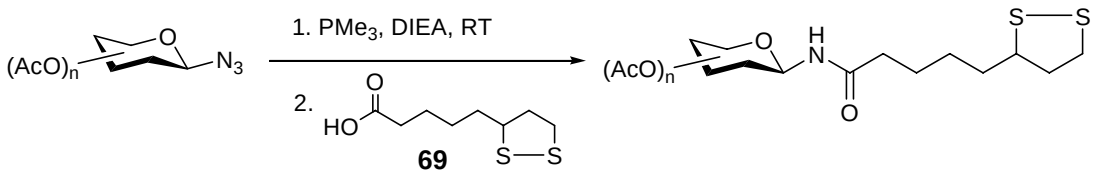

entry	starting material	product		yield[b] (%)
1	**63**	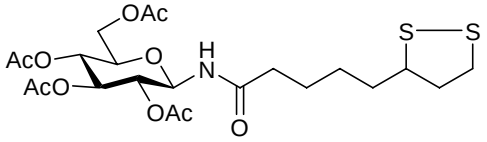	**70**	61
2	**64**	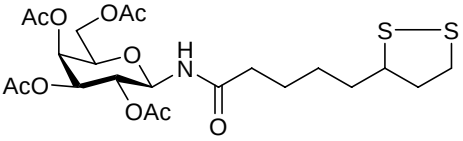	**71**	52
3	**65**	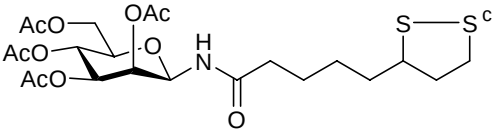	**72**	48
4	**66**	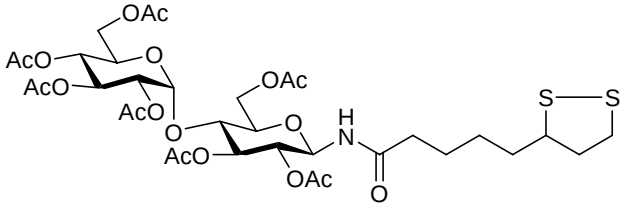	**73**	48
5	**67**	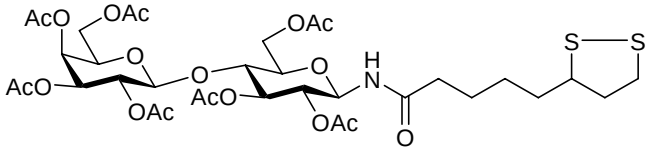	**74**	54

[a] All reactions were performed in dichloromethane at room temperature. D/L-thioctic acid **69** was added into *in situ* formed phosphorimine. [b] Isolated yields. [c] The reaction was performed in 1,2-dichloroethane at 95 °C to generate isoxazoline, which then coupled with thiopyridyl ester **83**. See experimental section for full reaction details.

All mono- and disaccharide azides which have β-confiugation were transformed into the β-linked glycoconjugates under these reaction conditions. However, mannose azide **65** has the α-configuration, which may not produce β-mannose conjugate **72**.

Therefore, a different reaction condition requires producing β-linkage of mannose conjugate. It was known that α-mannose azide **65** treated with triphenylphosphine at high temperature initially forms the α-phosphorimine **75**, which is then epimerized to the β-phosphorimine **76**. As soon as the β-phosphorimine **76** is produced, condensation occurs to generate isoxazoline **77** (Scheme 8).[84]

Scheme 8

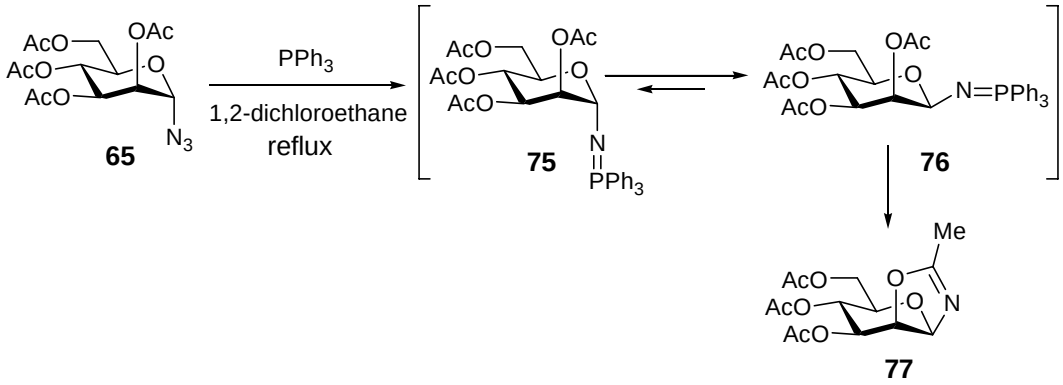

By utilizing a reaction condition producing α-stereochemistry, α-mannose azide **65** was converted into the isoxazoline intermediate **77**, and the resulting isoxazoline **77** was coupled with thiopyridyl ester **83** to facilitate the formation of β-linked mannose conjugate **72**.

The final task remaining was to deprotect the acetyl groups. Under basic condition, the desired products were readily prepared in good yields, and the results are summarized in Table 3.

Table 3. Deprotection of acetyl groups.

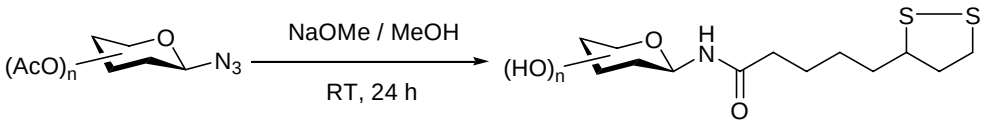

entry	product		yield[a] (%)
1	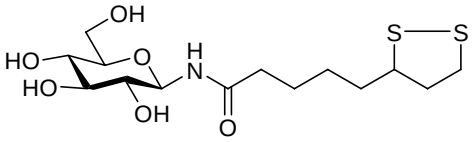	**78**	91
2	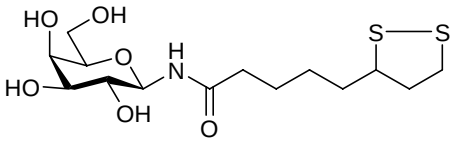	**79**	88
3	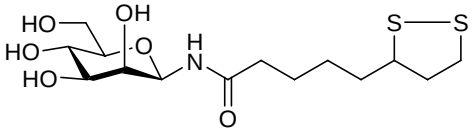	**80**	85
4	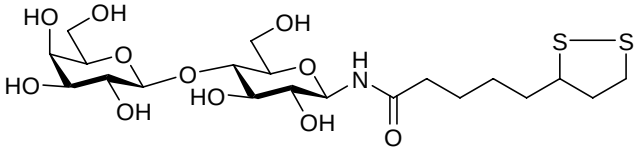	**81**	84

[a] Isolated yields except for entry 2. The yield of galactose disulfide **79** was based on the crude product. ^{1}H NMR showed that the crude product **79** was essentially pure.

Following the successful preparation of the β-N-linked glycoconjugates in a stereoselective manner, attention turned toward the construction of α-N-linkage utilizing isoxazoline formation.

It was shown that among the coupling reactions between isoxazoline and a variety of acid derivatives, thiopyridyl esters **48** in the presence of copper (II) chloride resulted in the production of α-adduct in excellent yield and stereoselectivity. Presumably, the coordination of copper to the pyridyl moiety increases the electrophilicity of the coupling partner.[83] Therefore, the thiopyridyl ester **83** was synthesized according to the modified

procedure of Mukaiyama.[88] The reaction of thioctic acid **69** with dipyridyl disulfide **82** in the presence of triphenylphosphine at room temperature produced the thiopyridyl ester **83** in excellent yield (Scheme 9).

Scheme 9

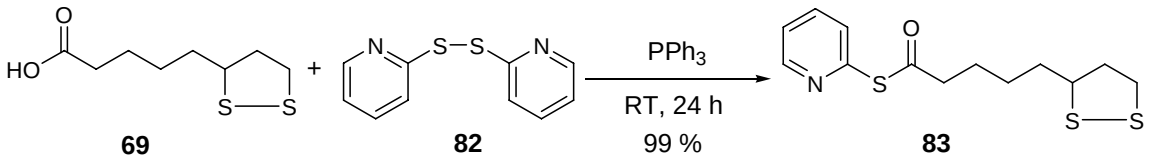

69 **82** **83**

With the desired coupling partner **83** in hand, β-glucose azide **63** was employed. Under the coupling conditions, the isoxazoline generated *in-situ* by the reaction of β-glucose azide **63** with triphenyl phosphine at 95 ^{o}C was coupled with thiopyridyl ester **83** to give exclusively the α-addcut **84** in moderate yields, which were sequentially deprotected to produce α-N-linked glucose conjugate **85**.

Under the same reaction conditions, β-lactose azide **67** was successfully converted into the α-N-linked lactose conjugate **87**. Table 4 summarizes the results of coupling reaction and deprotection.

Table 4. Synthesis of α-N-linked glycoconjugates tethered to thioctic acid.[a]

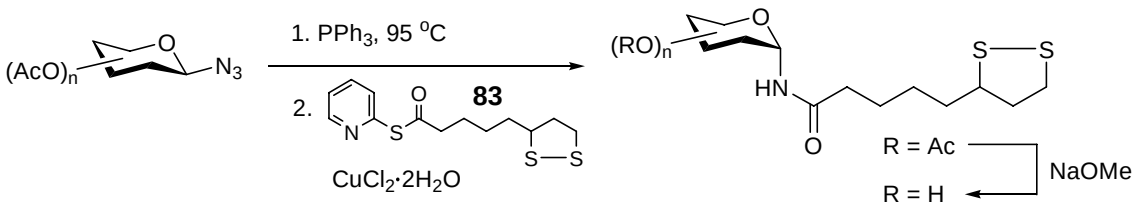

entry	starting material	product		yield (%)
1	**63**	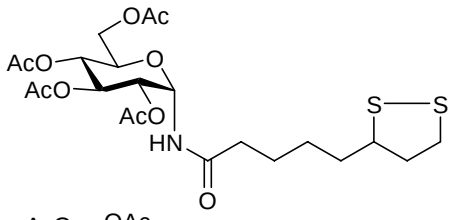	**84**	63[b]
2	**67**	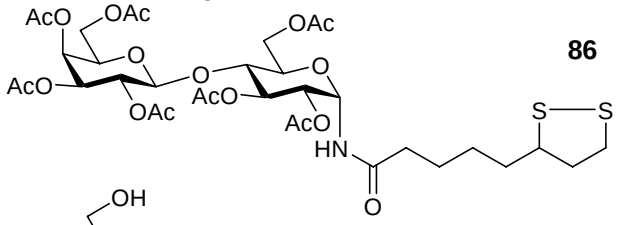	**86**	55[b]
3	**84**	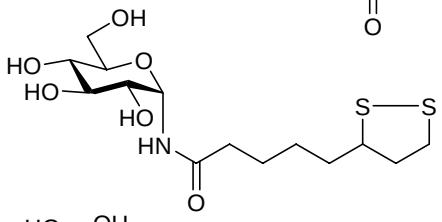	**85**	99[c]
4	**86**	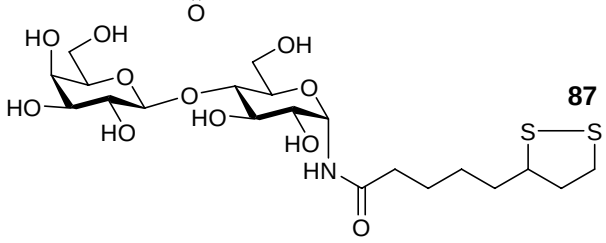	**87**	90[c]

[a] The coupling reactions were performed in 1,2-dichloroethane in the presence of 4Å molecular sieves. The thiopyridyl ester and the additive, respectively, were added at room temperature and run for 24 h. For the deprotection step, all reactions were performed in methanol at room temperature for 24 h. [b] Isolated yields. [c] Crude yields. ^{1}H NMR showed that the crude products were essentially pure.

It was our intention to show that the methodology developed by Damkaci and DeShong[83,84] can be used for the stereoselective synthesis of N-linked glycoconjugates anchored to thiol groups. The results of coupling reactions with thioctic acid or its

derivative demonstrated the feasibility. However, for the effective binding of proteins, carbohydrate moieties have to be extended enough from the surface. The tether length of thioctic acid utilized in coupling reactions is already set. Therefore, a simple and effective method for controlling the tether length is required. For this purpose, an alternative approach was employed. For the construction of β-linkage (Scheme 10), acetylated β-glucose azide **63** was allowed to react with trimethyl phosphine to generate β-phosphorimine, which was coupled with acid chloride **88** prepared by the literature[89] to provide acetylated β-glucose amide **89**. Displacement of the bromide with thioacetate, followed by removal of the acetate protecting groups with sodium methoxide in methanol under a nitrogen atmosphere and air oxidation afforded β-glucose disulfide **91** in 35 % overall yield.

Scheme 10

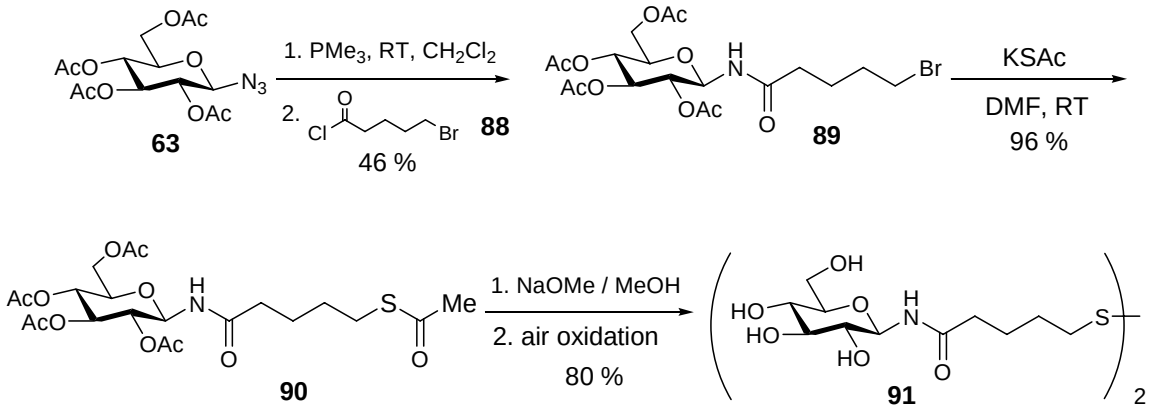

α-Glucose disulfide **94** was also synthesized by the similar manner in 42 % overall yield (Scheme 11).

Scheme 11

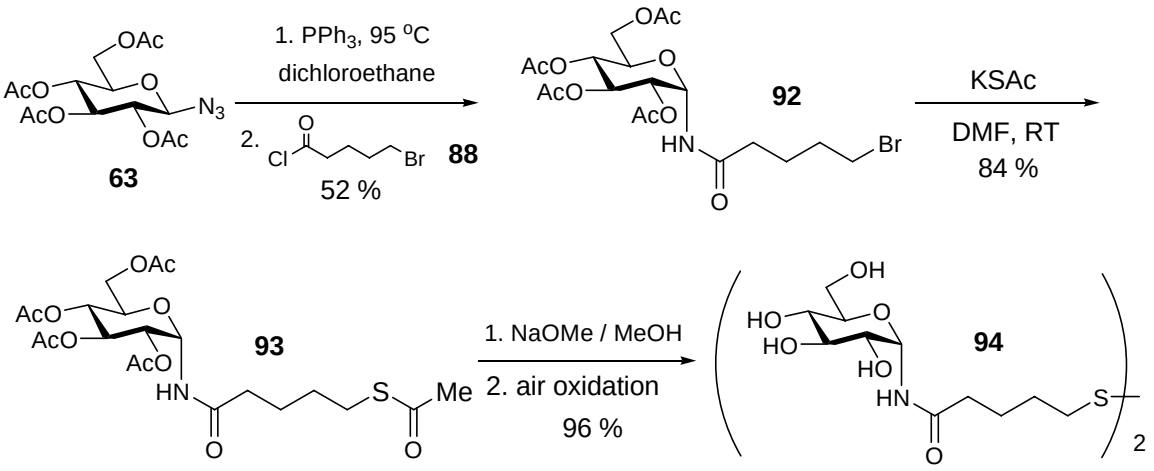

These results demonstrate that the tether length of N-linked glycoconjugates can be controlled by simply introducing acid halides **88** that have a different length during the coupling reactions.

Having the method that can control the stereochemistry and tether length of the glycoconjugates anchored to thiol groups, attention turned towards the immobilization of glycoconjugates on gold surfaces to investigate whether they are presented in oriented and homogeneous fashion with reproducibility. A variety of thiolated glycoconjugates were immobilized on gold surfaces and characterized their structural features on gold surfaces by atomic force microscopy, reflection Fourier transform infrared spectroscopy, and X-ray photoelectron spectroscopy with collaboration of Dr. Tarlov group in NIST.

Potentially, there are a number of conformations when glycoconjugates are immobilized on the gold surface (Figure 11), many of which may be unsuitable for the development of biosensors.

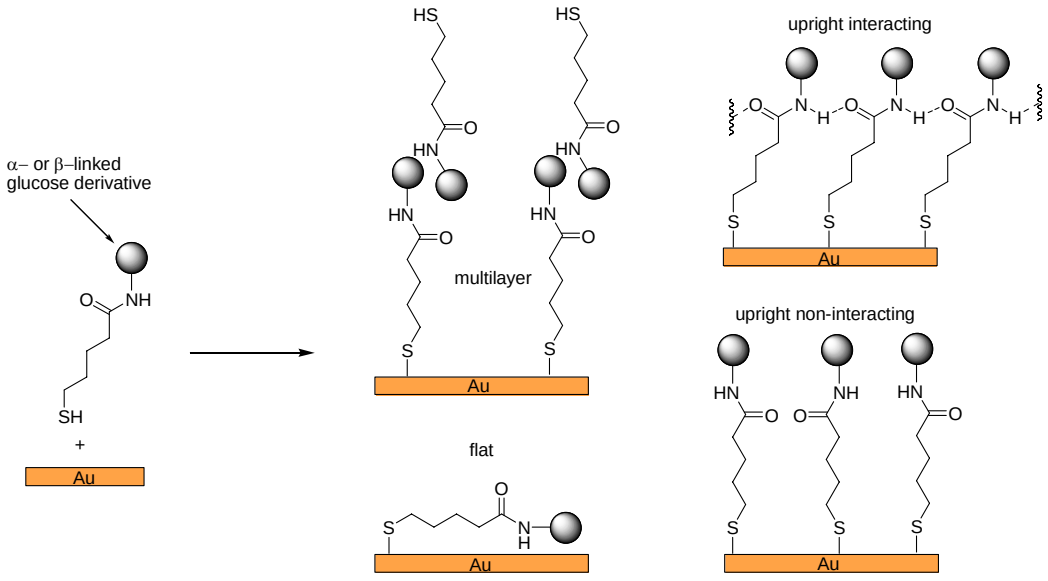

Figure 21. Possible conformations of thiol-anchored glycoconjugates adsorbed on gold surface.

The experimental data indicated that α- or β-linked glycoconjugates attach to gold in an upright interacting fashion via the thiol linker, and both glycoconjugates form monolayers with high packing densities comparable to those typically observed for alkanethiol monolayers on gold. Also the surface density is sensitive to the stereochemistry of the glycoconjugates. For details, see Appendix.

Synthesis of Glycoconjugates Anchored to Siloxanes

For the direct immobilization of carbohydrates on a glass surface including silica particles, it is required to introduce siloxane moieties to the terminal of glycoconjugates.

The hydrosilylation catalyzed by various transition metals (Pd, Pt, Rh, Ru, Co, and Ir) has been used for the formation of C-Si bond from unsaturated carbon bonds.[90-93] Mioskowski and co-workers have reported an excellent catalytic activity of platinum oxide (PtO_2) for the hydrosilylation reactions with a wide range of functional alkenes.[94]

In order to investigate the possibility of hydrosilylation reaction, β-glucose azide

63 was initially selected and coupled to 4-pentenoic acid **95** under β-linkage formation condition to give β-glucose pentenamide **96**. Using a modified hydrosilylation condition, β-glucose pentenamide **96** was treated with triethoxysilane in the presence of platinum oxide, which resulted in the formation of a mixture of desired adduct **97** and saturated adduct **98**. Analogous reactions with β-lactose azide **67** provided triethoxysilyl-β-lactose conjugate **100** and its saturated adduct **101**. Table 5 summaries the results of coupling reaction and hydrosilylation reaction.

Table 5. Stereoselective synthesis of glycoconjugates anchored to siloxane group.[a]

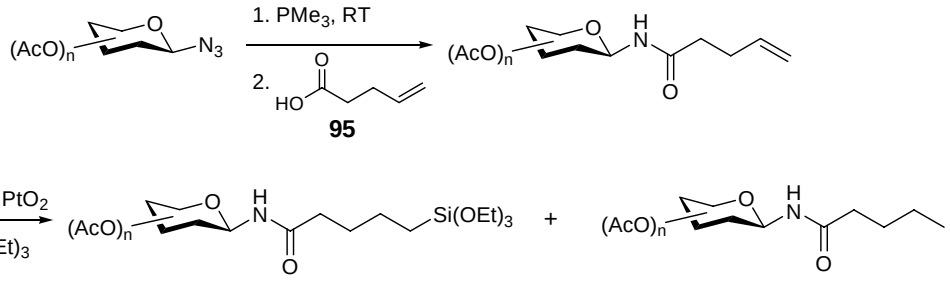

entry	R	coupling product yield[b] (%)	hydrosilylation product[c]	yield[d] (%)
1	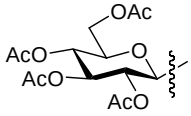	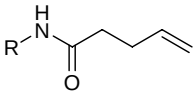 **96** 77	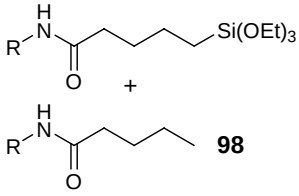 **97** + **98** **97**:**98** = 85:15	62
2	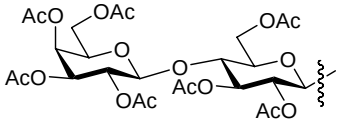	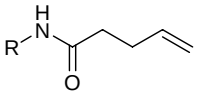 **99** 73	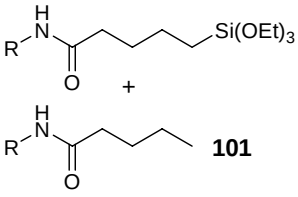 **100** + **101** **100**:**101** = 72:28	40

[a] The coupling reactions were performed in dichloromethane at room temperature for 24 h. The hydrosilylation reactions were performed in a sealed tube at 95 °C for 2 h. The hydrogenation reaction were performed in methanol for 2 h. [b] Isolated yield. [c] The mole ratio of two compounds was determined by GC and ^{1}H NMR. [d] Yield of the desired adduct. The yield was calculated on the basis of GC and ^{1}H NMR spectroscopy.

The presence of saturated adducts (**98** and **101**, respectively) in the mixture was confirmed by the hydrogenation of their corresponding glycosyl pentenamides (**96** and **99**, respectively). The formation of the saturated adduct presumably arises from the hydrogenation of glycosyl pentenamides on the surface of colloidal platinum particles generated during the reaction.[95]

Synthesis of Glycoconjugates Modified with Alkyl Chains

Our group has been interested in the surfactant-based vesicles as a drug carrier because of their stability and ease of preparation. Targeted delivery of toxic drugs, such as chemotherapeutic agents, is critical for enhancing the therapeutic index of the drug and reducing the toxic side effects to normal cells. To achieve targeted delivery of drugs, it is prerequisite to functionalize the surface of surfactant vesicles with targeting agents. Utilizing carbohydrate-receptor interactions, it was thought that the surface of surfactant vesicles could be functionalized with lipidated carbohydrates by insertion into the hydrophobic interior of vesicle bilayer.

Initially, β-glucose azide **63** was coupled with octanoic acid **102** as an alkyl chain under the reaction condition generating β-linkage. The resulting acetylated β-glucose-octanamide **103** was deprotected under basic condition to give the desired product **107**. More complex di- and trisaccharide conjugates were also obtained under the same reaction condition in moderate yield. The results are summarized in Table 6.

Table 6. Stereoselective synthesis of glycoconjugates modified with alky chain.[a]

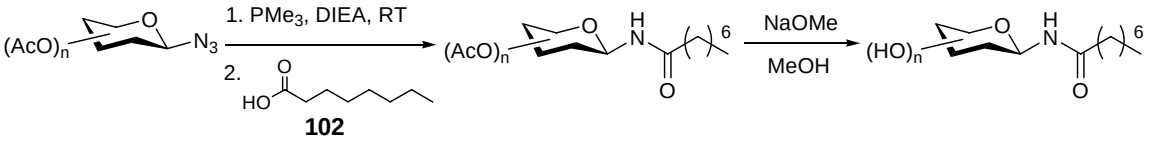

102

entry	product	R = Ac	yield[b] (%)	R = H	yield[c] (%)
1	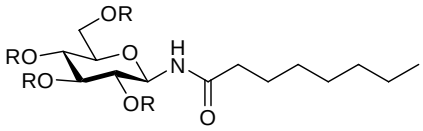	**103**	57	**107**	85
2	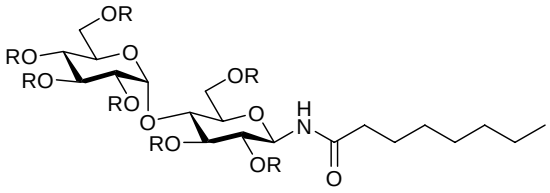	**104**	61	**108**	74
3	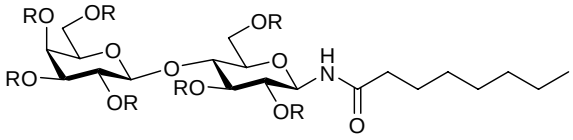	**105**	54	**109**	71
4	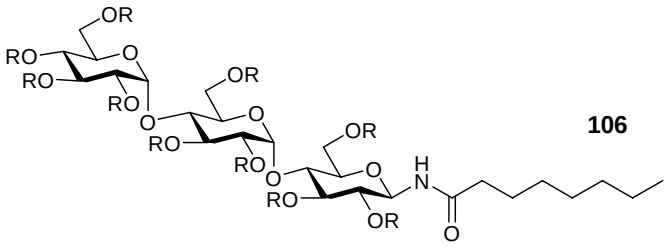	**106**	50	**110**	74

[a] Typical reaction conditions were used for the coupling reaction and deprotection reaction. See the experimental section for details. [b,c] Isolated yields.

The study of surface functionalization of surfactant vesicles with lipidated carbohydrates is discussed in Chapter 4.

CONCLUSIONS AND OUTLOOK

A variety of N-linked glycoconjugates tethered to thiol groups, siloxane group, and alkyl chain have been synthesized by the modified Staudinger reaction in a high

stereoselective manner. The possibility to control tether length has been successfully demonstrated. The generality of the coupling reaction has also been demonstrated by introducing the complex trisaccharide, maltotriose. During the chemical manipulation, the carbohydrate moieties remained intact. Therefore, this coupling methodology has the potential to allow for the synthesis of complex glycoconjugates with a range of linkers.

The glycoconjugates synthesized are being utilized for the development of biosensors. In the Dagenais group (Department of Electrical and Computer Engineering at UMCP), they utilize siloxane-anchored glycoconjugates to functionalize optical fibers. The Tarlov group in NIST utilizes thiol-anchored glycoconjugates to functionalize gold electrodes. The resulting optical and electrochemical sensors show excellent performance toward binding of lectins. These initial results hold promise for the biomedical applications with further development.

EXPERIMENTAL SECTION

General Experimental. All reagents and solvents were purchased from commercial suppliers and used without further purification unless otherwise noted.

Thin-layer chromatography (TLC) was performed on 0.25 mm Merck silica-coated glass plates treated with a UV-active binder, with compounds being identified in one or more of the following manners: UV (254 nm) or vanillin/sulfuric acid charring.

Melting points were taken in Kimax soft glass capillary tubes using a Thomas-Hoover Uni-Melt capillary melting point apparatus equipped with a calibrated thermometer and are corrected.

Infrared spectra were recorded on a Nicolet 5DXC FT-IR spectrophotometer. Band positions are given in reciprocal centimeters (cm^{-1}) and relative intensities are listed as br (broad), s (strong), m (medium) or w (weak).

^{1}H and ^{13}C NMR spectra were recorded on a Bruker DRX-400 MHz spectrometer. Chemical shifts are reported in parts per million (ppm) relative to $CDCl_3$ (δ 7.24). Coupling constants (*J* values) are given in hertz (Hz). Spin multiplicities are indicated by the following symbols: s (singlet), d (doublet), t (triplet), q (quartet), m (multiplet), br (broad).

Low resolution (LRMS) and high resolution (HRMS) mass spectra were obtained on a VG-7070E magnetic sector instrument.

Tetrahydrofuran (THF) was distilled from sodium/benzophenone. Methylene chloride (CH_2Cl_2), dimethyl formamide (DMF) and 1,2-dichloroethane were distilled from calcium hydride. Triphenylphosphine (Ph_3P) was recrystallized from hexane.

Glassware used in the reactions dried overnight in an oven at 120 ºC. All reactions were performed under an atmosphere of nitrogen unless otherwise noted.

All compounds were determined to be > 95 % pure by ^{1}H NMR spectroscopy unless otherwise noted.

Synthesis of Starting Materials

General procedure for the synthesis of glycosyl peracetate (Table 1). To a refluxing suspension of anhydrous NaOAc (4.0 equiv) in acetic anhydride (20 equiv) was added carbohydrate (1.0 equiv). The reaction mixture was refluxed for 3 h and cooled to 100 °C, then immediately transferred into ice-water mixture and stirred vigorously until a gum

formed. After decanting the aqueous layer, the gum was dissolved in CH_2Cl_2, washed with sat. aq. $NaHCO_3$, H_2O, dried over $MgSO_4$, filtered, and concentrated *in vacuo*. The crude product was purified by column chromatography on silica unless otherwise noted to give glycosyl peracetate.

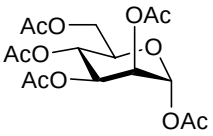

Mannose peracetate (59) (Table 1, entry 3). D-(+)-Mannose (5.00 g, 27.8 mmol), NaOAc (9.10 g, 111 mmol) and acetic anhydride (52.0 mL, 555 mmol). Without further purification, 10.0 g (93%) of mannose peracetate **(59)** as a mixture of anomers (**α**/**β**, 70/30, determined by ^{1}H NMR) was obtained. The crude mixture was used directly in the next step without further purification: R_f = 0.46 (hexane/EtOAc, 1/1); IR (CCl_4, cm^{-1}) 2959 (w), 1759 (s), 1369 (m), 1214 (s), 974 (m). The spectral data (^{1}H NMR) were identical to that previously reported by Vazquez.[96]

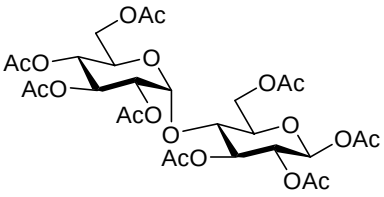

Maltose peracetate (60) (Table 1, entry 4). D-(+)-Maltose monohydrate (9.00 g, 25.0 mmol), NaOAc (8.20 g, 100 mmol) and acetic anhydride (47.0 mL, 500 mmol). Purification by column chromatography (hexane/EtOAc, 1/2) afforded 16.7 g (98%) of β-maltose peracetate **(60)** containing a significant amount of α-anomer (**α**/**β**, 28/72, determined by ^{1}H NMR) as a white foam: R_f = 0.61 (hexane/EtOAc, 1/2). The spectral data (IR, ^{1}H, and ^{13}C NMR) were identical to those previously reported by Damkaci.[84]

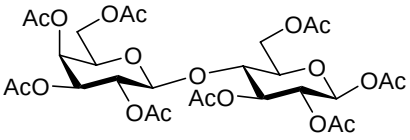

Lactose peracetate (61) (Table 1, entry 5). α-D-Lactose monohydrate (9.00 g, 25.0 mmol), NaOAc (8.20 g, 100 mmol) and acetic anhydride (47.0 mL, 500 mmol). Purification by column chromatography (hexane/EtOAc, 1/1), followed by two successive recrystallizations (CH_2Cl_2/ether/hexane) afforded 14.7 g (87%) of β-lactose peracetate **(61)** containing a trace amount of α-anomer (**α/β**, 7/93, determined by ^{1}H NMR) as a white solid: R_f = 0.21 (hexane/EtOAc, 1/1). The melting point and spectral data (IR, ^{1}H, and ^{13}C NMR) were identical to those previously reported by Damkaci.[84]

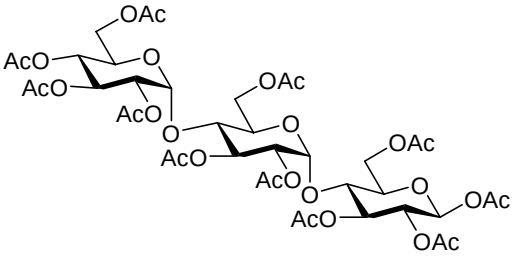

Maltotriose peracetate (62) (Table 1, entry 6). Maltotriose hydrate (1.00 g, 1.98 mmol), NaOAc (0.810 g, 9.90 mmol) and acetic anhydride (4.70 mL, 49.5 mmol). Purification by column chromatography (hexane/EtOAc, 1/3) afforded 1.83 g (96%) of β-maltotriose peracetate **(62)** containing a significant amount of α-anomer (**α/β**, 29/71, determined by ^{1}H NMR) as a white foam: R_f = 0.34 (hexane/EtOAc, 1/2); IR (CCl_4, cm^{-1}) 2959 (w), 1760 (s), 1368 (m), 1232 (s), 1037 (s); ^{1}H NMR (**β-anomer**, 400MHz, $CDCl_3$) δ 1.97 (s, 3H), 1.97 (s, 3H), 1.97 (s, 3H), 1.98 (s, 3H), 1.99 (s, 3H), 2.00 (s, 3H), 2.03 (s, 3H), 2.07 (s, 3H), 2.07 (s, 3H), 2.12 (s, 3H), 2.14 (s, 3H), 3.83-4.09 (m, 6H), 4.13 (dd, *J* = 12.4, 2.4, 1H), 4.22 (dd, *J* = 12.4, 3.4, 1H), 4.27 (dd, *J* = 12.4, 4.2, 1H), 4.40-4.46 (m, 2H), 4.71 (dd, *J* = 10.4, 4.0, 1H), 4.82 (dd, *J* = 10.4, 4.4, 1H), 4.93 (dd, *J* = 9.2, 8.1, 1H), 5.04 (t, *J* = 10.4, 1H), 5.24 (d, *J* = 4.0, 1H), 5.27-5.41 (m, 3H), 5.38 (d, *J* = 4.4, 1H), 5.71 (d, *J* = 8.1, 1H) ; ^{13}C NMR (**β-anomer**, 100 MHz, $CDCl_3$) δ 20.5, 20.5, 20.6, 20.6, 20.6, 20.7,

20.8, 20.8, 20.8, 20.8, 20.9, 61.3, 62.2, 62.6, 67.8, 68.5, 69.0, 69.3, 70.0, 70.4, 70.9, 71.6, 72.4, 72.9, 73.4, 75.1, 91.2, 95.6, 95.9, 168.8, 169.4, 169.6, 169.8, 169.8, 170.0, 170.3, 170.5, 170.5, 170.6, 170.6; HRMS (ESI) cacld. for $C_{40}H_{54}O_{27}Na$ [*M* + Na]$^+$ 989.2750, found 989.2765.

Synthesis of Glycosyl Azides

General Procedure for the Synthesis of Glycosyl Azide (Table 1). To a solution of glycosyl peracetate (1.0 equiv) in anhydrous CH_2Cl_2 was added trimethylsilyl azide (1.3 equiv), followed by 1.0 M solution of $SnCl_4$ (0.5 equiv). The resulting solution was stirred at room temperature for 24 h under a nitrogen atmosphere. The reaction mixture was diluted with CH_2Cl_2, washed with sat. aq. $NaHCO_3$, H_2O, dried over $MgSO_4$, filtered, and concentrated *in vacuo*. The crude product was purified by column chromatography on silica unless otherwise noted to give β-glycosyl azide. The α-anomer was rarely observed.

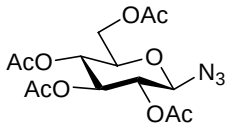

Peracetylated β-glucosyl azide (63) (Table 1, entry 1). β-D-Glucose pentaacetate **(57)** (10.0 g, 25.6 mmol), trimethylsilyl azide (4.40 mL, 33.3 mmol), and $SnCl_4$ (12.8 mL, 12.8 mmol). Purification by recrystallization (hexane/CH_2Cl_2) afforded 9.10 g (95%) of β-glucosyl azide **63** as a white solid: R_f = 0.14 (hexane/ether, 1/1); m.p. 126-127 °C (lit. m.p. 126-127 °C)[97]; IR (CCl_4, cm^{-1}) 2961 (w), 2119 (s), 1757 (s), 1543 (s), 1223 (s); ^{1}H NMR (400MHz, $CDCl_3$) δ 2.01 (s, 3H), 2.04 (s, 3H), 2.08 (s, 3H), 2.11 (s, 3H), 3.80 (ddd, *J* = 9.0, 4.8, 2.4, 1H), 4.18 (dd, *J* = 12.4, 2.4, 1H), 4.28 (dd, *J* = 12.4, 4.8, 1H), 4.65 (d, *J* = 9.0, 1H), 4.96 (t, *J* = 9.0, 1H), 5.11 (t, *J* =

9.0, 1H), 5.22 (t, *J* = 9.0, 1H); ^{13}C NMR (100 MHz, $CDCl_3$) δ 20.5, 20.5, 20.5, 20.7, 61.6, 67.8, 70.6, 72.5, 73.6, 87.9, 169.2, 169.3, 170.1, 170.6.

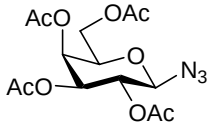

Peracetylated β-galactosyl azide (64) (Table 1, entry 2). β-D-Galactose pentaacetate **(58)** (3.00 g, 7.69 mmol), trimethylsilyl azide (1.30 mL, 9.99 mmol), and $SnCl_4$ (3.85 mL, 3.85 mmol). Purification by recrystallization (hexane/CH_2Cl_2) afforded 2.40 g (83%) of β-galactosyl azide **64** as white crystals: R_f = 0.32 (hexane/ether, 1/2). The melting point and spectral data (IR, ^{1}H, and ^{13}C NMR) were identical to those previously reported by Damkaci.[84]

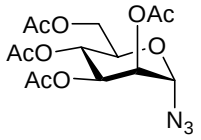

Peracetylated β-mannosyl azide (65) (Table 1, entry 3). Mannose pentaacetate **(59)** (2.86 g, 7.33 mmol), trimethylsilyl azide (1.16 mL, 8.79 mmol), and $SnCl_4$ (3.67 mL, 3.67 mmol). Purification by column chromatography (hexane/EtOAc, 1/1) afforded 2.65 g (97%) of β-mannosyl azide **65** as a light yellow gum: R_f = 0.58 (hexane/EtOAc, 1/1). The spectral data (IR, ^{1}H, and ^{13}C NMR) were identical to those previously reported by Damkaci.[84]

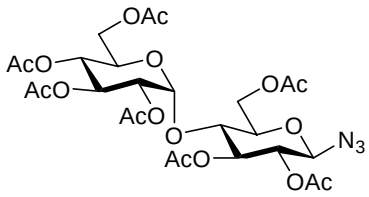

Peracetylated β-maltosyl azide (66) (Table 1, entry 4). Maltose peracetate **(60)** (1.67 g, 2.46 mmol), trimethylsilyl azide (0.430 mL, 3.20 mmol), and $SnCl_4$ (1.23 mL, 1.23 mmol). Purification by column chromatography (hexane/EtOAc, 1/1) afforded 1.50 g (92%) of β-maltosyl azide **66** as a white foam: R_f = 0.73 (hexane/ EtOAc, 1/2); The

spectral data (IR, ^{1}H, and ^{13}C NMR) were identical to those previously reported by Damkaci.[84]

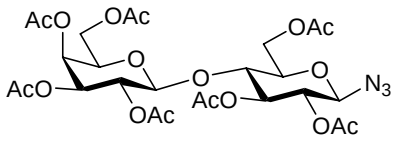

Peracetylated β-lactosyl azide (67) (Table 1, entry 5). Lactose peracetate **(61)** (2.65 g, 3.91 mmol), trimethylsilyl azide (0.670 mL, 5.08 mmol), and $SnCl_4$ (1.96 mL, 1.96 mmol). Purification by column chromatography (hexane/EtOAc, 1/1) afforded 2.30 g (89%) of acetylated β-lactosyl azide **67** as a white foam: R_f = 0.34 (hexane/ EtOAc, 1/1) The spectral data (IR, ^{1}H, and ^{13}C NMR) were identical to those previously reported by Damkaci.[84]

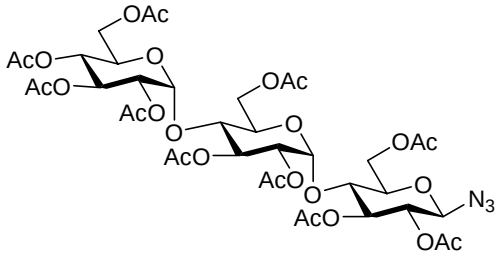

Peracetylated β-maltotriose azide (68) (Table 1, entry 6). Maltotriose peracetate **(62)** (1.54 g, 1.59 mmol), trimethylsilyl azide (0.250 mL, 1.91 mmol), and $SnCl_4$ (0.800 mL, 0.800 mmol). Without further purification, 1.40 g (93%) of β-maltotriosyl azide **68** as a colorless gum was obtained: R_f = 0.49 (hexane/ EtOAc, 1/2); ^{1}H NMR (400MHz, $CDCl_3$) δ 1.97 (s, 3H), 1.98 (s, 3H), 1.98 (s, 3H), 1.99 (s, 3H), 2.01 (s, 3H), 2.03 (s, 3H), 2.03 (s, 3H), 2.08 (s, 3H), 2.14 (s, 3H), 2.16 (s, 3H), 3.89 (ddd, *J* = 9.0, 4.0, 2.8, 1H), 3.89-3.99 (m, 4H), 4.03 (dd, *J* = 12.4, 2.4, 1H), 4.15 (dd, *J* = 12.4, 3.2, 1H), 4.22 (dd, *J* = 12.4, 3.6, 1H), 4.30 (dd, *J* = 12.0, 4.0, 1H), 4.44 (dd, *J* = 12.4, 2.0, 1H), 4.48 (dd, *J* = 12.0, 2.8, 1H), 4.69 (d, *J* = 9.0, 1H), 4.72 (dd, *J* = 9.6, 4.0, 1H), 4.76 (t, *J* = 9.0, 1H), 4.83 (dd, *J* = 10.4, 4.0, 1H), 5.05 (t, *J* = 9.6, 1H), 5.24 (t, *J* = 9.0, 1H), 5.25 (d, *J* = 4.0, 1H), 5.31-5.37 (m, 2H), 5.39

(d, J = 4.0, 1H); HRMS (ESI) cacld. for $C_{38}H_{51}O_{25}N_3Na$ $[M + Na]^+$ 972.2709, found 972.2706. The spectral data (IR and ^{13}C NMR) were identical to those previously reported by Damkaci.[84]

Synthesis of Acetylated Glycoconjugates

General Procedure A. Synthesis of β-N-linked Glycoconjugate

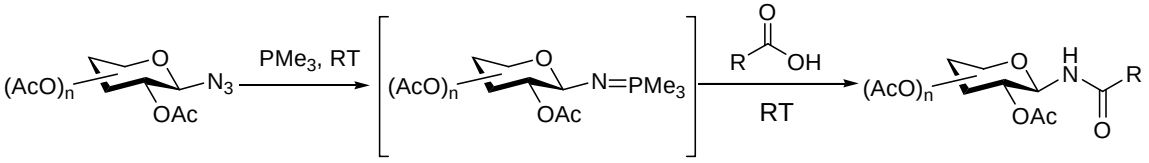

To a solution of acetylated β-glycosyl azide (1.0 equiv) in anhydrous CH_2Cl_2 was added diisopropylethylamine (2.0 equiv), followed by 1.0 M solution of PMe_3 (given equiv, typically 1.1 equiv). The reaction mixture was stirred at room temperature for 30 min and then a coupling partner (2.0 equiv) was added dropwise. After being stirred 24 h, the reaction mixture was diluted with CH_2Cl_2 and washed with brine, dried over $MgSO_4$, filtered, and concentrated *in vacuo*. The crude product was purified by column chromatography unless otherwise noted to give acetylated β-glycoconjugate.

General Procedure B. Synthesis of α-N-linked Glycoconjugate

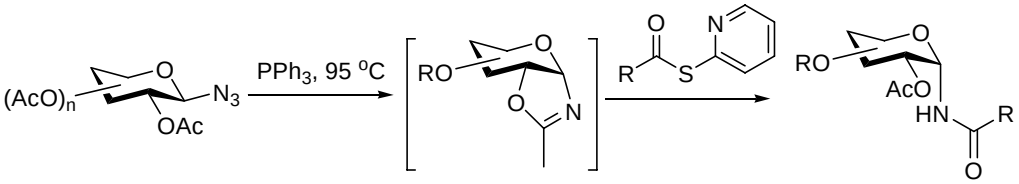

Acetylated β-glycosyl azide (1.0 equiv) and Ph_3P (1.1 equiv) were dissolved in anhydrous 1,2-dichloroethane in the presence of 4Å molecular sieves. The resulting

suspension was heated at 95 °C for 24 h without stirring to form isoxazoline intermediate and then cooled to room temperature. A coupling partner (1.3 equiv) and additive (1.3 equiv) were added. The reaction mixture was stirred at given temperature for 24 h and diluted with CH_2Cl_2. The molecular sieves were filtered, washed with H_2O and brine. The organic layer was dried over $MgSO_4$, filtered, and concentrated *in vacuo*. The crude product was purified by column chromatography unless otherwise noted to give acetylated α-glycoconjugate with a trace amount of β-anomer.

General Procedure C. Deprotection of Acetyl Group

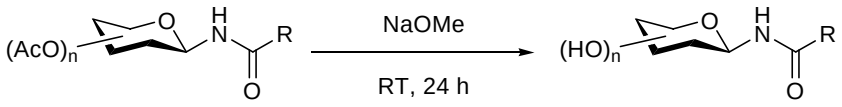

To a solution of acetylated glycoconjugate (1.0 equiv) in MeOH was added 0.2 M solution of sodium methoxide (given equiv) and then stirred at room temperature for 24 h under a nitrogen atmosphere. The reaction mixture was neutralized with Amberlite IR-120 resin or Dowex MAC-3 resin, filtered and concentrated *in vacuo*. The crude product was purified by a short column chromatography unless otherwise noted to give deacetylated glycoconjugate.

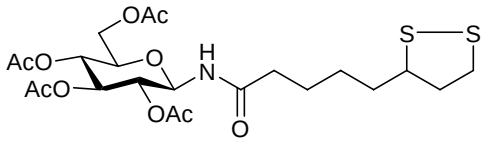

Acetylated β-glucosyl thioctanamide 70 (Table 2, entry 1). Amide **70** was prepared following general procedure A using acetylated β-glucosyl azide **63** (2.00 g, 5.36 mmol), diisopropylethylamine (1.90 mL, 10.7 mmol), Me_3P (6.43 mL, 6.43 mmol) and D/L-thioctic acid **69** (2.21 g, 10.7 mmol) as coupling partner. Purification by column

chromatography (hexane/EtOAc, 2/3) afforded 1.76 g (61%) of β-glucosyl thioctanamide **70** as a light yellow foam: R_f = 0.39 (hexane/EtOAc, 1/2); IR (CCl_4, cm^{-1}) 3432 (w), 2929 (w), 1755 (s), 1707 (m), 1550 (s), 1231 (s), 1055 (s); ^{1}H NMR (400MHz, $CDCl_3$,) δ 1.39-1.49 (m, 2H), 1.59-1.72 (m, 4H), 1.90 (sextet, *J* = 6.4, 1H), 2.02 (s, 3H), 2.03 (s, 3H), 2.05 (s, 3H), 2.08 (s, 3H), 2.16-2.23 (m, 2H), 2.45 (sextet, *J* = 6.4, 1H), 3.08-3.21 (m, 2H), 3.53-3.58 (m, 1H), 3.82 (ddd, *J* = 9.5, 4.0, 2.0, 1H), 4.08 (dd, *J* = 13.0, 2.0, 1H), 4.31 (dd, *J* = 13.0, 4.0, 1H), 4.91 (t, *J* = 9.5, 1H), 5.06 (t, *J* = 9.5, 1H), 5.25 (t, *J* = 9.5, 1H), 5.31 (t, *J*= 9.5, 1H), 6.21 (d, *J* = 9.5, 1H); ^{13}C NMR (100 MHz, $CDCl_3$) δ 20.6, 20.6, 20.7, 20.7, 24.7, 28.7, 28.7, 34.5, 36.2, 36.3, 38.4, 40.2, 40.2, 56.2, 61.6, 68.1, 70.6, 72.6, 73.5, 78.1, 169.1, 169.4, 170.1, 170.6, 172.4. There are three more carbons (25) than expected (22), due to the fact that racemic thioctic acid **69** was utilized. So a mixture of diastereomers was obtained.

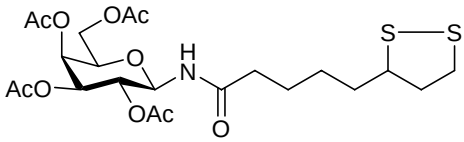

Acetylated β-galactosyl thioctanamide 71 (Table 2, entry 2). Amide **71** was prepared following general procedure A using acetylated β-galactosyl azide **64** (2.00 g, 5.36 mmol), diisopropylethylamine (1.90 mL, 10.7 mmol), Me_3P (6.43 mL, 6.43 mmol) and D/L-thioctic acid **69** (2.21 g, 10.7 mmol) as coupling partner. Purification by column chromatography (hexane/EtOAc, 1/1) afforded 1.50 g (52%) of acetylated β-galactosyl thioctanamide **71** as a light yellow foam: R_f = 0.28 (hexane/EtOAc, 1/1); IR (CCl_4, cm^{-1}) 3433 (w), 2934 (w), 1752 (s), 1704 (m), 1369 (m), 1225 (s), 1056 (m), 907 (m); ^{1}H NMR (400MHz, $CDCl_3$,) δ 1.33-1.45 (m, 2H), 1.55-1.72 (m, 4H), 1.87 (sextet, *J* = 6.5, 1H), 1.96 (s, 3H), 2.00 (s, 3H), 2.03 (s, 3H), 2.11 (s, 3H), 2.12-2.20 (m, 2H), 2.42 (sextet, *J* =

6.5, 1H), 3.05-3.18 (m, 2H), 3.50-3.54 (m, 1H), 3.98-4.03 (m, 1H), 4.06-4.12 (m, 2H), 5.06 (t, *J* = 9.0, 1H), 5.10 (dd, *J* = 9.0, 3.0, 1H), 5.20 (t, *J* = 9.0, 1H), 5.40 (d, *J* = 3.0, 1H), 6.22 (d, *J* = 9.0, 1H); ^{13}C NMR (100 MHz, $CDCl_3$) δ 20.5, 20.6, 20.6, 20.8, 24.7, 24.7, 28.6, 28.7, 34.5, 36.3, 36.3, 38.4, 40.2, 56.2, 61.0, 67.1, 68.3, 70.7, 72.2, 78.4, 169.7, 170.0, 170.3, 171.3, 172.8; HRMS (DEI) cacld. for $C_{22}H_{33}O_{10}N_1S_2$ [*M*]$^+$ 535.1546, found 535.1555. There are three more carbons (25) than expected (22), due to the fact that racemic thioctic acid **69** was utilized.

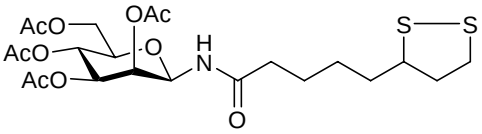

Acetylated β-mannosyl thioctanamide 72 (Table 2, entry 3). Amide **72** was prepared following general procedure B using acetylated β-mannosyl azide **65** (0.490 g, 1.31 mmol), PPh_3 (0.38 mg, 1.44 mmol), thiopyridyl ester **83** (0.510 g, 1.71 mmol) as coupling partner, and $CuCl_2{\cdot}2H_2O$ (0.290, 1.71 mmol) as an additive. Purification by column chromatography (hexane/EtOAc, 1/2) afforded 0.340 g (48%) of acetylated β-mannosyl thioctanamide **72** as a light yellow foam: R_f = 0.42 (hexane/EtOAc, 1/2); IR (CCl_4, cm^{-1}) 3448 (w), 2927 (m), 1759 (s), 1709 (m), 1368 (m), 1223 (s), 1057 (m); ^{1}H NMR (400MHz, $CDCl_3$,) δ 1.39-1.49 (m, 2H), 1.59-1.70 (m, 4H), 1.87 (sextet, *J* = 6.5, 1H), 1.95 (s, 3H), 2.02 (s, 3H), 2.07 (s, 3H), 2.15-2.22 (m, 2H), 2.22 (s, 3H), 2.44 (sextet, *J* = 6.5, 1H), 3.05-3.17 (m, 2H), 3.50-3.56 (m, 1H), 3.75 (ddd, *J* = 10.0, 5.2, 2.4, 1H), 4.05 (dd, *J* = 12.4, 2.4, 1H), 4.29 (dd, *J* = 12.4, 5.2, 1H), 5.08 (dd, *J* = 10.0, 3.0, 1H), 5.21 (t, *J* = 10.0, 1H), 5.34 (t, *J* = 3.0, 1H), 5.53 (d, *J* = 9.5, 1H), 6.08 (d, *J* = 9.5, 1H); ^{13}C NMR (100 MHz, $CDCl_3$) δ 20.5, 20.7, 20.8, 20.9, 24.7, 24.7, 28.7, 28.7, 34.6, 36.1, 38.5, 40.2, 40.2, 56.2, 56.3, 62.1, 65.1, 70.1, 71.6, 74.2, 75.9, 169.6, 169.8, 170.3, 170.7,

172.0. There are four more carbons (26) than expected (22), due to the fact that racemic thiopyridyl ester **83** was utilized.

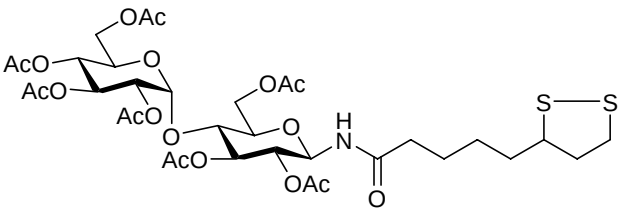

Acetylated β-maltosyl thioctanamide 73 (Table 2, entry 4). Amide **73** was prepared following general procedure A using acetylated β-maltosyl azide **66** (0.25 g, 0.38 mmol), diisopropylethylamine (0.070 mL, 0.42 mmol), Me_3P (0.49 mL, 0.49 mmol) and D/L-thioctic acid **69** (0.16 g, 0.76 mmol) as coupling partner. Purification by column chromatography (hexane/EtOAc, 2/3) afforded 0.15 g (48%) of β-maltosyl thioctanamide **73** as a light yellow foam: R_f = 0.41 (hexane/EtOAc, 1/2): IR (CCl_4, cm^{-1}) 3432 (w), 2931 (w), 1757 (s), 1706 (m), 1360 (m), 1225 (s), 1065 (m). The spectral data (^1H and ^{13}C NMR) were identical to those previously reported by Damkaci.[84]

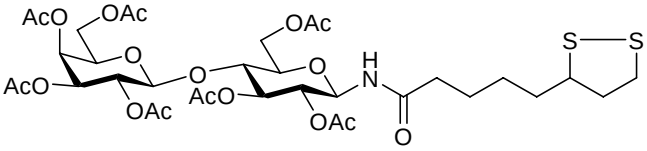

Acetylated β-lactosyl thioctanamide 74 (Table 2, entry 5). Amide **74** was prepared following general procedure A using acetylated β-lactosyl azide **67** (1.00 g, 1.51 mmol), diisopropylethylamine (0.530 mL, 3.02 mmol), Me_3P (1.81 mL, 1.81 mmol) and D/L-thioctic acid **69** (0.624 g, 3.02 mmol) as coupling partner. Purification by column chromatography (hexane/EtOAc, 1/2) afforded 0.670 g (54 %) of β-lactosyl thioctanamide **74** as a light yellow foam: R_f = 0.45 (hexane/EtOAc, 1/2); IR (CCl_4, cm^{-1})

3310 (w), 2930 (w), 1752 (s), 1706 (w), 1376 (m), 1219 (s). The spectral data (^{1}H and ^{13}C NMR) were identical to those previously reported by Damkaci.[84]

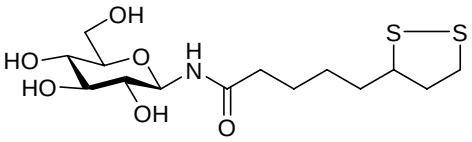

β-Glucosyl thioctanamide 78 (Table 3, entry 1). Amide **78** was prepared following general procedure C using acetylated β-glucosyl thioctanamide **70** (1.76 g, 3.29 mmol) and sodium methoxide (32.9 mL, 6.58 mmol). The reaction mixture was neutralized with Dowex MAC-3 resin. Purification by column chromatography (CH_2Cl_2/MeOH, 3/1) afforded 1.10 g (91%) of β-glucosyl thioctanamide **78** as an amorphous solid: R_f = 0.67 (CH_2Cl_2/MeOH, 3/1); IR (KBr, cm^{-1}) 3442 (br), 2917 (s), 1634 (s), 1549 (s), 1080 (s); ^{1}H NMR (400MHz, D_2O) δ 1.27-1.36 (m, 2H), 1.46-1.55 (m, 3H), 1.58-1.65 (m, 1H), 1.86 (sextet, *J* = 6.8, 1H), 2.20 (t, *J* = 7.2, 2H), 2.36 (sextet, *J* = 6.8, 1H), 3.02-3.13 (m, 2H), 3.21-3.30 (m, 2H), 3.36-3.43 (m, 2H), 3.55-3.61 (m, 2H), 3.74 (dd, *J* = 12.0, 2.4, 1H), 4.82 (d, *J* = 9.2, 1H); ^{13}C NMR (100 MHz, D_2O) δ 24.6, 27.7, 33.6, 35.4, 37.9, 40.1, 56.3, 60.4, 69.1, 71.6, 76.4, 77.4, 79.1, 178.2; HRMS (ESI) cacld. for $C_{14}H_{25}NO_6S_2Na$ $[M + Na]^+$ 390.1021, found 390.1022.

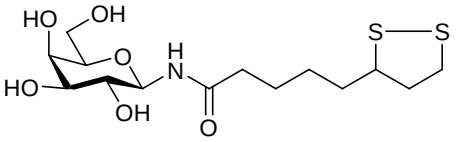

β-Galactosyl thioctanamide 79 (Table 3, entry 2). Amide **79** was prepared following general procedure C using acetylated β-galactosyl thioctanamide **71** (0.49 g, 0.93 mmol) and sodium methoxide (14 mL, 2.8 mmol). The reaction mixture was neutralized with Dowex MAC-3 resin. Without further purification, 0.30 g (88%) of β-galactosyl thioctanamide **79** as an amorphous solid was obtained: R_f = 0.67 (CH_2Cl_2/MeOH, 3/1); ^{1}H NMR

(400MHz, D_2O) δ 1.29-1.35 (m, 2H), 1.48-1.56 (m, 3H), 1.58-1.63 (m, 1H), 1.85 (sextet, *J* = 6.8, 1H), 2.20 (t, *J* = 7.2, 2H), 2.35 (sextet, *J* = 6.8, 1H), 3.03-3.12 (m, 2H), 3.48 (t, *J* = 9.2, 1H), 3.54-3.65 (m, 5H), 3.83 (d, *J* = 3.2, 1H), 4.76 (d, *J* = 9.2, 1H); ^{13}C NMR (100 MHz, D_2O) δ 24.6, 27.8, 33.6, 35.4, 37.9, 40.1, 56.3, 60.8, 68.5, 69.1, 73.3, 76.6, 79.5, 178.3; HRMS (ESI) cacld. for $C_{14}H_{25}NO_6S_2Na$ $[M + Na]^+$ 390.1021, found 390.1015.

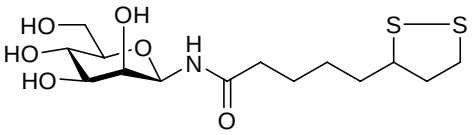

β-Mannosyl thioctanamide 80 (Table 3, entry 3). Amide **80** was prepared following general procedure C using acetylated β-mannosyl thioctanamide **72** (0.30 g, 0.56 mmol) and sodium methoxide (11 mL, 2.2 mmol). The reaction mixture was neutralized with Dowex MAC-3 resin. Purification by column chromatography (CH_2Cl_2/MeOH, 3/1) afforded 0.18 g (85%) of β-mannosyl thioctanamide **80** as an amorphous solid: R_f = 0.62 (CH_2Cl_2/MeOH, 3/1); IR (drop casting on CaF_2, cm^{-1}) 3320 (br), 2916 (w), 1650 (m), 1527 (w), 1073 (m); ^1H NMR (400MHz, D_2O) δ 1.29-1.35 (m, 2H), 1.46-1.56 (m, 3H), 1.58-1.65 (m, 1H), 1.84-1.89 (m, 1H), 2.22 (t, *J* = 7.2, 2H), 2.32-2.40 (m, 1H), 3.04-3.13 (m, 2H), 3.33 (ddd, *J* = 9.6, 6.0, 2.4, 1H), 3.47 (t, *J* = 9.6, 1H), 3.56-3.61 (m, 3H), 3.76 (dd, *J* = 12.4, 2.4, 1H), 3.80 (br d, *J* = 3.2, 1H), 5.08 (br s, 1H); ^{13}C NMR (100 MHz, D_2O) δ 24.6, 24.6, 27.7, 27.7, 33.6, 33.6, 35.0, 35.1, 37.9, 40.1, 56.3, 60.7, 66.2, 70.0, 73.2, 77.5, 77.6, 177.4. There are four more carbons (18) than expected (14), due to the fact that a mixture of diastereomers **72** was utilized.

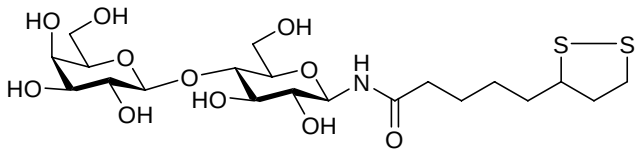

β-Lactosyl thioctanamide 81 (Table 3, entry 4). Amide **81** was prepared following general procedure C using acetylated β-lactosyl thioctanamide **74** (1.48 g, 1.80 mmol) and sodium methoxide (31.5 mL, 6.29 mmol). The reaction mixture was neutralized with Dowex MAC-3 resin. Purification by column chromatography (CH_2Cl_2/MeOH, 2/1) afforded 0.80 g (84%) of β-lactosyl thioctanamide **81** as an amorphous solid: R_f = 0.32 (CH_2Cl_2/MeOH, 3/1); IR (Neat, cm^{-1}) 3299 (br), 2921 (w), 1649 (m), 1538 (m), 1386 (m), 1019 (s); ^{1}H NMR (400MHz, D_2O,) δ 1.29-1.37 (m, 2H), 1.44-1.56 (m, 3H), 1.56-1.65 (m, 1H), 1.87 (sextet, *J* = 6.4, 1H), 2.22 (t, *J* = 7.2, 2H), 2.37 (sextet, *J* = 6.4, 1H), 3.04-3.13 (m, 2H), 3.29-3.33 (m, 1H), 3.42 (dd, *J* = 10.0, 7.6, 1H), 3.52-3.71 (m, 9H), 3.79-3.83 (m, 2H), 4.33 (d, *J* = 7.6, 1H), 4.85 (d, *J* = 9.2, 1H); ^{13}C NMR (100 MHz, D_2O) δ 24.6, 27.7, 33.6, 35.4, 37.9, 40.1, 56.3, 59.7, 60.9, 68.4, 70.8, 71.3, 72.4, 75.0, 75.2, 76.2, 77.6, 78.9, 102.7, 178.2; HRMS (FAB) cacld. for $C_{20}H_{36}O_{11}NS_2$ $[M + H]^+$ 530.1730, found 530.1716.

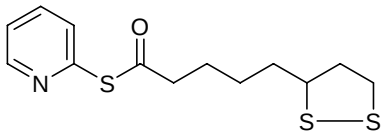

Thiopyridyl ester 83. (±)-Thioctic acid **(69)** (2.00 g, 9.69 mmol), Ph_3P (3.05 g, 11.6 mmol) and 2,2'-dipyridyl disulfide **82** (2.56 g, 11.6 mmol) were dissolved in 30 mL of anhydrous THF. The solution was stirred at room temperature for 24 h and then concentrated *in vacuo* to give the crude product. Purification by column chromatography (hexane/EtOAc, 2/1) afforded 2.87 g (99%) of (±)-thiopyridyl ester **83** as a yellow oil: R_f = 0.34 (hexane/EtOAc, 2/1); IR (CCl_4, cm^{-1}) 3057 (w), 2934 (s), 1711 (s), 1575 (s), 1425 (s), 1123 (m), 995 (m); ^{1}H NMR (400MHz, $CDCl_3$,) δ 1.43-1.53 (m, 2H), 1.63-1.77 (m, 4H), 1.87 (sextet, *J* = 6.8,

1H), 2.42 (sextet, *J* = 6.8, 1H), 2.69 (t, *J* = 7.4, 2H), 3.04-3.17 (m, 2H), 3.50-3.56 (m, 1H), 7.25 (ddd, *J* = 8.0, 5.0, 1.0, 1H), 7.57-7.59 (m, 1H), 7.71 (td, *J* = 8.0, 2.0, 1H), 8.58 (ddd, *J* = 5.0, 2.0, 1.0, 1H); ^{13}C NMR (100 MHz, $CDCl_3$) δ 25.0, 28.4, 34.5, 38.4, 40.1, 43.8, 56.1, 123.5, 130.1, 137.2, 150.1, 151.2, 196.1.

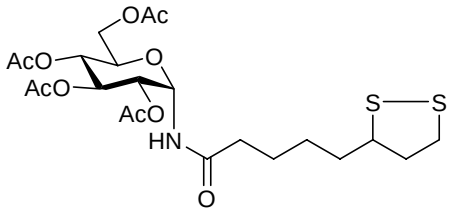

Acetylated α-glucosyl thioctanamide 84 (Table 4, entry 1). Amide **84** was prepared following general procedure B using acetylated β-glucosyl azide **63** (0.83 g, 2.2 mmol), Ph_3P (0.64 g, 2.5 mmol), thiopyridyl ester **83** (0.87 g, 2.9 mmol) as coupling partner and $CuCl_2 \cdot 2H_2O$ (0.50 g, 2.9 mmol) as additive. After the coupling partner and the additive were added, the resulting mixture was stirred at room temperature for 24 h. Purification by column chromatography (hexane/EtOAc, 1/1.5) afforded 0.75 g (63%) of acetylated α-glucosyl thioctanamide **84** as a light yellow foam: R_f = 0.39 (hexane/EtOAc, 1/2); IR (CCl_4, cm^{-1}) 3336 (br w), 2932 (m), 1755 (s), 1705 (m), 1219 (s), 1027 (m); ^{1}H NMR (400 MHz, $CDCl_3$) δ 1.38-1.51 (m, 2H), 1.55-1.73 (m, 4H), 1.80-1.92 (m, 1H), 1.99 (s, 3H), 2.00 (s, 6H), 2.04 (s, 3 H), 2.27 (br t, *J* = 7.3, 2H), 2.43 (sextet, *J* = 6.6, 1H), 3.05-3.18 (m, 2H), 3.50-3.56 (m, 1H), 3.89-3.92 (m, 1H), 4.01 (dd, *J* = 12.4, 2.2, 1H), 4.25 (dd, *J* = 12.4, 4.2, 1H), 5.03 (t, *J* = 10.0, 1H), 5.15 (dd, *J* = 10.0, 5.0, 1H), 5.33 (t, *J* = 10.0, 1H), 5.84 (br t, *J* = 7.3, 1H), 6.56 (d, *J* = 7.3, 1H); ^{13}C NMR (100 MHz, $CDCl_3$) δ 20.5, 20.5, 20.6, 20.7, 25.0, 28.7, 34.5, 36.2, 36.2, 38.4, 40.2, 56.3, 56.3, 61.7, 68.0, 68.3, 68.4, 70.1, 74.2, 169.0, 169.4, 170.3, 170.7, 173.3; HRMS (FAB) calcd. for $C_{22}H_{33}NO_{10}S_2Li$ $[M + Li]^+$ 542.1706, found 542.1708. There are two

more carbons (24) than expected (22), due to the fact that racemic thiopyridyl ester **83** was utilized.

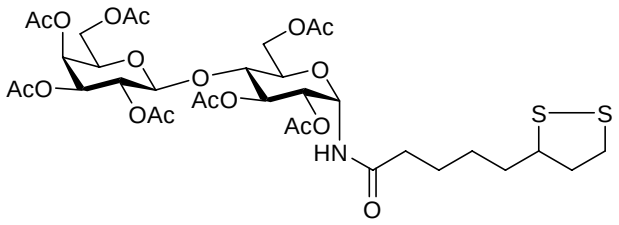

Acetylated α-lactosyl thioctanamide 86 (Table 4, entry 2). Amide **86** was prepared following general procedure B using acetylated β-lactosyl azide **67** (1.00 g, 1.51 mmol), Ph_3P (0.440 g, 1.66 mmol), thiopyridyl ester **83** (0.590 g, 1.97 mmol) as coupling partner and $CuCl_2 \cdot 2H_2O$ (0.340 g, 1.97 mmol) as additive. After the coupling partner and the additive were added, the resulting mixture was stirred at room temperature for 24 h. Purification by column chromatography (hexane/EtOAc, 2/3) afforded 0.690 g (55%) of acetylated α-lactosyl thioctanamide **86** as a light yellow foam: R_f = 0.45 (hexane/ EtOAc, 1/2); IR (CCl_4, cm^{-1}) 3260 (w), 2936 (w), 1759 (s), 1701 (w), 1376 (m), 1219 (s); ^1H NMR (400MHz, $CDCl_3$,) δ 1.38-1.53 (m, 2H), 1.58-1.73 (m, 4H), 1.83-1.92 (m, 1H), 1.93 (s, 3H), 2.01 (s, 3H), 2.02 (s, 3H), 2.03 (s, 3H), 2.04 (s, 3H), 2.07 (s, 3H), 2.12 (s, 3H), 2.27 (br t, *J* = 7.5, 2H), 2.43 (sextet, *J* = 6.5, 1H), 3.05-3.18 (m, 2H), 3.50-3.57 (m, 1H), 3.70-3.75 (m, 2H), 3.86 (dd, *J* = 7.0, 0.8, 1H), 4.03-4.13 (m, 3H), 4.33 (br d, *J* = 11.3, 1H), 4.44 (d, *J* = 8.0, 1H), 4.92 (dd, *J* = 10.0, 3.4, 1H), 5.03-5.09 (m, 2H), 5.28 (dd, *J* = 10.0, 8.0, 1H), 5.32 (dd, *J* = 3.4, 0.8, 1H), 5.76 (dd, *J* = 7.5, 5.5, 1H), 6.46 (br d, *J* = 7.5, 1H); ^{13}C NMR (100 MHz, $CDCl_3$) δ 20.5, 20.6, 20.6, 20.6, 20.7, 20.8, 20.8, 25.0, 28.7, 34.5, 36.2, 38.4, 40.2, 56.3, 60.8, 61.9, 66.6, 68.3, 69.0, 69.3, 69.8, 70.7, 70.8, 73.7, 75.8, 101.1, 169.2, 169.3, 169.9, 170.0, 170.0, 170.4, 170.4, 173.3; HRMS (FAB) cacld. for $C_{34}H_{49}O_{18}NS_2Cs$ [*M* + Cs]$^+$ 956.1445, found 956.1454.

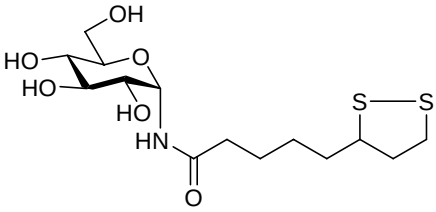

α-Glucosyl thioctanamide 85 (Table 4, entry 3). Amide **85** was prepared following general procedure C using acetylated α-glucosyl thioctanamide **84** (1.09 g, 2.04 mmol) and sodium methoxide (13.2 mL, 2.65 mmol). The reaction mixture was neutralized with Amberlite IR-120 resin. Without further purification, 0.740 g (99%) of α-glucosyl thioctanamide **85** as an amorphous solid was obtained. The ^{1}H NMR of the crude product indicated high purity: R_f = 0.67 (CH_2Cl_2/MeOH, 3/1); IR (KBr, cm^{-1}) 3378 (br), 2926 (s), 1662 (s), 1533 (s), 1060 (s); ^{1}H NMR (400MHz, D_2O) δ 1.21-1.31 (m, 2H), 1.43-1.63 (m, 4H), 1.79-1.87 (m, 1H), 2.17-2.27 (m, 2H), 2.29-2.37 (m, 1H), 3.01-3.08 (m, 2H), 3.27-3.35 (m, 2H), 3.54-3.68 (m, 5H), 5.43 (d, *J* = 5.6, 1H); ^{13}C NMR (100MHz, D_2O) δ 24.9, 24.9, 27.7, 27.8, 33.7, 33.7, 35.1, 35.2, 38.0, 40.1, 40.1, 56.3, 56.4, 60.3, 69.1, 69.2, 72.5, 72.9, 76.4, 178.6; HRMS (ESI) cacld. for $C_{14}H_{25}NO_6S_2Na$ $[M + Na]^+$ 390.1021, found 390.1013. There are six more carbons (20) than expected (14), due to the fact that a mixture of diastereomers **84** was utilized.

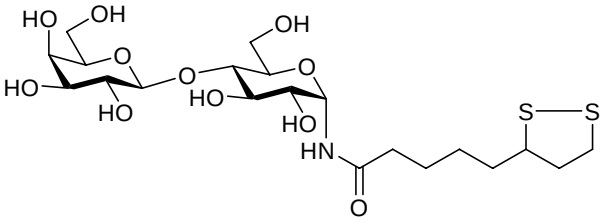

α-Lactosyl thioctanamide 87 (Table 4, entry 4). Amide **87** was prepared following general procedure C using acetylated α-lactosyl thioctanamide **86** (0.59 g, 0.72 mmol) and sodium methoxide (4.7 mL, 0.93 mmol). The reaction mixture was neutralized with Amberlite IR-120 resin. Without further purification, 0.340 g (90%) of α-lactosyl thioctanamide **87** as an amorphous solid was obtained. The ^{1}H NMR of the crude product indicated high purity: R_f = 0.32 (CH_2Cl_2/MeOH, 3/1); IR (Neat, cm^{-1}) 3317 (br), 2921 (w), 1654 (m), 1520 (m),

1386 (m), 1019 (s); ^{1}H NMR (400MHz, D_2O,) δ 1.24-1.32 (m, 2H), 1.44-1.56 (m, 3H), 1.56-1.66 (m, 1H), 1.79-1.89 (m, 1H), 2.19-2.28 (m, 2H), 2.33 (m, 1H), 3.00-3.13 (m, 2H), 3.41 (dd, *J* = 10.0, 7.8, 1H), 3.47-3.66 (m, 7H), 3.69-3.75 (m, 4H), 3.78 (d, *J* = 3.3, 1H), 4.31 (d, *J* = 7.8, 1H), 5.43 (d, *J* = 4.1, 1H); 13C NMR (100 MHz, D2O) δ 24.9, 27.7, 27.8, 33.7, 33.7, 35.2, 35.3, 38.1, 40.2, 40.2, 56.4, 56.5, 59.8, 61.0, 68.5, 69.0, 70.9, 71.3, 71.7, 72.5, 75.3, 76.2, 78.0, 102.8, 178.7; HRMS (FAB) cacld. for $C_{20}H_{35}O_{11}NS_2Cs$ [*M* + Cs]$^{+}$ 662.0706, found 662.0704. There are five more carbons (25) than expected (20), due to the fact that a mixture of diastereomers **86** was utilized.

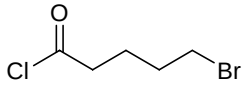

5-Bromopentanoyl chloride (88). Thionyl chloride (6.05 mL, 82.9 mmol) was added to a flask containing 5-bromovaleric acid (5.00 g, 27.6 mmol). The reaction mixture was refluxed for 2.5 h and concentrated *in vacuo*. Purification by vacuum distillation at 112 - 114 °C, 26 mmHg (lit. b.p. 102 - 104 °C, 15 mmHg)[89] afforded 4.80 g (87%) of acid chloride **88** as a colorless oil: IR (CCl_4, cm^{-1}) 2963 (w), 1800 (s), 1255 (w), 970 (w); ^{1}H NMR (400MHz, $CDCl_3$) δ 1.84-1.93 (m, 4H), 2.93 (t, *J* = 6.4, 2H), 3.39 (t, *J* = 6.4, 2H); ^{13}C NMR (100 MHz, $CDCl_3$) δ 23.6, 31.1, 32.4, 46.0, 173.4.

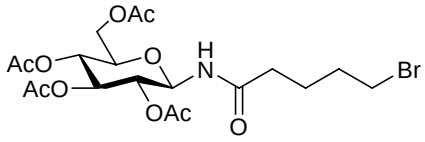

Acetylated β-glucose-5-bromopentanamide 89 (Scheme 10). Amide **89** was prepared following general procedure A using acetylated β-glucosyl azide **63** (1.00 g, 2.68 mmol), diisopropylethylamine (0.930 mL, 5.36 mmol), Me_3P (2.95 mL, 2.95 mmol) and acid chloride **88** (1.10 g, 5.36 mmol) as coupling partner. Purification by column

chromatography (hexane/EtOAc, 1/1) afforded 0.630 g (46%) of β-glucose-5-bromopentanamide **89** as a yellow gum: R_f = 0.37 (hexane/EtOAc, 2/3); IR (CCl_4, cm^{-1}) 3433 (w), 2959 (w), 1755 (s), 1705 (m), 1227 (s), 1041 (s); ^1H NMR (400MHz, $CDCl_3$,) δ 1.71-1.75 (m, 2H), 1.80-1.87 (m, 2H), 2.00 (s, 3H), 2.01 (s, 3H), 2.03 (s, 3H), 2.06 (s, 3H), 2.14-2.24 (m, 2H), 3.37 (t, *J* = 6.7, 2H), 3.79 (ddd, *J* = 9.6, 4.3, 2.1, 1H), 4.05 (dd, *J* = 12.5, 2.1, 1H), 4.29 (dd, *J* = 12.5, 4.3, 1H), 4.88 (t, *J* = 9.6, 1H), 5.04 (t, *J* = 9.6, 1H), 5.23 (t, *J* = 9.6, 1H), 5.29 (t, *J*= 9.6, 1H), 6.22 (d, *J* = 9.6, 1H); ^{13}C NMR (100 MHz, $CDCl_3$) δ 20.6, 20.6, 20.7, 20.7, 23.6, 31.9, 32.8, 35.4, 61.5, 68.1, 70.6, 72.6, 73.5, 78.1, 169.6, 169.8, 170.6, 171.1, 172.5; HRMS (FAB) cacld. for $C_{19}H_{29}O_9NBr^{79}$ $[M + H]^+$ 510.0975, found 510.0976.

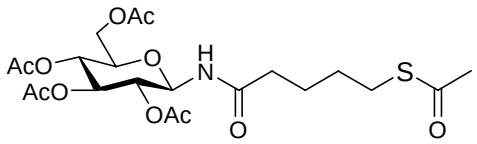

Acetylated β-glucose-5-thioacetyl pentanamide 90 (Scheme 10). To a solution of acetylated β-glucose-5-bromopentanamide **89** (0.610 g, 1.20 mmol) in 10 mL of anhydrous DMF was added potassium thioacetate (0.177 g, 1.55 mmol). The reaction mixture was stirred at room temperature for 20 h and then diluted with EtOAc (100 mL). After being washed with H_2O (3 × 100 mL), the organic layer was dried over $MgSO_4$ and concentrated *in vacuo*. Purification by column chromatography (hexane/EtOAc, 1/1) afforded 0.580 g (96%) of acetylated β-glucose-5-thioacetyl pentanamide **90** as a yellow gum: R_f = 0.30 (hexane/EtOAc, 2/3); IR (CCl_4, cm^{-1}) 3371 (w), 2944 (w), 1756 (s), 1696 (s), 1227 (s), 1040 (s); ^1H NMR (400MHz, $CDCl_3$,) δ 1.52-1.57 (m, 2H), 1.59-1.63 (m, 2H), 1.98 (s, 3H), 2.00 (s, 3H), 2.02 (s, 3H), 2.05 (s, 3H), 2.15-2.20 (m, 2H), 2.30 (s, 3H), 2.82 (td, *J* = 6.8, 2.4, 2H), 3.78 (ddd, *J* = 9.6, 4.4, 2.0, 1H), 4.04 (dd, *J* = 12.4, 2.0, 1H), 4.27 (dd, *J* =

12.4, 4.4, 1H), 4.87 (t, *J* = 9.6, 1H), 5.03 (t, *J* = 9.6, 1H), 5.22 (t, *J* = 9.6, 1H), 5.27 (t, *J*= 9.6, 1H), 6.28 (d, *J* = 9.6, 1H); ^{13}C NMR (100 MHz, $CDCl_3$) δ 20.5, 20.5, 20.6, 20.7, 24.0, 28.4, 28.9, 30.6, 35.8, 61.6, 68.1, 70.6, 72.7, 73.5, 78.1, 169.5, 169.8, 170.6, 171.0, 172.8, 195.9; HRMS (DEI) cacld. for $C_{21}H_{31}O_{11}NS$ $[M]^+$ 505.1618, found 505.1615.

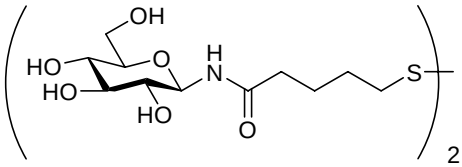

β-Glucose disulfide 91 (Scheme 10). Disulfide **91** was prepared following general procedure C using acetylated β-glucose-5-thioacetyl pentanamide **90** (0.54 g, 1.1 mmol) and sodium methoxide (7.0 mL, 1.4 mmol). After being stirred for 24 h under a nitrogen atmosphere, the reaction mixture was exposed to air for an additional 24 h to complete the oxidation of the thiol group to the disulfide. The reaction mixture was neutralized with Amberlite IR-120 resin. Without further purification, 0.25 g (80%) of β-glucose disulfide **91** as an amorphous solid was obtained. The ^{1}H NMR of the crude product indicated high purity (> 95%): R_f = 0.34 ($MeOH/CH_2Cl_2$, 1/3); IR (neat, cm^{-1}) 3293 (br), 2921 (w), 1654 (m), 1544 (s), 1020 (s); ^{1}H NMR (400MHz, D_2O) δ 1.59 (br s, 4H), 2.23 (br s, 2H), 2.63 (br s, 2H), 3.22-3.31 (m, 2H), 3.37-3.44 (m, 2H), 3.59 (dd, *J* = 12.4, 5.2, 1H), 3.74 (dd, *J* = 12.4, 2.0, 1H), 4.82 (d, *J* = 9.2, 1H); ^{13}C NMR (100 MHz, D_2O) δ 23.7, 27.6, 35.1, 37.5, 60.4, 69.1, 71.6, 76.4, 77.4, 79.1, 177.9; HRMS (FAB) cacld. for $C_{22}H_{40}O_{12}N_2S_2Cs$ $[M + Cs]^+$ 721.1077, found 721.1077.

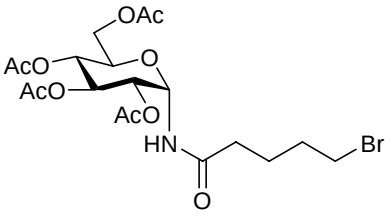

Acetylated α-glucose-5-bromopentanamide 92 (Scheme 11). Amide **92** was prepared following general procedure B using β-glucosyl azide **63** (0.20 g, 0.54 mmol), Ph_3P (0.15 g, 0.59 mmol) and acid chloride **88** (0.21 g, 1.1 mmol) as coupling partner. After formation of the isoxazoline intermediate, the reaction mixture was stirred at 95 °C for 24 h. Purification by column chromatography (hexane/EtOAc, 1/1) afforded 0.14 g (52%) of acetylated α-glucose-5-bromopentanamide **92** as a yellow gum: R_f = 0.28 (hexane/EtOAc, 1/1); IR (CCl_4, cm^{-1}) 3445 (w), 2959 (w), 1755 (s), 1705 (m), 1223 (s), 1033 (m); ^{1}H NMR (400 MHz, $CDCl_3$) δ 1.75-1.79 (m, 4H), 2.00 (s, 3H), 2.02 (s, 6 H), 2.05 (s, 3H), 2.32 (br s, 2H), 3.50-3.55 (m, 2H), 3.86-3.90 (m, 1H), 4.03 (dd, *J* = 12.4, 2.2, 1H), 4.25 (dd, *J* = 12.4, 4.4, 1H), 5.03 (t, *J* = 9.7, 1H), 5.16 (dd, *J* = 9.7, 5.4, 1 H), 5.34 (t, *J* = 9.7, 1H), 5.85 (dd, *J* = 7.4, 5.4, 1H), 6.53 (d, *J* = 7.4, 1H); ^{13}C NMR (100 MHz, $CDCl_3$) δ 20.5, 20.6, 20.6, 20.7, 22.7, 31.7, 35.5, 44.4, 61.7, 68.1, 68.3, 68.3, 70.2, 74.2, 168.9, 169.4, 170.5, 170.7, 173.0.

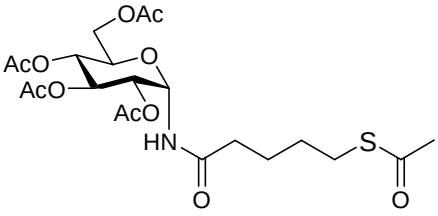

Acetylated α-glucose-5-thioacetyl pentanamide 93 (Scheme 11). To a solution of acetylated α-glucose-5-bromopentanamide **92** (0.12 g, 0.24 mmol) in 3 mL of DMF was added potassium thioacetate (0.035 g, 0.31 mmol). The reaction mixture was stirred at room temperature for 20 h and then diluted with 50 mL of EtOAc. After being washed with H_2O (3 × 100 mL), the organic layer was dried over $MgSO_4$, filtered, and concentrated *in vacuo*. Purification by column chromatography (hexane/EtOAc, 1/1) afforded 0.10 g (84%) of acetylated α-glucose-5-thioacetyl pentanamide **93** as a yellow

gum: R_f = 0.30 (hexane/EtOAc, 2/3); IR (CCl_4, cm^{-1}) 3386 (w), 2959 (w), 1755 (s), 1697 (m), 1227 (s); ^{1}H NMR (400 MHz, $CDCl_3$) δ 1.59-1.64 (m, 2H), 1.66-1.72 (m, 2H), 2.00 (s, 3H), 2.01 (s, 6H), 2.05 (s, 3 H), 2.30-2.35 (m, 5H), 2.85-2.88 (m, 2H), 3.85-3.88 (m, 1H), 4.03 (dd, *J* = 12.4, 2.8, 1H), 4.25 (dd, *J* = 12.4, 4.4, 1H), 5.04 (t, *J* = 9.6, 1H), 5.16 (dd, *J* = 9.6, 5.6, 1H), 5.37 (t, *J* = 9.6, 1H), 5.86 (dd, *J* = 7.6, 5.6, 1H), 6.75 (d, *J* = 7.6, 1H); ^{13}C NMR (100 MHz, $CDCl_3$) δ 20.5, 20.6, 20.6, 20.7, 24.3, 28.0, 29.0, 30.6, 35.5, 61.8, 68.0, 68.4, 68.4, 70.2, 74.2, 169.0, 169.4, 170.4, 170.7, 173.4, 197.4; HRMS (FAB) calcd. for $C_{21}H_{32}O_{11}NS$ [*M* + H]$^+$ 506.169, found 506.169.

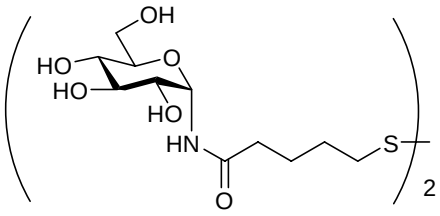

α-Glucose disulfide 94 (Scheme 11). Disulfide **94** was prepared following general procedure C using acetylated α-glucose-5-thioacetyl pentanamide **93** (0.082 g, 0.16 mmol) and sodium methoxide (1.0 mL, 0.21 mmol). After being stirred for 24 h under a nitrogen atmosphere, the reaction mixture was exposed to air for additional 24 h to complete the oxidation of the thiol group to the disulfide. The reaction mixture was neutralized with Amberlite IR-120 resin. Without further purification, 0.046 g (96%) of α-glucose disulfide **94** as an amorphous solid was obtained. The ^{1}H NMR of the crude product indicated high purity: R_f = 0.34 ($MeOH/CH_2Cl_2$, 1/3); IR (neat, cm^{-1}) 3272 (br), 2921 (w), 1654 (m), 1528 (s), 1020 (s); ^{1}H NMR (400MHz, D_2O) δ 1.56-1.58 (m, 4H), 2.22-2.28 (m, 2H), 2.59-2.62 (m, 2H), 3.27-3.35 (m, 2H), 3.55-3.68 (m, 4H), 5.43 (d, *J* = 5.6, 1H); ^{13}C NMR (100 MHz, D_2O) δ 23.9, 27.5, 34.9, 37.4, 60.3, 69.1, 69.2, 72.5, 72.9, 76.4, 178.5; HRMS (FAB) cacld. for $C_{22}H_{41}O_{12}N_2S_2$ [*M* + H]$^+$ 589.2101, found 589.2080.

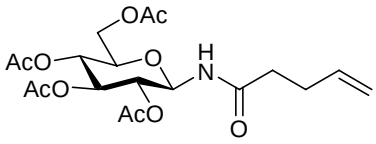

Acetylated β-glucose-4-pentenamide 96 (Table 5). Amide **96** was prepared following general procedure A using acetylated β-glucosyl azide **63** (3.00 g, 8.04 mmol), diisopropylethylamine (2.80 mL, 16.1 mmol), Me_3P (9.64 mL, 9.64 mmol) and 4-pentenoic acid **(95)** (1.61 g, 16.1 mmol) as coupling partner. Purification by column chromatography (hexane/EtOAc, 2/3) afforded 2.65 g (77%) of acetylated β-glucose-4-pentenamide **96** as a white foam: R_f = 0.50 (hexane/EtOAc, 1/2); IR (CCl_4, cm^{-1}) 3432 (w), 3080 (w), 2955 (w), 1759 (s), 1709 (s), 1509 (s), 1227 (s), 909 (m); ^1H NMR (400MHz, $CDCl_3$) δ 1.99 (s, 3H), 2.00 (s, 3H), 2.02 (s, 3H), 2.05 (s, 3H), 2.18-2.36 (m, 4H), 3.79 (ddd, *J* = 9.5, 4.4, 2.2, 1H), 4.05 (dd, *J* = 12.4, 2.2, 1H), 4.28 (dd, *J* = 12.4, 4.4, 1H), 4.86 (t, *J* = 9.5, 1H), 4.98 (dd, *J* = 10.3, 1.6, 1H), 5.02 (dd, *J* = 17.3, 1.6, 1H), 5.03 (t, *J* = 9.5, 1H), 5.23 (t, *J* = 9.5, 1H), 5.28 (t, *J* = 9.5, 1H), 5.70-5.80 (m, 1H), 6.20 (d, *J* = 9.5, 1H); ^{13}C NMR (100 MHz, $CDCl_3$) δ 20.6, 20.6, 20.7, 20.7, 28.8, 35.6, 61.6, 68.1, 70.5, 72.6, 73.5, 78.1, 115.8, 136.3, 169.5, 169.8, 170.6, 171.0, 172.5; HRMS (FAB) cacld. for $C_{19}H_{28}O_{10}N$ $[M + H]^+$ 430.1713, found 430.1708.

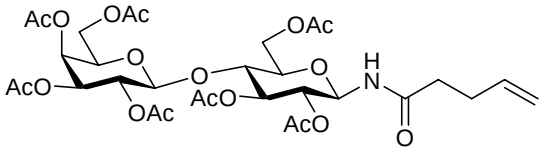

Acetylated β-lactose-4-pentenamide 99 (Table 5). Amide **99** was prepared following general procedure A using acetylated β-lactose azide **67** (2.00 g, 3.02 mmol), diisopropylethylamine (1.60 mL, 9.07 mmol), Me_3P (3.63 mL, 3.63 mmol) and 4-pentenoic acid **95** (0.910 g, 9.07 mmol) as coupling partner. Purification by column chromatography (hexane/EtOAc, 1/2) afforded 1.58 g (73%) of

acetylated β-lactose-4-pentenamide **99** as a white foam: R_f = 0.33 (hexane/EtOAc, 1/2); IR (CCl_4, cm^{-1}) 3436 (w), 3083 (w), 2943 (w), 1755 (s), 1704 (m), 1227 (s), 1052 (s); ^1H NMR (400MHz, $CDCl_3$) δ 1.94 (s, 3H), 2.01 (s, 3H), 2.02 (s, 3H), 2.02 (s, 3H), 2.04 (s, 3H), 2.09 (s, 3H), 2.13 (s, 3H), 2.18-2.36 (m, 4H), 3.67-3.76 (m, 2H), 3.82-3.85 (m, 1H), 4.01-4.14 (m, 3H), 4.40 (dd, *J* = 12.4, 1.4, 1H), 4.42 (d, *J* = 8.0, 1H), 4.79 (t, *J* = 9.4, 1H), 4.91 (dd, *J* = 10.4, 3.4, 1H), 4.96 (dd, *J* = 10.3, 1.5, 1H), 5.01 (dd, *J* = 18.8, 1.5, 1H), 5.06 (dd, *J* = 10.4, 8.0, 1H), 5.18 (t, *J* = 9.4, 1H), 5.26 (dd, *J* = 9.4, 8.7, 1H), 5.32 (dd, *J* = 3.4, 1.0, 1H), 5.69-5.78 (m, 1H), 6.11 (d, *J* = 9.4, 1H); ^{13}C NMR (100 MHz, $CDCl_3$) δ 20.5, 20.6, 20.6, 20.6, 20.7, 20.7, 20.9, 28.8, 35.6, 60.8, 61.9, 66.6, 68.9, 70.7, 70.9, 71.0, 72.3, 74.4, 75.9, 77.9, 100.9, 115.8, 136.3, 168.9, 169.2, 170.1, 170.1, 170.3, 170.3, 171.2, 172.3; HRMS (FAB) cacld. for $C_{31}H_{44}O_{18}N$ $[M + H]^+$ 718.2558, found 718.2562.

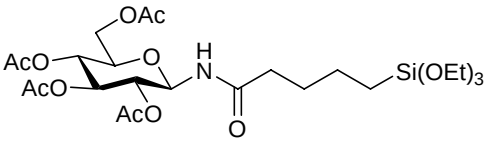

Acetylated β-glucose-5-(triethoxysilyl)pentanamide 97 (Table 5). To a sealed tube were added acetylated β-glucose-4-pentenamide **96** (0.800 g, 0.687 mmol), triethoxysilane (1.53 g, 9.32 mmol), platinum oxide (PtO_2, 21.0 mg, 93.0 μmol), and 2.8 mL of THF. The tube was charged with nitrogen and sealed. The resulting mixture was stirred at 95 ^oC for 2 h. After cooling to room temperature, the crude product was filtered through activated charcoal with ethanol and concentrated. Purification by column chromatography (hexane/EtOAc, 1/1) afforded 0.77 g of a mixture of siloxane amide **97** and saturated amide **98** (**97/98**, 85/15 mol ratio, determined by GC and ^1H NMR spectroscopy). The yield of acetylated β-glucose-5-(triethoxysilyl)pentanamide **97** was calculated on the basis of mol ratio to give 0.68 g (62%) as a colorless gum: R_f = 0.36

(hexane/EtOAc, 1/1); IR (CCl_4, cm^{-1}) 3432 (w), 2973 (m), 1755 (s), 1707 (m), 1511 (m), 1224 (s), 956 (w) ^{1}H NMR (**97**, 400MHz, $CDCl_3$) δ 0.57-0.62 (m, 2H), 1.19 (t, *J* = 7.0, 9H), 1.35-1.42 (m, 2H), 1.57-1.63 (m, 2H), 1.99 (s, 3H), 2.00 (s, 3H), 2.02 (s, 3H), 2.05 (s, 3H), 2.14-2.20 (m, 2H), 3.77 (q, *J* = 7.0, 6H), 3.78-3.82 (m, 1H), 4.04 (dd, *J* = 12.4, 2.0, 1H), 4.28 (dd, *J* = 12.4, 4.4, 1H), 4.88 (t, *J* = 9.5, 1H), 5.04 (t, *J* = 9.5, 1H), 5.22 (t, *J* = 9.5, 1H), 5.28 (t, *J* = 9.5, 1H), 6.16 (d, *J* = 9.5, 1H); ^{13}C NMR (**97**, 100 MHz, $CDCl_3$) δ 10.2, 18.3 (x 3), 20.6, 20.6, 20.6, 20.7, 22.5, 28.4, 36.3, 58.3 (x 3), 61.6, 68.1, 70.5, 72.6, 73.5, 78.1, 169.5, 169.8, 170.6, 171.1, 173.2; ^{29}Si NMR (**97**, 79.5 MHz, $CDCl_3$, externally referenced to TMS at 0 ppm) δ −45.6; HRMS (FAB) cacld. for $C_{25}H_{43}O_{13}NSiLi$ $[M + Li]^+$ 600.2664, found 600.2694.

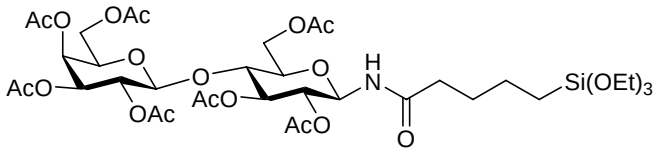

Acetylated β-lactose-5-(triethoxysilyl)pentanamide 100 (Table 5). To a sealed tube were added acetylated β-lactose-4-pentenamide **99** (0.310 g, 0.430 mmol), triethoxysilane (0.350 g, 2.16 mmol), platinum oxide (PtO_2, 5.00 mg, 22.0 μmol), and 0.7 mL of THF. The tube was charged with nitrogen and sealed. The resulting mixture was stirred at 95 ^{o}C for 2 h. After cooling to room temperature, the crude product was filtered through activated charcoal with ethanol and concentrated. Purification by column chromatography (hexane/EtOAc, 1/1) afforded 0.200 g of a mixture of siloxane amide **100** and saturated amide **101** (**100/101**, 72/28 mol ratio, determined by ^{1}H NMR spectroscopy). The yield of acetylated β-lactose-5-(triethoxysilyl)pentanamide **100** was calculated on the basis of mol ratio to give 0.15 g (40%) as a white foam: R_f = 0.47

(hexane/EtOAc, 2/3) ; IR (CCl_4, cm^{-1}) 3305 (w), 2974 (m), 1752 (s), 1703 (m), 1225 (s), 956 (m); ^{1}H NMR (**100**, 400MHz, $CDCl_3$) δ 0.56-0.61 (m, 2H), 1.18 (t, *J* = 7.0, 9H), 1.34-1.41 (m, 2H), 1.54-1.62 (m, 2H), 1.93 (s, 3H), 2.01 (s, 3H), 2.01 (s, 3H), 2.02 (s, 3H), 2.05 (s, 3H), 2.09 (s, 3H), 2.14 (s, 3H), 2.08-2.18 (m, 2H), 3.77 (q, *J* = 7.0, 6H), 3.67-3.85 (m, 3H), 4.01-4.14 (m, 3H), 4.37-4.40 (m, 1H), 4.41 (d, *J* = 8.0, 1H), 4.79 (t, *J* = 9.5, 1H), 4.90 (dd, *J* = 10.5, 3.4, 1H), 5.07 (dd, *J* = 10.5, 8.0, 1H), 5.17 (t, *J* = 9.5, 1H), 5.27 (br t, *J* = 9.5, 1H), 5.32 (br d, *J* = 3.4, 1H), 6.07 (d, *J* = 9.5, 1H); ^{13}C NMR (**100**, 100 MHz, $CDCl_3$) δ 10.2, 18.3 (x 3), 20.5, 20.6, 20.6, 20.6, 20.6, 20.7, 20.9, 22.5, 28.4, 36.3, 58.3 (x 3), 60.8, 61.9, 66.6, 68.9, 70.7, 70.9, 71.0, 72.3, 74.4, 75.9, 77.9, 100.9, 168.9, 169.3, 170.1, 170.1, 170.3, 170.3, 171.3, 173.0; ^{29}Si NMR (**100**, 79.5 MHz, $CDCl_3$, externally referenced to TMS at 0 ppm) δ –45.5; HRMS (FAB) cacld. for $C_{37}H_{59}O_{21}NSiCs$ [*M* + Cs]$^+$ 1014.2403, found 1014.2426.

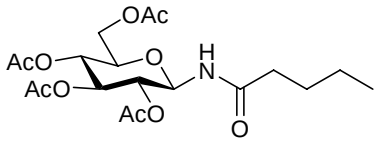

Acetylated β-glucosyl pentanamide 98 (Table 5). Acetylated β-glucose-4-pentenamide **96** (130 mg, 0.303 mmol) and palladium on carbon (5%, 64.0 mg, 30.3 μmol) were stirred in 5 mL of MeOH under 1 atm of hydrogen for 1 h. The reaction mixture was filtered and concentrated. Without further purification, 120 mg (98%) of acetylated β-glucosyl pentanamide **98** as a white foam was obtained: R_f = 0.29 (hexane/EtOAc, 1/1); IR (CCl_4, cm^{-1}) 3436 (w), 2961 (m), 1755 (s), 1707 (s), 1512 (s), 1224 (s), 1039 (s); ^{1}H NMR (400MHz, $CDCl_3$) δ 0.87 (t, *J* = 7.2, 3H), 1.25-1.31 (m, 2H), 1.51-1.56 (m, 2H), 1.99 (s, 3H), 2.00 (s, 3H), 2.01 (s, 3H), 2.05 (s, 3H), 2.07-2.22 (m, 2H), 3.79 (ddd, *J* = 9.6, 4.4, 2.0, 1H), 4.04 (dd, *J* = 12.4, 2.0, 1H), 4.28 (dd, *J* = 12.4, 4.4, 1H), 4.89 (t, *J* = 9.6, 1H),

5.03 (t, *J* = 9.6, 1H), 5.23 (t, *J* = 9.6, 1H), 5.28 (t, *J* = 9.6, 1H), 6.19 (d, *J* = 9.6, 1H); ^{13}C NMR (100 MHz, $CDCl_3$) δ 13.7, 20.6, 20.6, 20.6, 20.7, 22.2, 27.2, 36.4, 61.6, 68.1, 70.5, 72.6, 73.5, 78.1, 169.6, 169.8, 170.6, 171.0, 173.4; HRMS (DEI) cacld. for $C_{19}H_{29}O_{10}N$ $[M]^+$ 431.1791, found 431.1776.

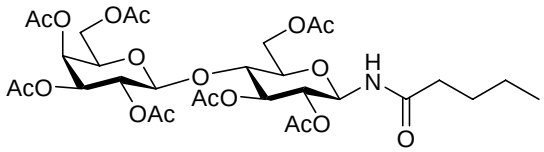

Acetylated β-lactosyl pentanamide 101 (Table 5). Acetylated β-lactose-4-pentenamide **99** (42 mg, 59 μmol) and palladium on carbon (5%, 12 mg, 5.9 μmol) were stirred in 5 mL of MeOH under 1 atm of hydrogen for 2 h. The reaction mixture was filtered and concentrated. Without further purification, 40 mg (94%) of acetylated β-lactosyl pentanamide **101** as a white foam was obtained: R_f = 0.29 (hexane/EtOAc, 1/2); IR (CCl_4, cm^{-1}) 3438 (w), 2960 (w), 1753 (s), 1706 (m), 1225 (s), 1048 (s); ^{1}H NMR (400MHz, $CDCl_3$) δ 0.87 (t, *J* = 7.4, 3H), 1.22-1.35 (m, 2H), 1.49-1.59 (m, 2H), 1.94 (s, 3H), 2.01 (s, 3H), 2.02 (s, 3H), 2.03 (s, 3H), 2.05 (s, 3H), 2.09 (s, 3H), 2.13 (s, 3H), 2.08-2.20 (m, 2H), 3.69-3.77 (m, 2H), 3.82-3.86 (m, 1H), 4.02-4.15 (m, 3H), 4.40 (dd, *J* = 12.4, 1.4, 1H), 4.44 (d, *J* = 8.0, 1H), 4.80 (t, *J* = 9.5, 1H), 4.91 (dd, *J* = 10.4, 3.4, 1H), 5.08 (dd, *J* = 10.4, 8.0, 1H), 5.19 (t, *J* = 9.5, 1H), 5.27 (t, *J* = 9.5, 1H), 5.32 (br d, *J* = 3.4, 1H), 6.07 (d, *J* = 9.5, 1H); ^{13}C NMR (100 MHz, $CDCl_3$) δ 13.6, 20.5, 20.6, 20.6, 20.6, 20.6, 20.8, 20.9, 22.2, 27.2, 36.4, 60.8, 61.9, 66.6, 68.9, 70.7, 70.9, 71.0, 72.3, 74.4, 76.1, 78.0, 100.9, 168.9, 169.2, 170.1, 170.1, 170.3, 170.4, 171.3, 173.2; HRMS (FAB) cacld. for $C_{31}H_{45}O_{18}NCs$ $[M + Cs]^+$ 852.1691, found 852.1706.

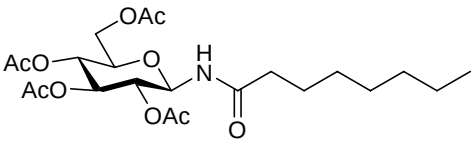

Acetylated β-glucosyl octanamide 103 (Table 6). Amide **103** was prepared following general procedure A using β-glucosyl azide **63** (0.520 g, 1.39 mmol), diisopropylethylamine (0.360 g, 2.79 mmol), PMe_3 (1.67 mL, 1.67 mmol), and octanoic acid **(102)** (0.400 g, 2.79 mmol). Purification by column chromatography (hexane/EtOAc, 2/1) afforded 0.376 g (57%) of acetylated β-glucosyl octanamide **103** as a colorless gum: R_f = 0.48 (hexane/ EtOAc, 1/1); IR (CCl_4, cm^{-1}) 3434 (w), 2957 (m), 1759 (s), 1708 (m), 1507 (m), 1228 (s); ^1H NMR (400MHz, $CDCl_3$) δ 0.85 (t, *J* = 7.2, 3H), 1.23 (br s, 8H), 1.54-1.57 (m, 2H), 1.99 (s, 3H), 2.01 (s, 3H), 2.02 (s, 3H), 2.05 (s, 3H), 2.11-2.18 (m, 2H), 3.80 (ddd, *J* = 9.6, 4.0, 2.0, 1H), 4.05 (dd, *J* = 12.4, 2.0, 1H), 4.29 (dd, *J* = 12.4, 4.0, 1H), 4.89 (t, *J* = 9.6, 1H), 5.04 (t, *J* = 9.6, 1H), 5.23 (t, *J* = 9.6, 1H), 5.28 (t, *J* = 9.6, 1H), 6.15 (d, *J* = 9.6, 1H); ^{13}C NMR (100 MHz, $CDCl_3$) δ 14.0, 20.6, 20.6, 20.6, 20.7, 22.6, 25.1, 28.9, 29.0, 31.6, 36.7, 61.6, 68.1, 70.6, 72.7, 73.5, 78.1, 169.6, 169.9, 170.6, 171.0, 173.4; HRMS (FAB) cacld. for $C_{22}H_{36}O_{10}N$ $[M + H]^+$ 474.2339, found 474.2340.

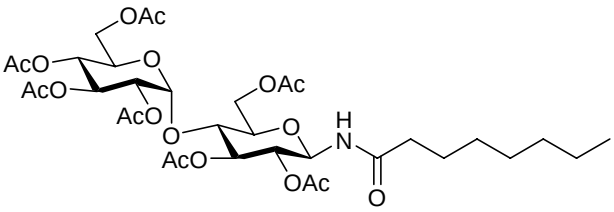

Acetylated β-maltosyl octanamide 104 (Table 6). Amide **104** was prepared following general procedure A using β-maltosyl azide **66** (1.05 g, 1.58 mmol), diisopropylethylamine (0.410 g, 3.17 mmol), PMe_3 (2.06 mL, 2.06 mmol), and octanoic acid **(102)** (0.460 g, 3.17 mmol). Purification by column chromatography (hexane/EtOAc, 1/2) afforded 0.730 g (61%) of acetylated β-maltosyl octanamide **104** as a white foam: R_f = 0.18 (hexane/ EtOAc, 1/1); IR (CCl_4, cm^{-1}) 3410 (w), 2952 (w), 1758 (s), 1708 (w), 1367 (w), 1230 (s), 1043 (m); ^1H

NMR (400MHz, $CDCl_3$) δ 0.84 (t, *J*=7.0, 3H), 1.23 (br s, 8H), 1.53-1.64 (m, 2H), 1.97 (s, 3H), 1.98 (s, 3H), 2.00 (s, 3H), 2.00 (s, 3H), 2.04 (s, 3H), 2.07 (s, 3H), 2.11 (s, 3H), 2.09-2.18 (m, 2H), 3.77 (ddd, *J* = 9.5, 4.0, 2.4, 1H), 3.89 (ddd, *J* = 10.0, 3.8, 2.2, 1H), 3.94 (t, *J* = 9.5, 1H), 4.01 (dd, *J* = 12.4, 2.2, 1H), 4.20 (dd, *J* = 12.4, 3.8, 1H), 4.21 (dd, *J* = 12.4, 4.0, 1H), 4.39 (dd, *J* = 12.4, 2.4, 1H), 4.73 (t, *J* = 9.5, 1H), 4.83 (dd, *J* = 10.0, 4.0, 1H), 5.03 (t, *J* = 10.0, 1H), 5.25 (t, *J* = 9.5, 1H), 5.30-5.38 (m, 3H), 6.02 (d, *J* = 9.5, 1H); ^{13}C NMR (100 MHz, $CDCl_3$) δ 14.0, 20.6, 20.6, 20.6, 20.6, 20.7, 20.8, 20.8, 22.5, 25.1, 28.9, 29.0, 31.6, 36.6, 61.4, 62.8, 67.9, 68.5, 69.2, 70.0, 71.3, 72.6, 73.9, 74.9, 77.6, 95.5, 169.5, 169.6, 169.8, 170.4, 170.5, 170.7, 171.1, 173.2; HRMS (ESI) cacld. for $C_{34}H_{52}O_{18}N$ $[M + H]^+$ 762.3184, found 762.3192.

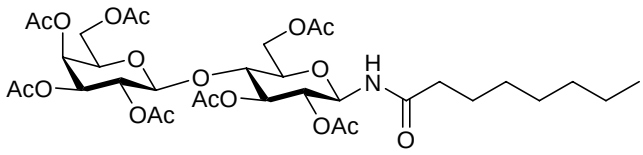

Acetylated β-lactosyl octanamide 105 (Table 6). Amide **105** was prepared following general procedure A using β-lactosyl azide **67** (0.480 g, 0.726 mmol), diisopropylethylamine (0.187 g, 1.45 mmol), PMe_3 (0.871 mL, 0.871 mmol), and octanoic acid **(102)** (0.210 g, 1.45 mmol). Purification by column chromatography (hexane/EtOAc, 1/2) afforded 0.300 g (54%) of acetylated β-lactosyl octanamide **105** as a white foam: R_f = 0.45 (hexane/ EtOAc, 1/2); IR (CCl_4, cm^{-1}) 3309 (w), 2957 (m), 1756 (s), 1707 (m), 1369 (s), 1221 (s), 1050 (s); ^1H NMR (400MHz, $CDCl_3$) δ 0.81 (t, *J* = 7.2, 3H), 1.20 (br s, 8H), 1.49-1.53 (m, 2H), 1.91 (s, 3H), 1.98 (s, 3H), 1.99 (s, 3H), 2.00 (s, 3H), 2.01 (s, 3H), 2.06 (s, 3H), 2.10 (s, 3H), 2.05-2.17 (m, 2H), 3.66-3.75 (m, 2H), 3.81-3.84 (m, 1H), 3.99-4.12 (m, 3H), 4.37 (dd, *J* = 12.0, 1.2, 1H), 4.41 (d, *J* = 8.0, 1H), 4.77 (t, *J* = 9.2, 1H), 4.89 (dd, *J* = 10.0, 3.2, 1H),

5.05 (dd, *J* = 10.0, 8.0, 1H), 5.16 (t, *J* = 9.2, 1H), 5.24 (t, *J* = 9.2, 1H), 5.30 (d, *J* = 3.2, 1H), 6.12 (d, *J* = 9.2, 1H); ^{13}C NMR (100 MHz, $CDCl_3$) δ 13.9, 20.4, 20.5, 20.6, 20.6, 20.6, 20.7, 20.8, 22.5, 25.1, 28.8, 28.9, 31.5, 36.5, 60.8, 61.9, 66.5, 68.9, 70.6, 70.8, 70.9, 72.2, 74.3, 75.9, 77.8, 100.8, 168.9, 169.2, 169.9, 170.1, 170.2, 170.3, 171.1, 173.2; HRMS (FAB) cacld. for $C_{34}H_{51}O_{18}NCs$ $[M + Cs]^+$ 894.2160, found 894.2137.

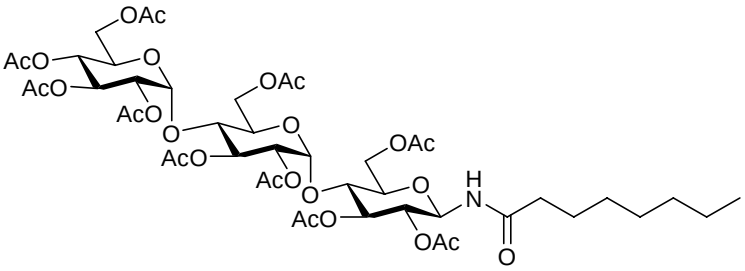

Acetylated β-maltotriosyl octanamide 106 (Table 6). Amide **106** was prepared following general procedure A using β-maltotriosyl azide **68** (1.16 g, 1.22 mmol), diisopropylethylamine (0.320 g, 2.44 mmol), PMe_3 (1.59 mL, 1.59 mmol), and octanoic acid **(102)** (0.350 g, 2.44 mmol). Purification by column chromatography (hexane/EtOAc, 1/2) afforded 0.640 g (50%) of acetylated β-maltotriosyl octanamide **106** as a white foam: R_f = 0.37 (hexane/ EtOAc, 1/2); IR (CCl_4, cm^{-1}) 3412 (w), 2958 (m), 1758 (s), 1709 (m), 1368 (m), 1233 (s), 1040 (s); ^{1}H NMR (400MHz, $CDCl_3$) δ 0.81-0.87 (m, 3), 1.24 (br s, 8H), 1.53-1.56 (m, 2H), 1.97 (s, 3H), 1.98 (s, 3H), 1.98 (s, 3H), 1.98 (s, 3H), 2.00 (s, 3H), 2.01 (s, 3H), 2.04 (s, 3H), 2.07 (s, 3H), 2.12 (s, 3H), 2.14 (s, 3H), 2.09-2.18 (m, 2H), 3.80 (ddd, *J*=9.4, 4.0, 2.6, 1H), 3.87-3.99 (m, 4H), 4.02 (dd, *J* = 12.4, 2.2, 1H), 4.13 (dd, *J* = 12.2, 2.7, 1H), 4.22 (dd, *J* = 12.4, 3.5, 1H), 4.28 (dd, *J* = 12.2, 4.0, 1H), 4.39 (dd, *J* = 12.2, 2.6, 1H), 4.44 (dd, *J* = 12.2, 1.5, 1H), 4.71 (dd, *J* = 10.3, 4.1, 1H), 4.72 (t, *J* = 9.4, 1H), 4.82 (dd, *J* = 10.0, 4.0, 1H), 5.04 (t, *J* = 10.0, 1H), 5.22 (d, *J* = 4.1, 1H), 5.26 (t, *J* = 9.4, 1H), 5.30-5.38 (m, 4H), 6.00 (d, *J* = 9.4, 1H); ^{13}C NMR (100 MHz, $CDCl_3$) δ 14.0, 20.6, 20.6, 20.6, 20.6,

20.6, 20.7, 20.8, 20.8, 20.9, 20.9, 22.6, 25.1, 28.9, 29.0, 31.6, 36.7, 61.3, 62.2, 62.9, 67.9, 68.5, 69.0, 69.3, 70.1, 70.4, 71.4, 71.6, 72.4, 73.7, 73.9, 74.8, 77.6, 95.6, 95.8, 169.5, 169.5, 169.6, 169.8, 170.3, 170.5, 170.5, 170.6, 170.7, 171.1, 173.2; HRMS (ESI) cacld. for $C_{46}H_{68}O_{26}N$ $[M + H]^+$ 1050.4029, found 1050.3988.

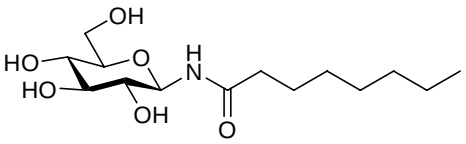

β-Glucosyl octanamide 107 (Table 6). Amide **107** was prepared following general procedure C using acetylated β-glucosyl octanamide **103** (0.320 g, 0.680 mmol) and NaOMe (6.80 mL, 1.35 mmol). The reaction mixture was neutralized with Dowex MAC-3 resin. Purification by column chromatography (CH_2Cl_2/MeOH, 6/1) afforded 0.177 g (85%) of β-glucosyl octanamide **107** as an amorphous solid: R_f = 0.17 (CH_2Cl_2/MeOH, 6/1); IR (ATR, Ge window, cm^{-1}) 3430 (br), 2918 (w), 1628 (s), 1545 (s), 1077 (s); ^{1}H NMR (400MHz, DMSO) δ 0.85 (t, *J* = 7.1, 3H), 1.23 (br s, 8H), 1.42-1.50 (m, 2H), 2.05-2.09 (m, 2H), 2.99-3.12 (m, 3H), 3.15 (t, *J* = 9.0, 1H), 3.39 (br d, *J* = 11.4, 1H), 4.61 (br d, *J* = 11.4, 1H), 4.45 (br s, 1H), 4.68 (t, *J* = 9.0, 1H), 4.87 (br s, 3H), 8.23 (d, *J* = 9.0, 1H); ^{13}C NMR (100 MHz, DMSO) δ 14.0, 22.1, 24.9, 28.5, 28.7, 31.2, 35.4, 60.9, 70.0, 72.5, 77.6, 78.5, 79.4, 172.5; HRMS (FAB) cacld. for $C_{14}H_{28}O_6N$ $[M + H]^+$ 306.1917, found 306.1927.

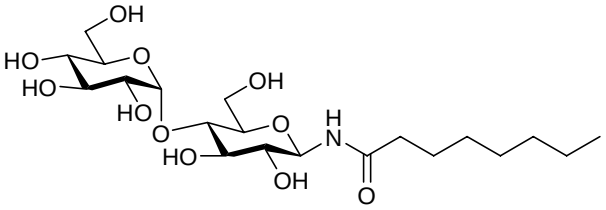

β-Maltosyl octanamide 108 (Table 6). Amide **108** was prepared following general procedure C using acetylated β-maltosyl octanamide **104** (0.37 g, 0.49 mmol) and NaOMe (17 mL, 3.4 mmol). The reaction mixture was neutralized with Dowex MAC-3 resin. Purification by column

chromatography (CH_2Cl_2/MeOH, 3/1) afforded 0.17 g (74%) of β-maltosyl octanamide **108** as an amorphous solid: R_f = 0.38 (CH_2Cl_2/MeOH, 3/1); IR (Drop casting on CaF_2, cm^{-1}) 3331 (br), 2926 (m), 1664 (m), 1546 (m), 1377 (w); ^{1}H NMR (400MHz, D_2O) δ 0.71 (t, *J* = 7.9, 3H), 1.13-1.16 (m, 8H), 1.43-1.51 (m, 2H), 2.15-2.19 (m, 2H), 3.26 (t, *J* = 9.3, 1H), 3.27 (t, *J* = 9.3, 1H), 3.43 (dd, *J* = 10.0, 3.9, 1H), 3.49-3.76 (m, 9H), 4.81 (d, *J* = 9.3, 1H), 5.28 (d, *J* = 3.9, 1H); ^{13}C NMR (100 MHz, D_2O) δ 13.2, 21.8, 24.9, 27.9, 28.0, 30.8, 35.7, 60.3, 60.4, 69.2, 71.5, 71.6, 72.5, 72.7, 75.9, 76.0, 76.9, 78.9, 99.4, 178.7; HRMS (ESI) cacld. for $C_{20}H_{38}O_{11}N$ $[M + H]^+$ 468.2445, found 468.2445.

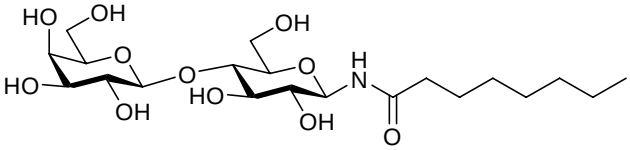

β-Lactosyl octanamide 109 (Table 6). Amide **109** was prepared following general procedure C using acetylated β-lactosyl oactanamide **105** (0.230 g, 0.300 mmol) and NaOMe (10.6 mL, 2.11 mmol). The reaction mixture was neutralized with Dowex MAC-3 resin. Purification by column chromatography (CH_2Cl_2/MeOH, 2/1) afforded 0.100 g (71%) of β-lactosyl octanamide **109** as an amorphous solid: R_f = 0.28 (CH_2Cl_2/MeOH, 3/1); IR (drop casting on CaF_2, cm^{-1}) 3269 (br), 2919 (m), 1655 (m), 1548 (m), 1373 (w); ^{1}H NMR (400MHz, D_2O) δ 0.72 (t, *J* = 6.8, 3H), 1.13-1.17 (m, 8H), 1.44-1.51 (m, 2H), 2.18 (t, *J* = 7.2, 2H), 3.27-3.32 (m, 1H), 3.41 (dd, *J* = 9.2, 7.6, 1H), 3.51-3.69 (m, 8H), 3.78-3.81 (m, 2H), 4.32 (d, *J* = 8.0, 1H), 4.84 (d, *J* = 9.2, 1H); ^{13}C NMR (100 MHz, D_2O) δ 13.2, 21.8, 24.9, 27.9, 28.0, 30.8, 35.7, 59.7, 60.9, 68.4, 70.8, 71.3, 72.4, 75.0, 75.2, 76.3, 77.6, 78.9, 102.7, 178.7; HRMS (FAB) cacld. for $C_{20}H_{38}O_{11}N$ $[M + H]^+$ 468.2445, found 468.2465.

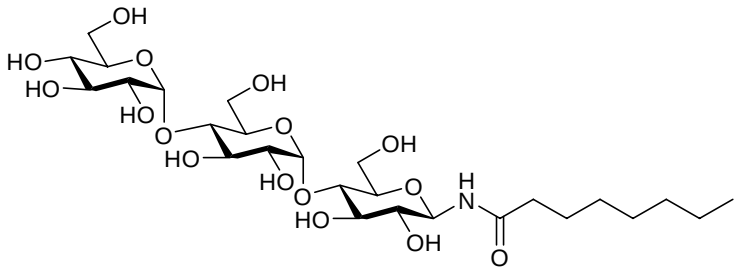

β-Maltotriosyl octanamide 110 (Table 6). Amide **110** was prepared following general procedure C using acetylated β-maltotriosyl octanamide **106** (0.43 g, 0.41 mmol) and NaOMe (21 mL, 4.1 mmol). The reaction mixture was neutralized with Dowex MAC-3 resin. Purification by column chromatography (CH_2Cl_2/MeOH, 2/1) afforded 0.19 g (74%) of β-maltotriosyl octanamide **110** as an amorphous solid: R_f = 0.17 (CH_2Cl_2/MeOH, 3/1); IR (drop casting on CaF_2, cm^{-1}) 3338 (br), 2927 (m), 1653 (m), 1544 (m), 1375 (w); ^{1}H NMR (400MHz, D_2O) δ 0.73 (t, *J* = 6.8, 3H), 1.15-1.18 (m, 8H), 1.45-1.51 (m, 2H), 2.17-2.21 (m, 2H), 3.28 (t, *J* = 9.2, 1H), 3.29 (t, *J* = 9.2, 1H), 3.44-3.86 (m, 16H), 4.84 (d, *J* = 9.2, 1H), 5.27 (d, *J* = 4.0, 1H), 5.29 (d, *J* = 3.6, 1H); ^{13}C NMR (100 MHz, D_2O) δ 13.2, 21.8, 24.9, 27.9, 28.0, 30.8, 35.7, 60.3, 60.3, 60.3, 69.2, 71.0, 71.4, 71.5, 71.6, 72.6, 72.7, 73.2, 75.9, 76.2, 76.5, 76.8, 78.9, 99.3, 99.6, 178.7; HRMS (FAB) cacld. for $C_{26}H_{47}O_{16}NNa$ [*M* + Na]$^+$ 652.2793, found 652.2806.

Chapter 3: Preparation and Characterization of Carbohydrate-Functionalized Gold Nanospheres for the Detection of Pathogens

INTRODUCTION

Since many biomolecules are tens of nanometers in size, it has been thought that accurately designed nanomaterials can be incorporated into biological systems. As a result, a variety of well-defined nanostructures possessing novel properties have emerged as versatile tools for biological and biomedical applications.[98-102] Among them, colloidal gold nanospheres are especially promising in biological applications because of their easy of preparation and bioconjugation, non-toxicity and stability.

Gold nanospheres (AuNSs) are easily prepared by the citrate reduction of auric acid with sodium citrate reported by Turkevich and co-workers in 1951[103] and refined by Frens in 1973.[104] The size of the nanospheres are controlled ranging from 16 nm to 147 nm by changing the sodium citrate concentration.[104] Typically, the formation of nanospheres is monitored by the generation of a deep red colored colloidal suspension. Citrate-capped AuNSs are very stable and are easily functionalized with various ligands containing thiol groups by the displacement of citrate caps. Another popular method for the synthesis of AuNSs is two phase synthesis reported by Brust and co-workers in 1994.[105] This method allows the direct synthesis of thermally and air stable AuNSs of 1-3 nm. In synthesis, the gold salt ($AuCl_4^-$) is transferred from aqueous solution to toluene using tetraoctylammonium bromide as a phase-transfer agent and then reduced by sodium borohydride in the presence of dodecanethiol to produce thiol-stabilized AuNSs (Scheme

12). The formation of nanospheres is monitored also by the generation of a deep brown color in the organic phase.

Scheme 12

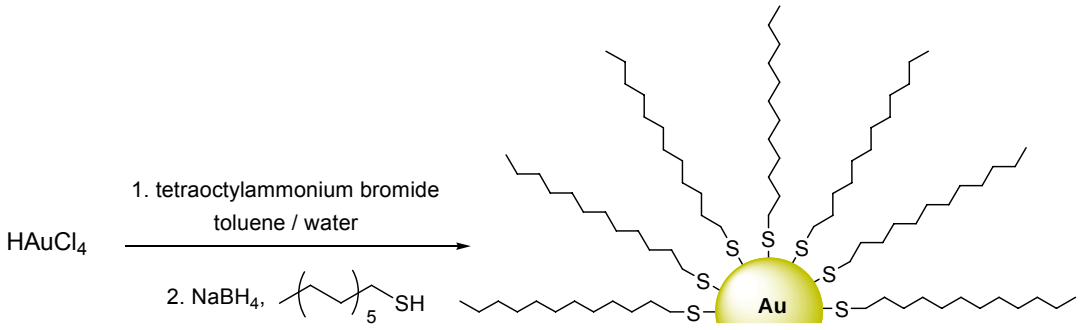

In addition to easy fabrication, gold is non-toxic in biological systems. Recent *in vitro* studies performed by Wyatt showed that gold nanospheres with a variety of surface modifiers are non-toxic to human cells.[106] Furthermore, gold nanospheres have unique optical properties arising from surface plasmon resonance (SPR).

SPR results from the collective oscillation of electrons in the conduction band of the metal nanoparticles upon incoming light. It depends on the shape, size, and dielectric constants of both the metal and the surrounding materials.[107-109] For gold nanospheres, this resonance is observed in the visible spectral region at ca. 520 nm, which results in the brilliant red color of the nanosphere suspensions.[103] The SPR of gold nanospheres is sensitive to the adsorption of molecules on the particle surface and to the coupling of other particles, leading to a shift in λ_{max}.[103,107-109] Upon the excitation of the SPR, the optical properties including absorption, scattering, and emission of gold nanospheres are dramatically enhanced.[110] Based on the sensitivity of SPR and the SPR-enhanced properties, gold nanospheres hybridized with proteins or DNA have been utilized for the biological and biomedical applications including biosensor, diagnostics, drug delivery, and the photothermal therapy of cancer.[103,110-112]

The tremendous advantages of gold nanospheres have recently attracted great attention in the field of glycobiology. As a result, the first generation of new hybrid materials made of gold nanospheres and biologically relevant carbohydrates has been shown in 2001 by Penadés and co-workers.[113] In fact, this approach extends tools for studying the structure and function of carbohydrates from two-dimensional (2D) microarrays to three-dimensional (3D) system in nanoscale. Although 2D microarrays allow high-throughput evaluation of carbohydrate functions to a variety of macromolecules, the study is mainly limited *in vitro*. By mimicking the situation encountered on cell surfaces, the multiple presentations of carbohydrates on the nanoscale-globular surface (3D) are promising for the study of carbohydrate-involved biological processes *in vivo*.

Literature Survey for Carbohydrate-Functionalized Gold Nanospheres: Synthetic Effort and Their Applications

Penadés group is the pioneer in the area of carbohydrate-functionalized AuNSs. They prepared various glycoconjugates anchored to thiol group for the functionalization of gold nanospheres (Scheme 13). The reaction of corresponding carbohydrates with thioacetyl alcohol **111** under the trichloroacetimidate method in the presence of a C-2 participating group (such as acyl), followed by the deprotection provided dimeric β-O-linked glucose **112**, lactose **113**, maltose **114**, and tumor antigen Lewis^x conjugates **115**, respectively (Scheme 13).[113,114]

Scheme 13

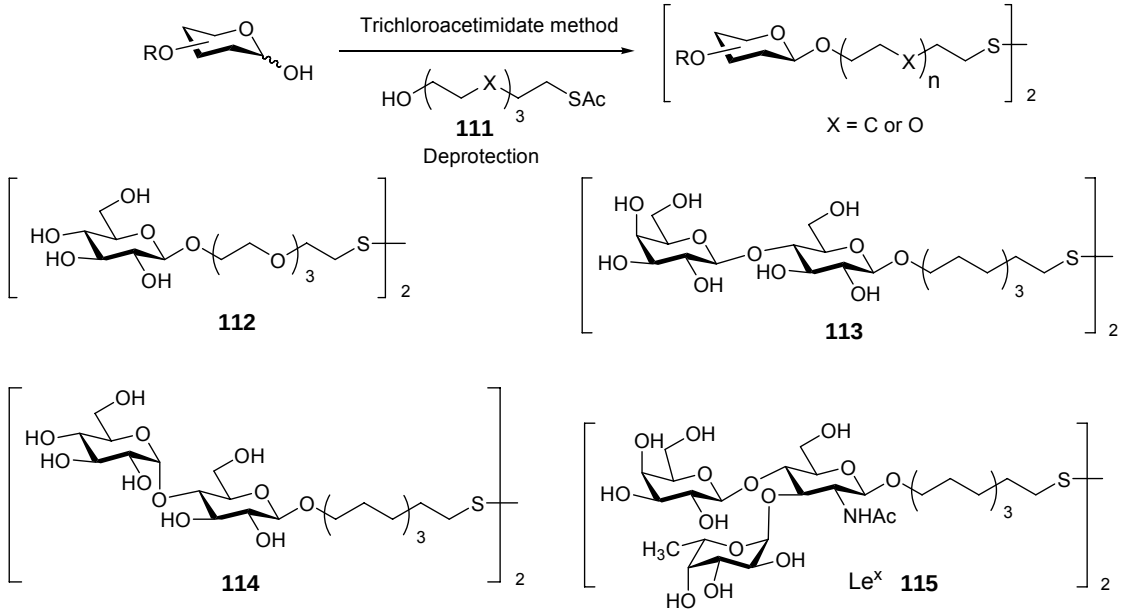

Using the modification of the Brust method,[105] preparation of carbohydrate-functionalized AuNSs (**116**, **117**, **118**, and **119**) was accomplished by adding a methanolic solution of the corresponding glycoconjugates to an aqueous solution containing tetrachloroauric acid, followed by subsequent reduction with sodium borohydride (Scheme 14).[114] The resulting dark brown-gold nanospheres are highly water soluble, stable in solution for years, and showed a permanent magnetism which is an unusual property for gold nanospheres.[115] The presence of carbohydrate moieties was confirmed by ^{1}H-NMR and IR spectroscopy. The core size of gold nanospheres (< 2 nm) was determined by transmission electron microscopy (TEM).

Scheme 14

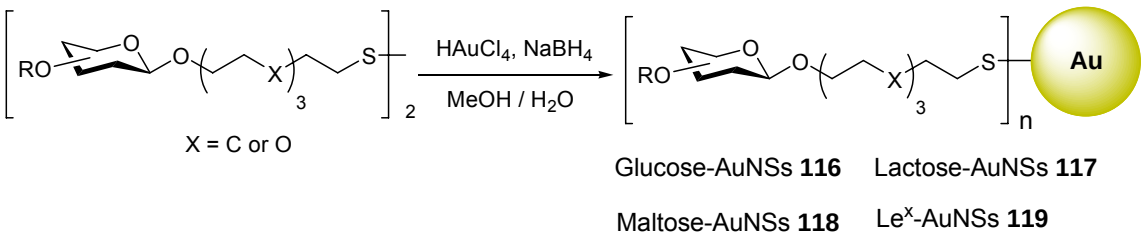

The resulting carbohydrate-functionalized gold nanospheres have been utilized in a variety of applications. For example, Le^X-functionalized AuNSs **119** were utilized for probing calcium ion mediated carbohydrate-carbohydrate interactions,[113,116] which have been implicated in cell recognition.[117] The possibility of carbohydrate-functionalized AuNSs as tools for anti-adhensive therapy was demonstrated *in vivo*.[118] Mice injected with tumor cells pre-incubated with lactose-functionalized AuNSs **117** suppressed tumor progression about 70 %, compared with the group inoculated only with tumor cells.[118]

Chen and co-workers prepared mannose-functionalized AuNSs **114** by the Brust method with mannose conjugates **113** anchored to a thiol group (Scheme 15).[119] The α-O-linked mannose conjugate **113** was synthesized by the reaction of acetylated mannosyl bromide **110** with pentenyl alcohol **111** under the Koenigs-Knorr condition, followed by the deprotection of the resulting acetylated mannose conjugate **112** (Scheme 15).

Scheme 15

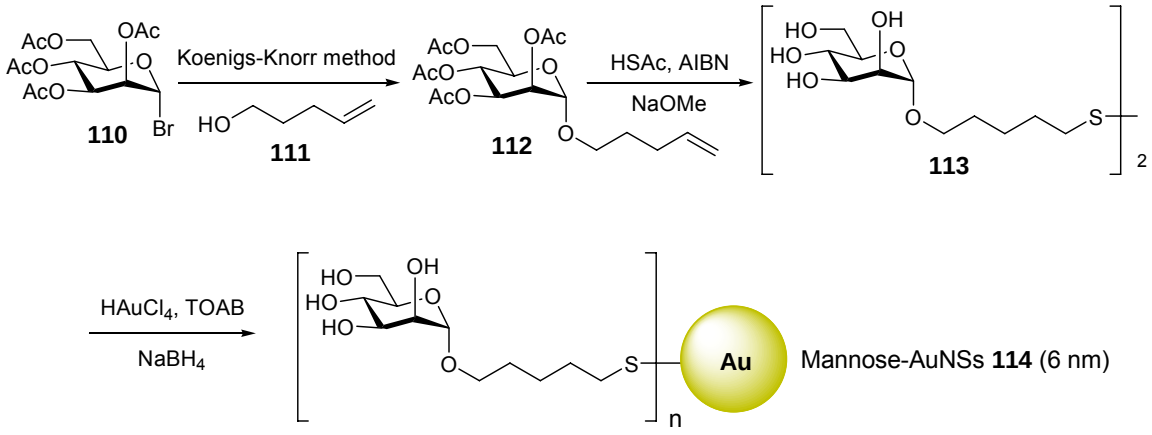

The size of gold nanospheres **114** (6±1 nm, mean diameter) was determined by TEM, and the UV-visible spectrum of particles **114** showed a clear SPR band at 520 nm. The presence of mannose conjugate **113** was confirmed by ^{1}H NMR. Mannose-functionalized AuNSs **114** were utilized to demonstrate the specificity of carbohydrate-

receptor interaction. When mannose-functionalized AuNSs **114** were incubated with two *E. coli* strains ORN178 (expresses mannose receptor FimH) and ORN208 (deficient on the FimH gene), mannose-functionalized AuNSs **114** recognized only ORN178 strain and were visualized by TEM.[119] Later on, they utilized carbohydrate-functionalized AuNSs as affinity probes for the efficient separation and enrichment of target proteins.[120] When galactose-functionalized AuNSs prepared by a similar manner in Scheme 4 were incubated with a mixture of proteins, a galactophilic lectin *Pseudomonas aeruginosa* was captured by the galactose-functionalized AuNSs, separated by centrifugation, and detected by MALDI-TOF mass spectrometry. The strong affinity results from the multivalent interaction between the galactose residues on the gold surface and *Pseudomonas aeruginosa* lectins.

Gervay-Hague and co-workers prepared monosaccharide-functionalized gold nanospheres (Scheme 16).[121] The synthesis of glycosides **116** was performed by the reaction of corresponding carbohydrate **115** with nitromethane under basic condition to provide β-C-linked glycosides **116**. Hydrogenation of glycosides **116** over palladium/charcoal, followed by coupling with bi-functional linker **118** afforded glycosyl conjugates **119**. Under the Penadés conditions,[114] glucose- and galactose-functionalized AuNSs (**120** and **121**) were produced as dark-brown powders.

Scheme 16

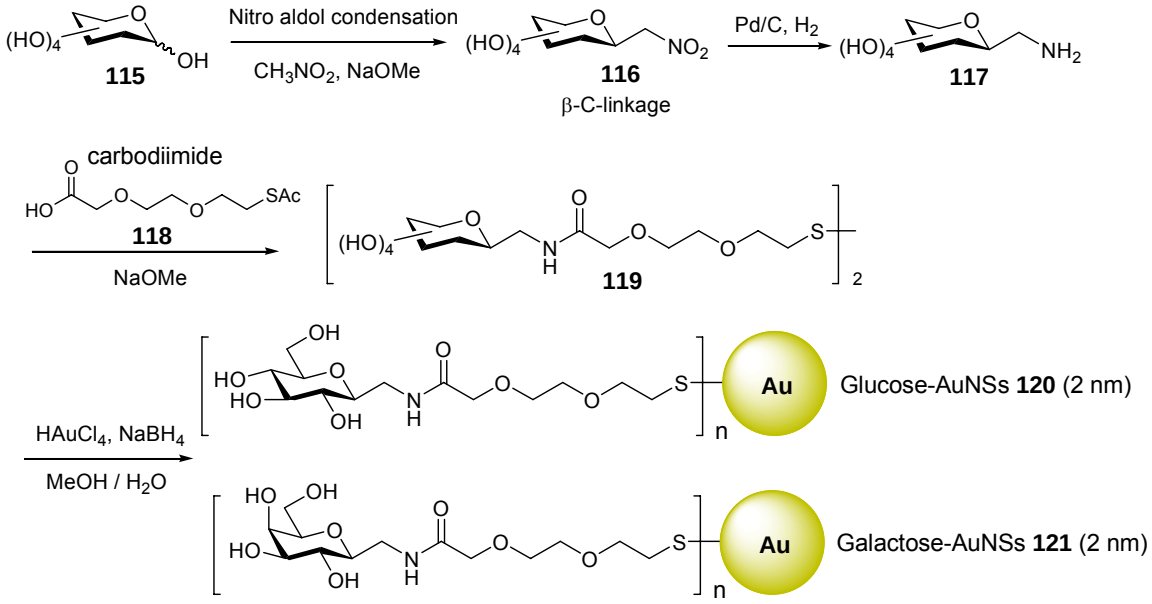

The particle sizes were measured by TEM and atomic force microscopy (AFM). The presence of carbohydrate moieties and tethers were confirmed by IR and ^{1}H NMR spectroscopy. These gold nanospheres (**120** and **121**) were utilized to investigate the multivalent interactions with recombinant glycoprotein 120 (gp 120), which initiates HIV infection, by a biotin-NeutrAvidin adhesion assay. The results indicated that the binding activity of carbohydrate-functionalized AuNSs (**120** and **121**) to recombinant gp 120 were 300 times greater than corresponding dimers **119**, demonstrating the importance of polyvalent display of carbohydrates on the gold nanospheres.

Barchi and co-workers synthesized gold nanospheres **122** functionalized with Thomsen-Friedenreich disaccharide,[122] which is a human tumor-associated carbohydrate antigen, by a modified procedure of that reported by Brust and co-workers.[105] These particles **122** showed *in vitro* activity against tumor growth and inhibited lung metastasis *in vivo* against an implanted metastatic breast cancer cell line.

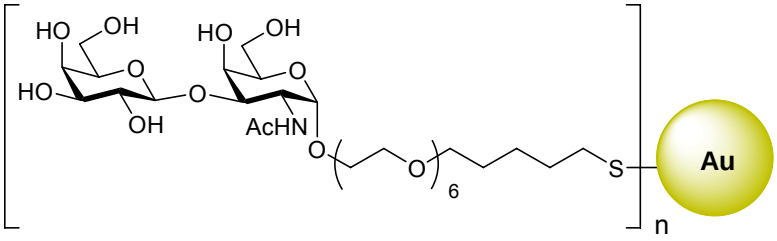

Thomsen-Friedenreich disaccharide AuNSs **122** (1-2 nm)

Kataoka and co-workers prepared carbohydrate-functionalized gold nanospheres through the immobilization of carbohydrate conjugates onto the gold nanospheres presenting poly(ethylene glycol) (PEG) derivatives (Scheme 17).[123] Thiol-stabilized AuNSs **124** (mean diameter of 8.9 nm determined by TEM) were first prepared by the reduction of auric acid with sodium borohydride in the presence of PEG derivatives **123**. The PEG terminal acetal groups were then converted to aldehydes **125** by acid treatment. The condensation of PEG terminal aldehyde groups **125** with a mixture of lactose and mannose derivatives (**126** and **127**) by reductive amination produced imines, which were reduced to generate gold nanospheres **128** containing both lactose and mannose (Scheme 17). The authors also controlled the density of carbohydrates on the surface by changing the ratio of lactose and mannose derivatives (**126** and **127**). The presence of lactose moieties on gold nanospheres was confirmed by the assay with *Recinus communis* agglutinin (RCA_{120}), a divalent lectin specifically recognizing β-galactose residue, by monitoring the change of the SPR band.

Scheme 17

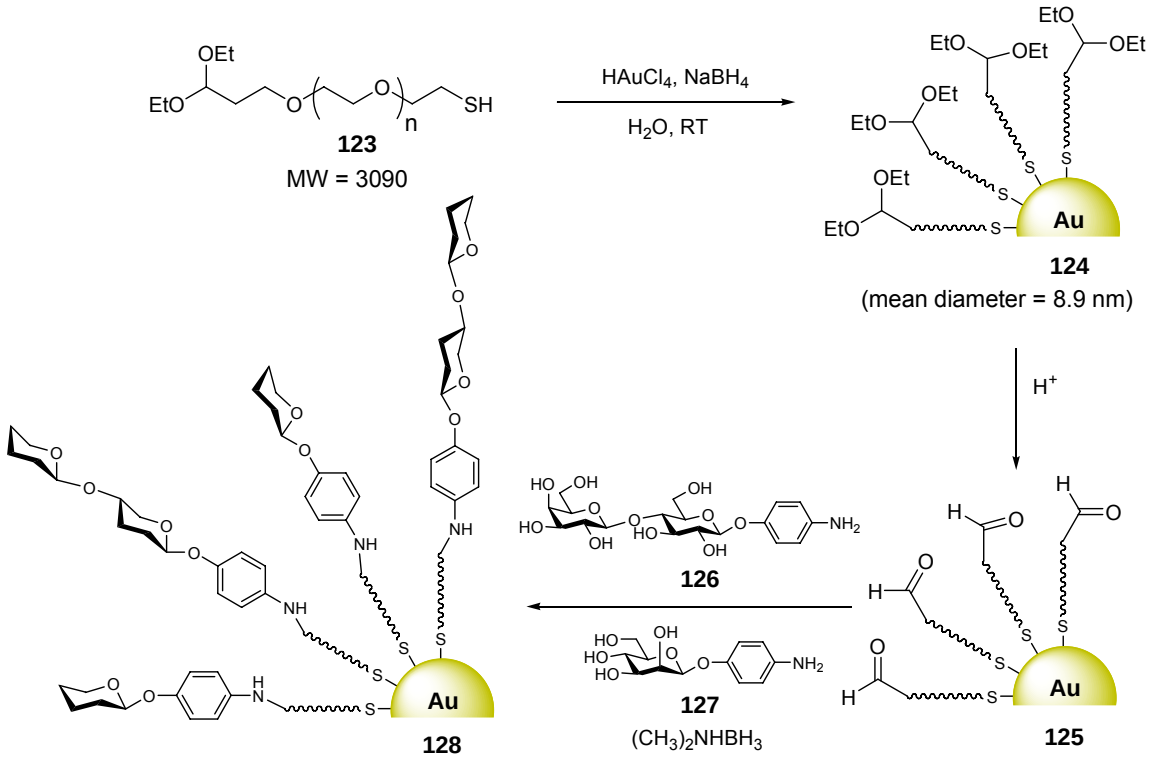

Russell and co-workers prepared lactose-functionalized AuNSs **134** (Scheme 18).[124] The β-O-linked lactose derivative **132** was synthesized by the reaction of peracetylated lactose **129** with bromoethanol **130** using the Koenigs-Knorr method. The bromide of lactose derivative **131** was then displaced by thioacetate, followed by deprotection of acetyl groups provided thiolated lactose derivative **132**. Lactose-functionalized AuNSs **134** (16 nm, mean diameter) were prepared by citrate reduction of auric acid, followed by the self-assembly of thiolated lactose derivative **132** on the pre-formed, citrate-capped AuNSs **133** (Scheme 18).[124] Similarly, they also prepared glucose, mannose, and lactose-functionalized gold nanospheres controlling tether length.[124]

Scheme 18

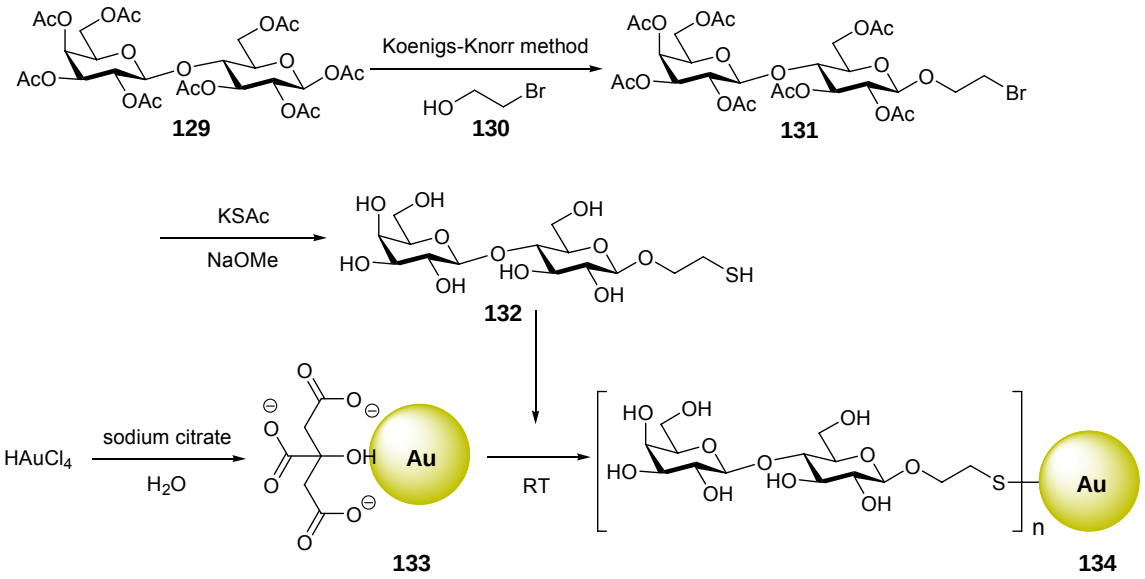

The lactose-functionalized AuNSs **134** were utilized to demonstrate calcium-mediated carbohydrate-carbohydrate interactions by monitoring the SPR band. Visibly, the solution containing lactose-functionalized AuNSs **134** changed color from red to purple following the addition of calcium ions, suggesting calcium-induced aggregation.[124] Recently, the authors reported a colorimetric assay to detect cholera toxin utilizing lactose-functionalized AuNSs **134** by mimicking the interactions between carbohydrates of GM1 ganglioside and the receptor presented on the cholera toxin.[125] The AuNSs **134** selectively recognized cholera toxin and responded with a color change of the solution. The simple color change of the bioassay provided a selective detection and quantification of cholera toxin within 10 minutes.

As discussed above, it is unambiguous that carbohydrate-functionalized gold nanospheres are fascinating tools for the study of their biological functions. Their unique properties, including the easy preparation, functionalization, biosafety, and stability, inspired us to develop cellular probes to detect pathogens. For these purposes, it is

important to control the size of gold nanospheres because of their size-dependent optical properties and their lifetime in bloodstream against physiological barriers[126] such as the renal system, the reticular endothelial system (RES), and liver. Accordingly, the goal of research in this section was to prepare carbohydrate-functionalized gold nanospheres with tunable size and to characterize the bioactivity of carbohydrates on the surface of gold nanospheres.

RESULTS AND DISCUSSION

Preparation of Carbohydrate-Functionalized Gold Nanospheres

In order to control the size of gold nanospheres, two different methods were utilized: (1) *in-situ* reduction of auric acid with sodium borohydride in the presence of glycoconjugates to provide small particles, and (2) a stepwise method where glycoconjugates were self-assembled on the surface of pre-formed, citrate-capped gold nanospheres to provide particles with larger diameters. For the surface functionalization of gold nanospheres, β-glucosyl thioctanamide **78** and β-lactosyl thioctanamide **81** (Scheme 19) were selected because of the structural simplicity of the carbohydrate moiety. The methodology that would be perfected using these two systems would be a model for more complex oligosaccharide. In addition, the presence of the disulfide functionality on the tether would ensure a strong attachment to gold surface.

Via Sodium Borohydride Reduction in the Presence of Carbohydrate Conjugates

The preparation of carbohydrate-functionalized gold nanospheres with diameters smaller than 2 nm was accomplished using an adaptation of Penadés's procedure

(Scheme 19).[114] A methanolic solution of the corresponding glycoconjugate (**78** or **81**) was added into an aqueous solution of tetrachloroauric acid. The resulting mixture was reduced with sodium borohydride to generate a dark suspension. The dark suspension was stirred at room temperature for 3 h, and then the solvent was removed. Purification by centrifugal filtration afforded carbohydrate-functionalized AuNSs (**135** or **136**).

Scheme 19

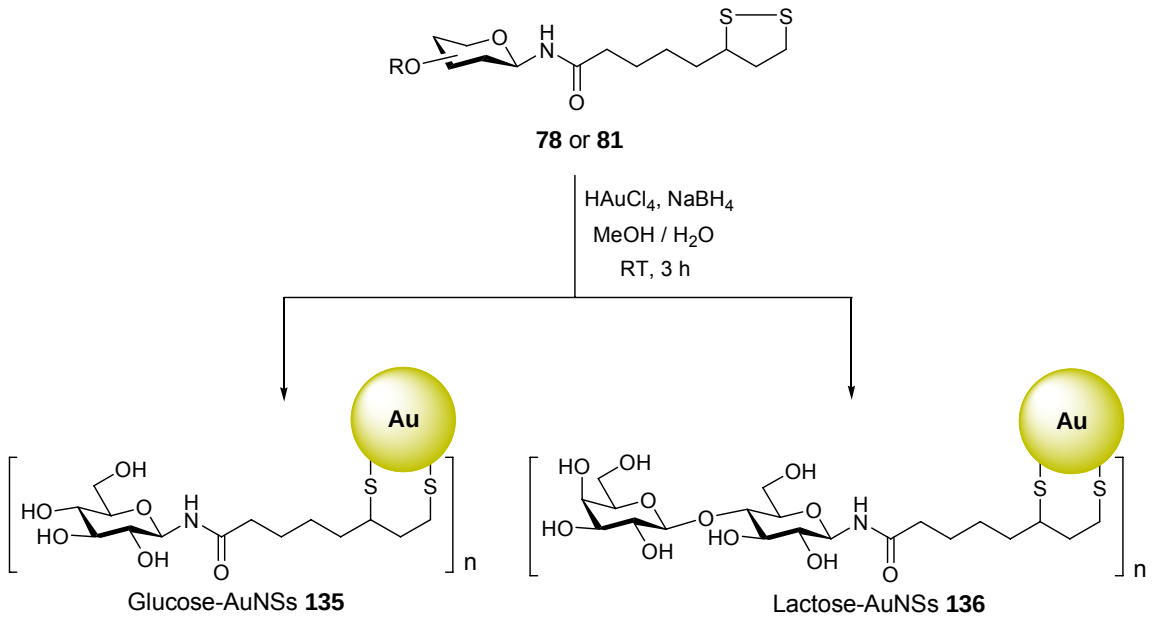

These functionalized nanospheres were characterized by UV-visible, FT-IR, X-ray photoelectron spectroscopy (XPS), and TEM. The size information of each nanospheres was obtained by TEM. Figure 22a and 22b shows TEM images with inset size distribution of glucose-functionalized AuNSs **135** and lactose-functionalized AuNSs **136**, respectively. Both AuNSs (**135** and **136**) showed small core diameters ranging from 0.5 nm to 4 nm with a mean core size of 1.8 nm for glucose-AuNSs **135**, and 1.9 nm for lactose-AuNSs **136**. It was known that UV-visible absorption spectra of gold nanospheres present a size-dependent SPR band at around 520 nm, and the SPR band is little or absent for gold nanospheres with core size less than 2 nm, as well as for bulk gold.[127,128] In the

absorption spectra (Figure 22c), AuNSs **135** and **136** showed no SPR band ca. 520 nm, which is in good agreement with TEM images obtained and UV-visible data reported.[127,128]

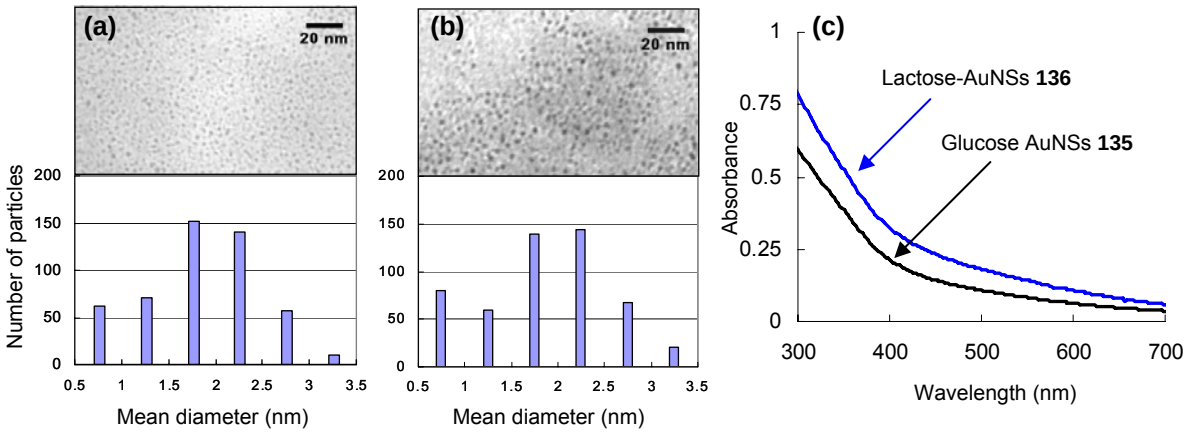

Figure 22. TEM images with inset size distribution histograms and UV-visible absorption spectra of carbohydrate-functionalized AuNSs. (a) glucose-AuNSs **135**, d_{core} = 1.8 ± 0.6 nm. (b) lactose-AuNSs **136**, d_{core} = 1.9 ± 0.7 nm. (c) no SPR band was observed at ca. 520 nm.

The presence of glycoconjugates (**78** or **81)** on the surface of gold nanospheres was confirmed by XPS and FT-IR spectroscopies. FT-IR spectra of both AuNSs **135** and **136** showed an amide functional group at around 1655 cm^{-1} (amide I band, C=O stretching) and at around 1530 cm^{-1} (amide II band, a combination of C-N stretching and C-N-H bending). A broad band at around 3360 cm^{-1} for O-H, N-H stretching, and C-H stretching at around 2920 cm^{-1} were also observed.

The XPS spectra of AuNSs **135** and **136** exhibited both gold core (Au 4f) and glycoconjugate-based peaks (S 2p, C 1s, and O 1s). The absence of nitrogen peaks is due possibly to the insensitivity of the technique to detect a small amount of nitrogen.[129] Figure 23 shows the Au 4f and S 2p regions of the XPS spectra of each AuNSs (**135** and **136**). The broad doublet peak observed in each region indicated that a single gold and a

single sulfur species were present. The binding energies measured for Au $4f_{7/2}$ and Au $4f_{5/2}$ of each nanospheres are at around 83.4 eV and 87.2 eV, respectively, suggesting that the gold atoms in the nanospheres are largely in the bulk state.[105] The binding energies of S $2p_{3/2}$ for each AuNSs (**135** and **136**) were observed at 161.3 eV and 161.8 eV, respectively, suggesting that glycoconjugates (**78** and **81)** bound to the surface of gold nanospheres as a thiolate species.[130]

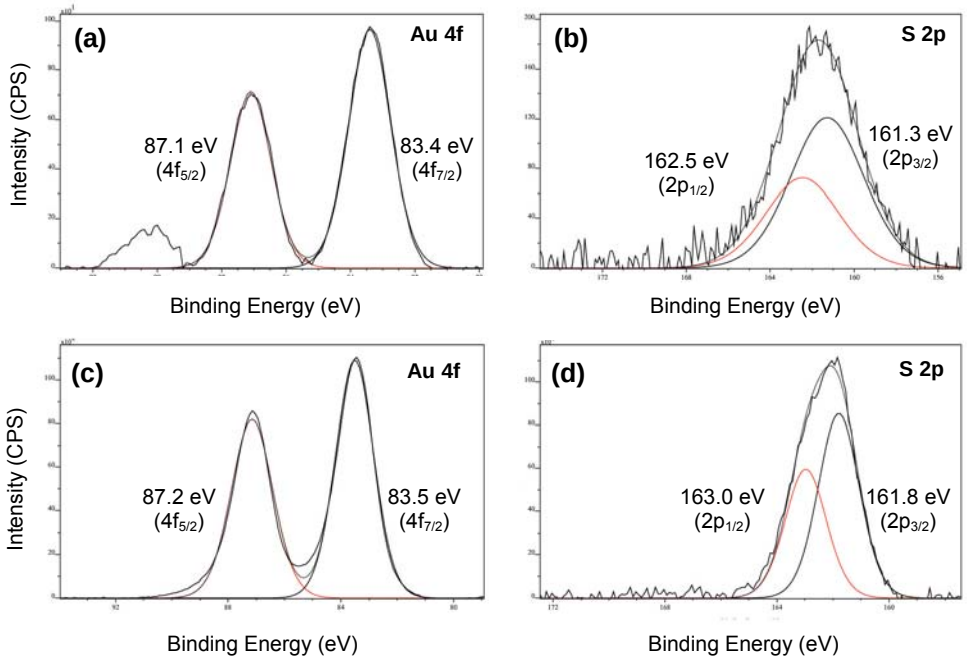

Figure 23. Au 4f and S 2p regions of XPS spectra of carbohydrate-functionalized AuNSs. (a) and (b) for glucose-AuNSs **135**. (c) and (d) for lactose-AuNSs **136**. The numbers in each spectrum correspond to the binding energies.

The preparation of carbohydrate-functionalized gold nanospheres using Penadés's procedure was successful. However, under these conditions a significant amount of gold nanospheres **135** and **136** were aggregated during the purification steps. In addition, occasionally this procedure gave a wide size distribution. That is presumably due to the heterogeneous reaction conditions where gold nanospheres (insoluble in methanol) are

immediately formed by adding sodium borohydride into a mixture of auric acid in water and glycoconjugates in methanol. Therefore, a more reliable method was required.

To achieve this goal, Penadés's procedure was modified slightly by using a single solvent (water) instead of using a mixture of methanol and water. Into an aqueous solution containing a mixture of auric acid and glycoconjugate (**78** or **81**), an aqueous solution of sodium borohydride was added (Scheme 19). As expected, the color of the solution was changed from a light yellow to a dark brown, indicating the formation of gold nanospheres. However, no dark suspension was generated. TEM images and UV-visible spectra of glucose-AuNSs **137** and lactose-AuNSs **138** showed homogeneous particles sizes with mean diameters of 1.7 ± 0.6 nm and 1.5 ± 0.4 nm for glucose-AuNSs **137** and lactose-AuNSs **138**, respectively.

Via Citrate Reduction and Self-Assembly of Carbohydrate Conjugates

The preparation of gold nanospheres with larger diameters was achieved by modification of the procedure reported by Frens.[104] An aqueous solution of sodium citrate was added into a boiling solution of tetrachloroauric acid in water. In few seconds, the color of the boiling solution was changed from a light yellow to a corresponding color (see the Table 7), indicating the formation of gold nanospheres. By altering the amount of citrate added, it was possible to systematically alter the size of the nanospheres produced. The results for the preparation of citrate-capped gold nanospheres are summarized in Table 7 and Figure 24.

Table 7. Experimental data for the preparation of citrate-capped gold nanospheres.[a]

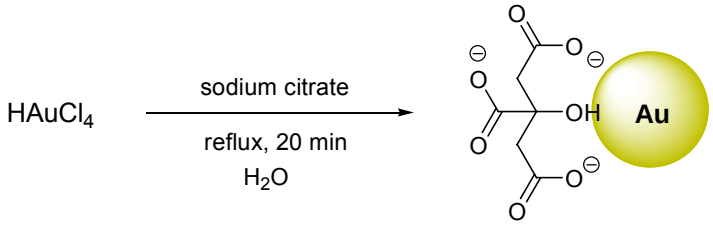

entry	citrate amount[b] (mL)	particle size[c] (nm)	solution color	SPR absorption at λ_{max}	particle concentration[g] (nM)
1	0.5	73.2 ± 18.6[d]	Brown[e]	540 nm[f]	-
2	1.0	28.3 ± 5.7[d]	Purple	524 nm	1.54
3	1.5	18.1 ± 2.2	Dark red	520 nm	6.63
4	2.0	15.8 ± 1.6	Dark red	520 nm	10.1
5	3.0	15.3 ± 1.3	Dark red	520 nm	11.1
6	4.0	aggregated	–	–	–

[a] The reaction was performed at reflux for 20 min with 100 mL of $HAuCl_4$ solution (1.47 mM in H_2O). See the experimental section for details. [b] 0.34 M of citrate solution was used. [c] The size of each particles was determined by TEM. [d] Relatively broad size distribution observed in TEM. [e] Tyndall effect of the scattered light was observed. [f] Broad SPR band was observed. See the experimental section for UV-visible spectra. [g] The concentration of particle solution was determined according to the literature.[131]

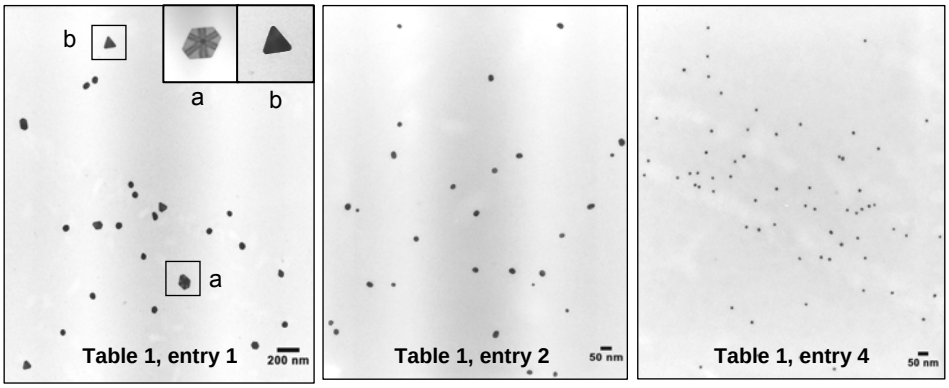

Figure 24. Representative TEM images of citrate-capped gold nanospheres.

By this method, citrate-capped AuNSs with mean diameter ranging from 15 nm to 73 nm were prepared. The size of citrate-capped AuNSs depended on the amount of citrate solution. As the amount of citrate solution was increased, the size of particles

decreased. When 4.0 mL of citrate solution was introduced (Table 7, entry 6), most particles aggregated and settled out of solution. Interestingly, a variety of morphologies were observed in the particles (Table 7, entry 1 and Figure 24) formed with the smallest amount of citrate solution.

Citrate-capped AuNSs provided an intense SPR band at ca. 520 nm except for the largest particles (Table 7, entry 1). The intensity of the absorbances decreased along with decreasing size (from entry 2 to entry 5). For the largest particles (Table 7, entry 1), the intensity and the position of the SPR band were decreased and largely red-shifted, respectively. Moreover, the shape of the SPR band was broadened, indicating broad size distribution which is a good agreement with the TEM image (Figure 24).

The concentrations of the gold nanospheres were determined to be within a range of ca. 10 nM, based on the size and absorbance.[131] The concentration of the largest particles could not be determined due to the broad size distribution and various shapes.

This method overcomes the main disadvantage of direct synthesis of gold nanospheres, where the size of nanospheres formulated via the reduction of auric acid with sodium borohydride in the presence of the ligands are dependent on both the concentration of ligand and reducing agent, which means that it is difficult to reproducibly control the size of particles. By this method, however, the size of particles are controlled only by the concentration of citrate as a reducing and stabilizing agent, and the resulting particles can be functionalized with various ligands by the displacement of citrate-caps without altering the size of particles.

It was our intention to prepare gold nanospheres > 2 nm by citrate reduction, but the smallest particles that could be prepared by this method was ca. 15 nm (Table 7). In

order to prepare gold nanospheres sized between 2 and 15 nm, the reduction method had to be altered. Therefore, gold salts were reduced with sodium borohydride in the presence of sodium citrate according to the literature[132] to produce citrate-capped AuNSs **139** with a mean diameter of 4.5±1.4 nm (Figure 25a). As anticipated, the resulting colloidal suspension showed the intense SPR band at the wavelength of 518 nm (Figure 3b).

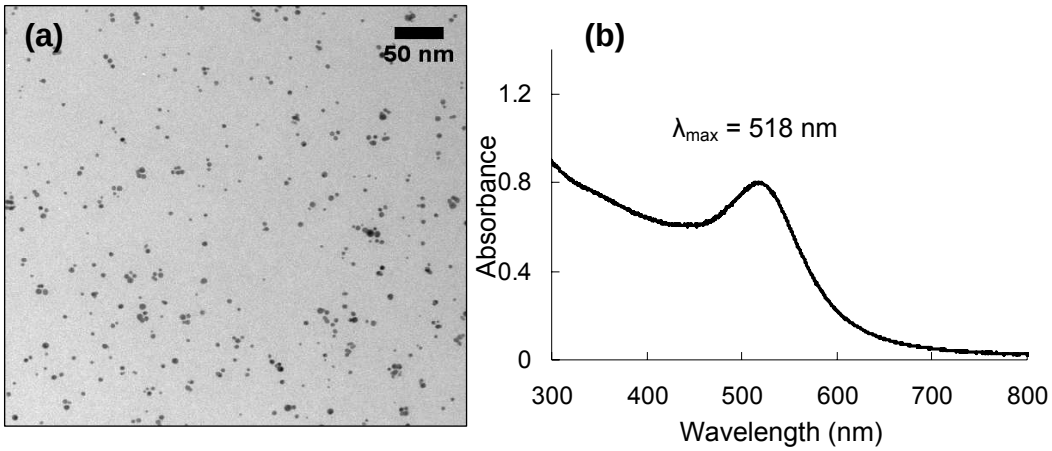

Figure 25. TEM image (a) and UV-visible spectrum (b) of citrate-capped AuNSs **139** (4.5±1.4 nm).

Displacement of Citrates with Carbohydrate Conjugates

Having prepared a variety of citrate-capped gold nanospheres, the study of a displacement reaction of citrate-caps on the surface of gold nanospheres with glycoconjugates was undertaken. As an initial study, a solution of glucosyl thioctianamide **78** in water was mixed with the solution of citrate-capped AuNSs (Table 7, entry 4, ca. 16 nm) (Scheme 20).

Scheme 20

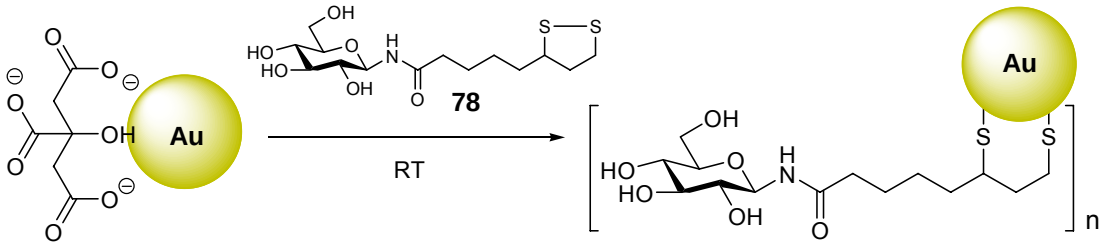

ca. 16 nm (Table 1, entry 4)

Upon mixing two solutions, the solution color suddenly turned blue, and gold nanospheres precipitated. The resulting black suspension was stirred at room temperature for 3 days. During this time, the black suspension disappeared and the solution gradually recovered a red color (Figure 26). The glucose-AuNSs **140** were then purified by a centrifugal filtration, followed by a size exclusive column chromatography (SEC). Galactose-AuNSs **141**, mannose-AuNSs **142**, and lactose-AuNSs **143** were prepared by an analogous process.

Figure 26. Monitoring the displacement reaction of citrate-capped AuNSs (Table 7, entry 4, 16 nm) with glucosyl thioctanamide **78** as a function of time.

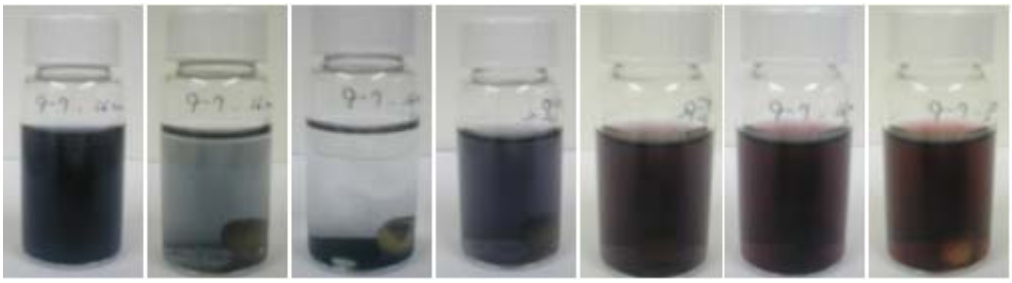

As mixed | 90 min | 90 min[a] | 22 h | 30 h | 50 h | 72 h

[a] The reaction vial was removed from the stirrer and allowed to sit for 1 min. All the particles were settled out of solution.

The absorption spectra (Figure 27) of glucose-AuNSs **140** and lactose-AuNSs **143** showed that the displacement of citrate-caps with glycoconjugates resulted in a small

shift of λ_{max} (from 520 nm to 524 nm), indicating a change in the dielectric property of the particle surface due to the presence of the thiolated glycoconjugates.[124]

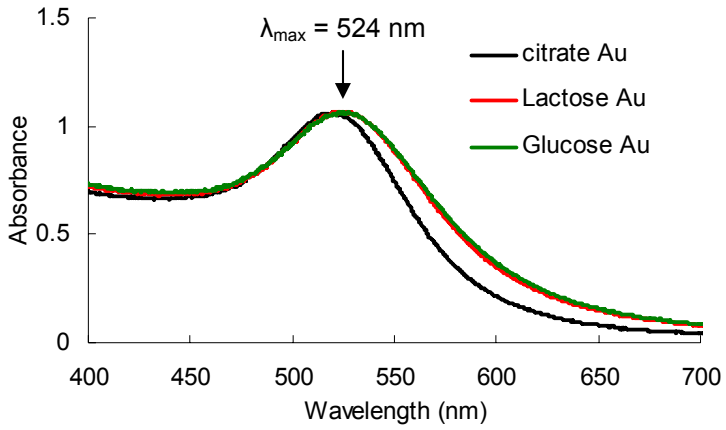

Figure 27. UV-visible absorption spectra of 16 nm citrate-capped AuNSs, glucose-AuNSs **140**, and lactose AuNSs **143**.

The preparation of glucose-AuNSs **144** and lactose-AuNSs **145** with 4.5 nm diameters were accomplished by the displacement reaction described above with the citrate-capped AuNSs **139**.

Bioassay of Carbohydrate-Functionalized Gold Nanospheres using Lectins

Following the successful preparation of carbohydrate-functionalized gold nanospheres by the displacement reaction of citrate-capped gold nanospheres with thiolated glycoconjugates, attention turned toward investigating the bioavailability of carbohydrate-functionalized gold nanospheres. While we had demonstrated that the surface of gold nanospheres could be functionalized with glycoconjugates, there was no evidence available on how these materials were oriented on the surface. Base on our previous studies on gold films reported in Appendix, it was anticipated that the conjugates were oriented "away from the surface" as was observed in self-assembled

monolayers (SAMs). If this were the case, then it was expected that lectin binding to the nanospheres would occur, leading to aggregation. On the other hand, if the glycoconjugates were to "lay on the surface", it was anticipated that aggregation would not occur (Scheme 21).

Scheme 21

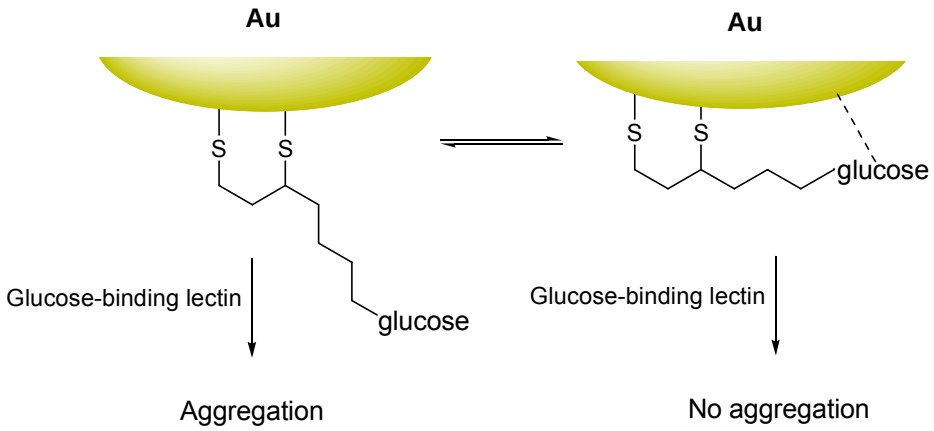

Lectins are carbohydrate-binding proteins that are widely distributed in nature, including microorganisms, plants and animals. Lectins presented on the cell surface play roles as receptors to mediate cell-cell interactions by the recognition of carbohydrates on apposing cells.[133,134] A lectin, concanavalin A (Con A) binds selectively to the monosaccharides mannose and glucose and to polysaccharides with terminal glucose or mannose residues.[135,136] Another lectin, peanut agglutinin (PNA) binds selectively to the monosaccharide galactose and to oligosaccharides with terminal galactose residues.[137,138] Both of lectins are homotetramers at physiological pH, and each monomer possesses one saccharide binding site.[139-141] Thus, it is anticipated that they would bind multiple carbohydrates and result in aggregation, followed by precipitation if there are corresponding carbohydrate-functionalized gold nanospheres (Scheme 22).

Scheme 22

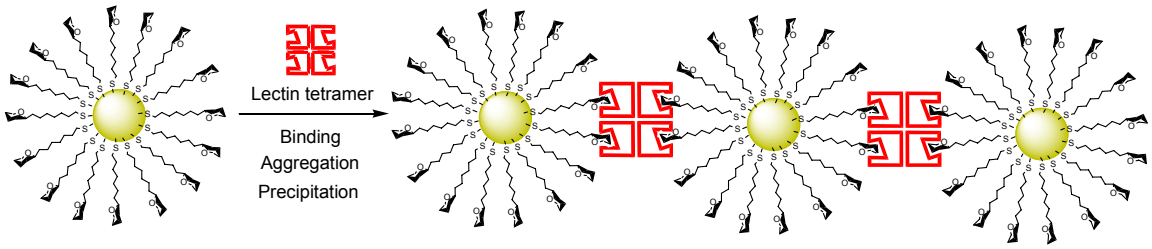

When Con A was added into a solution of glucose-AuNSs **144** (4.5 nm-diametered), aggregation occurred and completely settled out of solution within 2 h (Figure 28a). TEM images (Figure 28b, 28c, and 28d) show Con A-induced aggregation of glucose-AuNSs **144**. Before addition of Con A, the particles were dispersed on the grid (Figure 28b). Upon addition of Con A, aggregation occurred and the particles were brought together to form networks (Figure 28c and 28d). Similarly, PNA-induced aggregation of lactose-AuNSs **145** is shown in the second row of Figure 28.

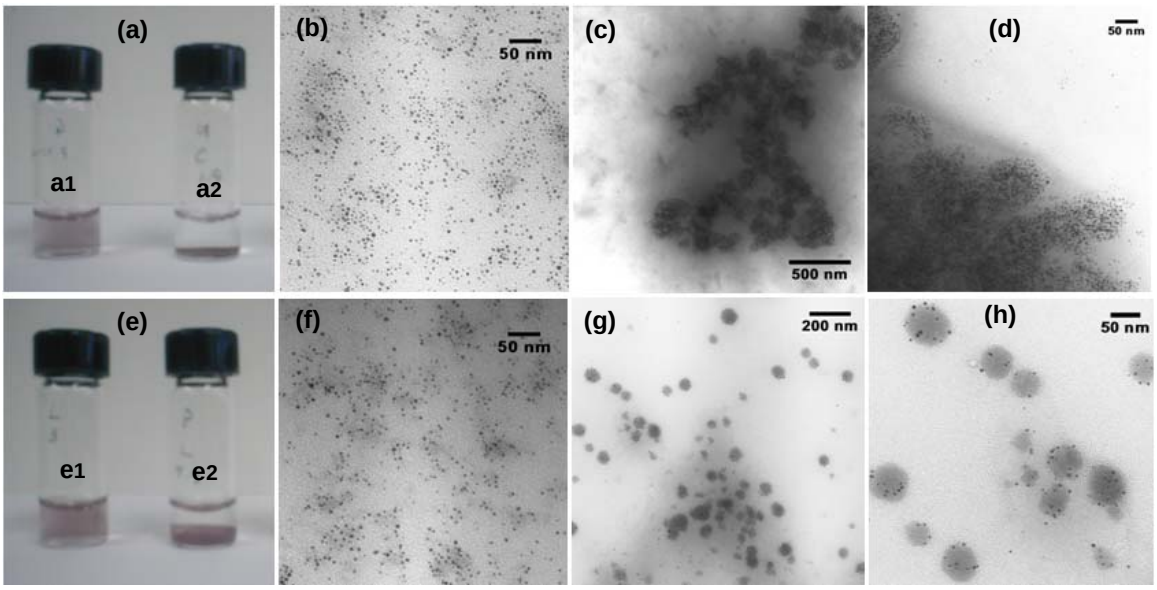

Figure 28. Photographs and TEM images of lectin-induced aggregation. (a1) photograph of glucose-AuNSs **144** and (a2) 2 h after addition of Con A (1.0 μM). (b) TEM image of glucose-AuNSs **144**. (c) 30 min after addition of Con A (1.0 μM) and (d) magnification of (c). (e1) photograph of lactose-AuNSs **145** and (e2) 2 h after addition of PNA (4.0 μM). (f) TEM image of lactose-AuNSs **145**. (g) 30 min after addition of PNA (4.0 μM) and (h) magnification of (g).

Aggregation depended on the concentration of Con A added. Figure 29a shows UV-visible absorption spectra for the aggregation of glucose-AuNSs **144** as a function of Con A concentration. As the concentration of Con A increased, the SPR band shifted toward longer wavelengths and the turbidity increased due to the scattering induced by aggregates.[142]

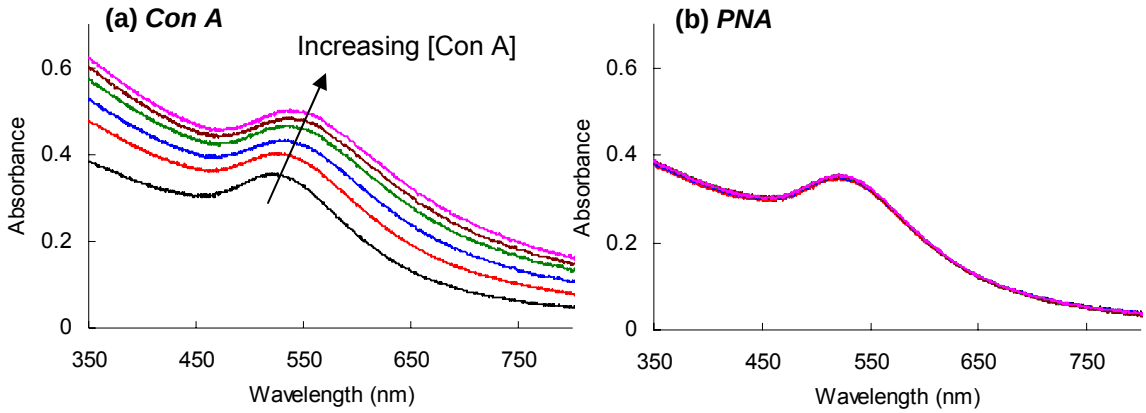

Figure 29. Changes in the UV-visible spectra of glucose-AuNSs **144** on addition of different concentration of (a) Con A and (b) PNA. From bottom to top, 0, 0.1, 0.2, 0.3, 0.4, and 0.5 μM of lectins. Spectra were obtained 40 min after addition of lectins.

The task remaining was to confirm whether the aggregation was induced by the specific recognition of Con A to glucose residues on the surface of gold nanospheres, rather than electronic interactions. Therefore, control experiments were performed with PNA possessing galactose specificity. When different concentrations of PNA were added into a suspension of the glucose-AuNSs **144**, no change in the UV-visible absorption spectra were observed (Figure 29b), indicating that there is no aggregation in the presence of PNA. An analogues set of experiments using lactose-AuNSs **145** with Con A gave no aggregation.

CONCLUSIONS AND OUTLOOK

The preparation and surface functionalization of gold nanospheres with carbohydrates have been achieved by two methods: (1) *in-situ* reduction of gold salt in the presence of glycoconjugates to provide ca. 2 nm particles and (2) a stepwise method where glycoconjugates were self-assembled on the surface of pre-formed, citrate-capped gold nanospheres to provide nanospheres with diameters of 15-73 nm. Bioactivity of the carbohydrates on the surface of gold nanospheres has been demonstrated using agglutination assays. These results indicate that gold nanospheres display multiple presentations of carbohydrates, and the carbohydrates on the gold surface preserve their function.

The development of cellular probes to detect pathogens utilizing glycosylated gold nanospheres is underway with collaboration of the Stein group (Department of Cell Biology and Molecular Genetics, UMCP). The initial results show their potential. Lactose-AuNSs **138** (mean diameter, 1.5 nm) *in vitro* targeted *Neisseria gonorrhoeae*, which is a human pathogen causing gonorrhea, and the pathogen was visualized under a conventional optical microscopy owing to the enhanced scattering of AuNSs **138** bound on the pathogen.

In addition, bis-functionalized gold nanoparticles serve as the basis of TRIAD, a novel vaccine system. Immunized mice with a gold nanosphere-based vaccine (TRIAD) composed of an oligosaccharide derived from *N. gonorrhoeae* and a synthetic peptide (PADRE) showed no observable adverse effects and generated significant levels of IgG response after a single immunization. Further research for the vaccine development is also underway.

EXPERIMENTAL SECTION

General. All chemicals were purchased from commercial suppliers and used without further purification unless noted otherwise. MilliQ water (Millipore, 18 MΩ) was used throughout.

Instrumentation. UV-visible absorption spectra were recorded using an Ocean Optics USB 2000 Spectrometer. **Transmission electron microscopy (TEM)** measurements were performed using a ZEISS EM10 CA. Samples for TEM analysis were prepared by drop casting 5 μL of the sample onto a formvar coated copper grid. Images were recorded on film and scanned from the negatives. Particle sizes and distributions were analyzed using Image J.[143] **Infrared spectra** were recorded on a Nicolet 5DXC FT-IR spectrophotometer. Band positions are given in reciprocal centimeters (cm^{-1}) and relative intensities are listed as br (broad), s (strong), m (medium) or w (weak). **X-ray photoelectron spectroscopy (XPS)** measurements were performed on a Kratos AXIS 165 spectrometer. The samples were prepared by the direct deposition of gold nanospheres onto a carbon tape.

Preparation of Carbohydrate-Functionalized Gold Nanospheres

Via Sodium Borohydride Reduction in the Presence of Carbohydrate Conjugates

General procedure: A solution of glycoconjugate (12 mM, 3 equiv) in MeOH was added into a solution of $HAuCl_4 \cdot 3H_2O$ (25 mM, 1 equiv) in H_2O. Under vigorous stirring at room temperature, a freshly prepared aqueous solution of $NaBH_4$ (1.0 M, 22 equiv) was added to form a dark suspension. The resulting suspension was stirred at room temperature for 3 h. The solvent was evaporated *in vacuo* below 40 ºC. The residue was

dissolved in H_2O and purified by centrifugal filtration (Centriplus YM-30, MWCO = 30kD). This process was repeated three times until the nanoparticles were free of starting glycoconjugate (checking by TLC). The aqueous residue in the Centriplus filter was collected and precipitated by addition of MeOH. The precipitated gold nanospheres were centrifuged and resuspended (by vortexing) in MeOH. This process was also repeated three times, decanted, and dried *in vacuo* to afford gold nanospheres as a dark-brown solid.

Glucose-AuNSs 135. AuNSs **135** were prepared following the general procedure using β-glucosyl thioctanamide **78** (44 mg, 0.12 mmol), $HAuCl_4 \cdot 3H_2O$ (16 mg, 0.040 mmol) and $NaBH_4$ (33 mg, 0.88 mmol). After purification, 15 mg of glucose-AuNSs **135** (1.8 nm, mean diameter) was obtained as a dark-brown solid: IR (KBr, cm^{-1}) 3410 (br), 2919 (w), 1650 (m, amide I band), 1539 (m, amide II band), 1409 (w), 1076 (s).

Lactose-AuNSs 136. AuNSs **136** were prepared following the general procedure using β-lactosyl thioctanamide **81** (64 mg, 0.12 mmol), $HAuCl_4 \cdot 3H_2O$ (16 mg, 0.040 mmol) and $NaBH_4$ (33 mg, 0.88 mmol). After purification, 6 mg of lactose-AuNSs **136** (1.9 nm, mean diameter) was obtained as a dark-brown solid: IR (KBr, cm^{-1}) 3374 (br), 2920 (w), 1654 (m, amide I band), 1540 (m, amide II band), 1414 (w), 1073 (s).

Glucose-AuNSs 137 and **lactose-AuNSs 138** were prepared following the general procedure except for the concentration of tetrachloroauric acid (30 mM used instead of 25 mM) and purification procedures.

Glucose-AuNSs 137. To a solution of β-glucosyl thioctanamide **78** (16.2 mg, 44.1 μmol) in H_2O was added a solution of $HAuCl_4$ (5.00 mg, 14.7 μmol) in H_2O. Under vigorous

stirring at room temperature, a freshly prepared aqueous solution of $NaBH_4$ (12.2 mg, 0.323 mmol) was added, and the resulting solution was stirred at room temperature for 2 h. The solution was neutralized by adding an aqueous solution of HCl (0.2 M) and then purified using size exclusive column chromatography (GE Healthcare, PD-10, Sephadex-G25 medium). The suspension of glucose-AuNSs **137** was stored at 4 ^{o}C. TEM analysis (Mean ± std dev): 1.7 ± 0.6 nm.

Lactose-AuNSs 138 were prepared following the procedure described above using β-lactosyl thioctanamide **81** (23.4 mg, 44.1 μmol), $HAuCl_4$ (5.00 mg, 14.7 μmol) and $NaBH_4$ (12.2 mg, 0.323 mmol). TEM analysis (Mean ± std dev): 1.5 ± 0.4 nm.

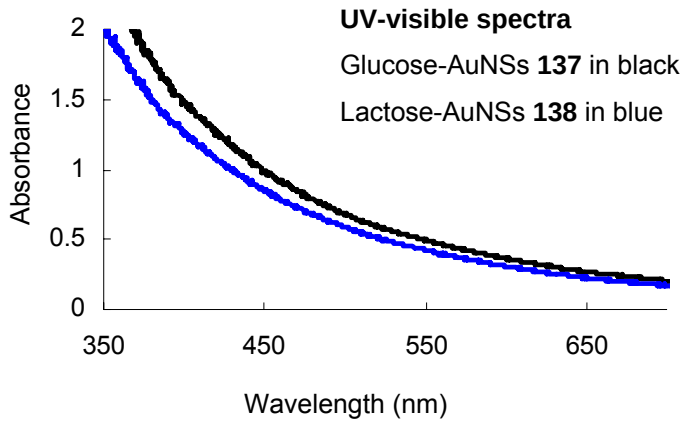

Figure 30. UV-visible absorption spectra of AuNSs **137** and **138**.

A General Procedure for the Preparation of Citrate-Capped Gold Nanospheres with a Mean Diameter Ranging from 15 nm to 73 nm is as follows: an aqueous solution of sodium citrate dihydrate (given mL, 0.340 M) was added into a boiling solution of $HAuCl_4$ (100 mL, 1.47 mM in H_2O). In few seconds, the color of the boiling solution changed from a light yellow to a corresponding color (typically deep red, see the experimental data below), indicating the formation of gold nanospheres. The reaction

mixture was refluxed for 20 min and then cooled at room temperature. The particle suspension was stored at 4 ^{o}C. The experimental data is shown below.

Experimental data for the preparation of citrate-capped gold nanospheres.

entry	citrate amount (mL)	particle size (nm)	solution color	SPR absorption at λ_{max}	particle concentration (nM)
1	0.5	73.2 ± 18.6	Brown	540 nm	-
2	1.0	28.3 ± 5.7	Purple	524 nm	1.54
3	1.5	18.1 ± 2.2	Dark red	520 nm	6.63
4	2.0	15.8 ± 1.6	Dark red	520 nm	10.1
5	3.0	15.3 ± 1.3	Dark red	520 nm	11.1
6	4.0	aggregated	-	-	-

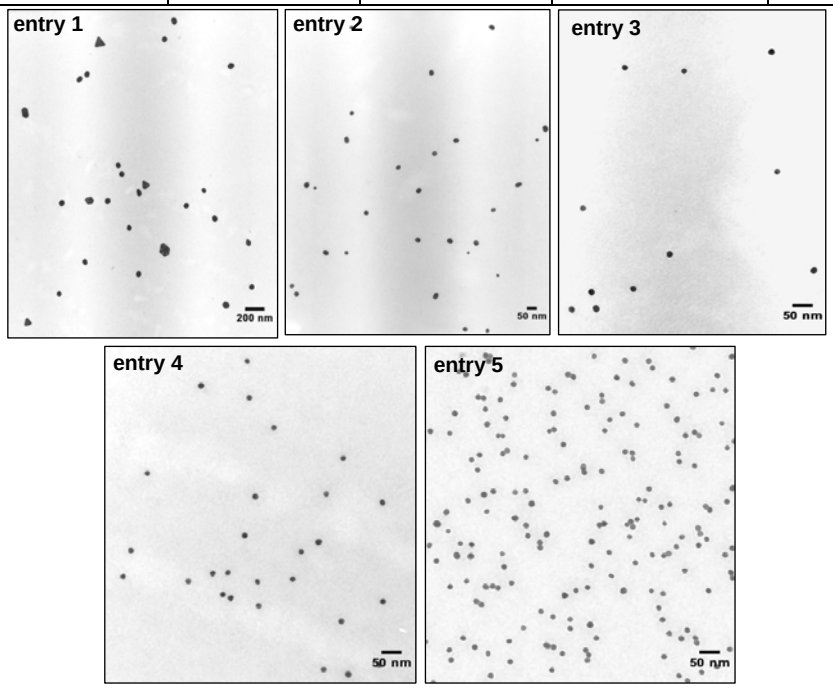

Figure 31. TEM images of citrate-capped gold nanospheres.

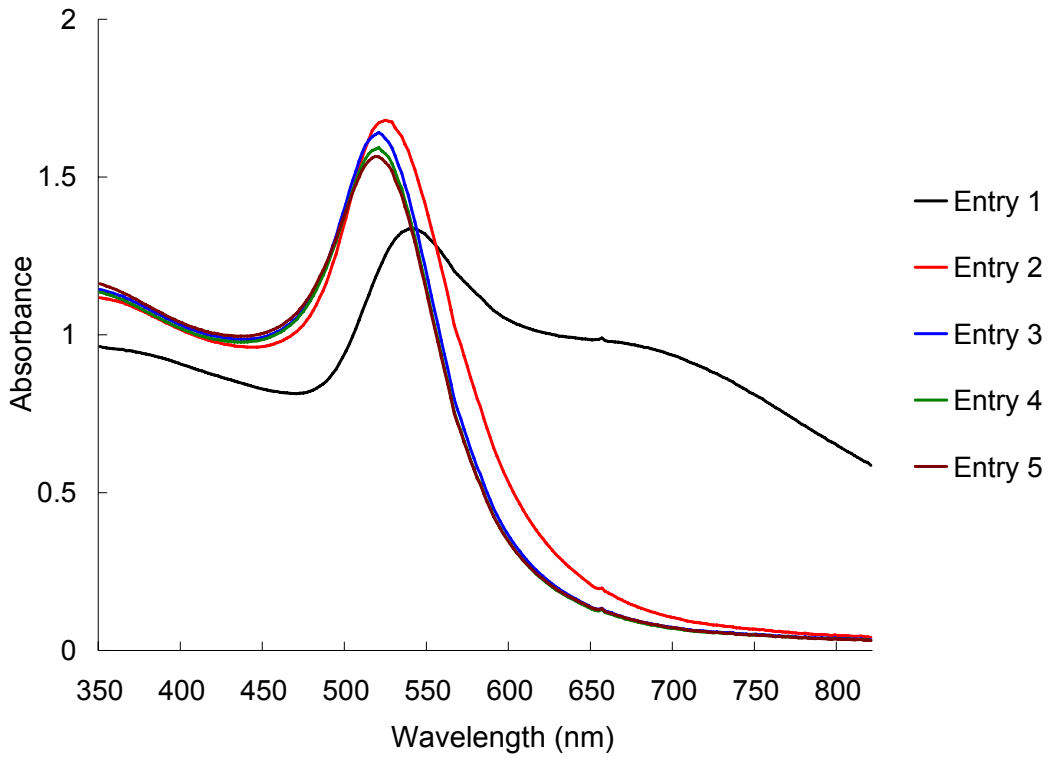

Figure 32. UV-visible spectra of citrate-capped AuNSs. The sample was prepared by diluting 1 mL of each particle solution with 2 mL of water.

Citrate-capped gold nanospheres 139 with a mean diameter of 4.5 nm. A solution of $HAuCl_4$ (1.00 mL, 29.4 mM in H_2O, Alfa Aesar) was added into 90.0 mL of H_2O at room temperature. After being stirred for 1 min, a solution of sodium citrate (2.00 mL, 38.8 mM in H_2O) was added, followed by a fresh solution of $NaBH_4$ (1.00 mL, 0.0750 % in 38.8 mM of sodium citrate). The red-colored solution was stirred for 10 min and stored at 4 ^oC.

A General Procedure for the Displacement of Citrate-Caps on the Gold Nanospheres (Table 7, entry 4) with Glycoconjugates is as follows: To an aqueous solution of glycoconjugates (10.0 mL, 1.58 mM in H_2O) was added a solution of citrate-capped gold nanospheres (5.00 mL, Table 7, entry 4). The resulting mixture was stirred at room temperature until a deep red color of the solution was observed. Typically, the

displacement reaction took 2 - 3 days to completely replace citrates. The particle solution was then purification by centrifugal filtration (Centriplus YM-30, MWCO = 30kD, repeated two times with pure water) and a size exclusive column chromatography (GE Healthcare, PD-10, Sephadex-G25 medium). Finally, carbohydrate-functionalized gold nanospheres were stored at 4 ^{o}C.

Glucose-AuNSs 140 (16 nm as a mean diameter) were prepared with citrate-capped gold nanospheres (5.0 mL, Table 7, entry 4) and glucosyl thioctanamide **78** (10 mL, 1.58 mM).

Galactose-AuNSs 141 (16 nm, mean diameter) were prepared with citrate-capped gold nanospheres (5.0 mL, Table 7, entry 4) and galactosyl thioctanamide **79** (10 mL, 1.58 mM).

Mannose-AuNSs 142 (16 nm, mean diameter) were prepared with citrate-capped gold nanospheres (5.0 mL, Table 7, entry 4) and mannosyl thioctanamide **80** (10 mL, 1.58 mM).

Lactose-AuNSs 143 (16 nm, mean diameter) were prepared with citrate-capped gold nanospheres (5.0 mL, Table 7, entry 4) and lactosyl thioctanamide **81** (10 mL, 1.58 mM).

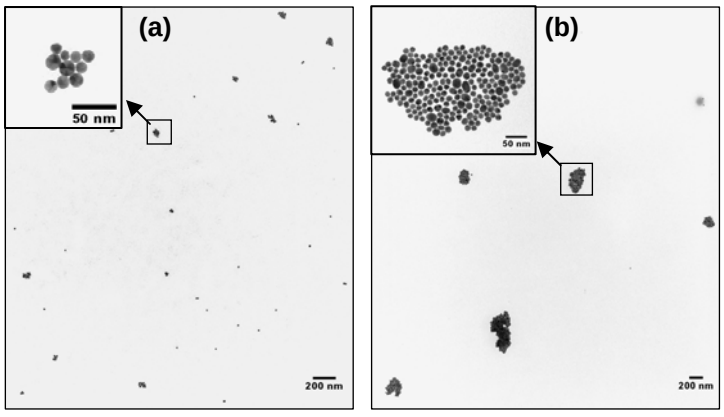

Figure 33. TEM images of (a) glucose-AuNSs **140** and (b) lactose- AuNSs **143**.

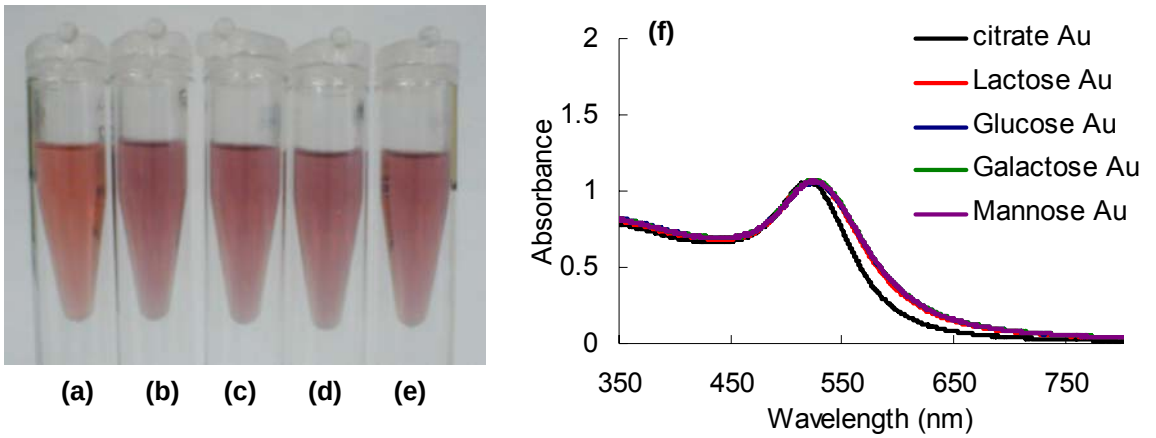

Figure 34. Photographs of (a) citrate-capped AuNSs (Table 7, entry 4), (b) glucose-AuNSs **140**, (c) galactose-AuNSs **141**, (d) mannose-AuNSs **142**, (e) lactose-AuNSs **143**, and (f) UV-visible spectra of individual particle suspension.

A General Procedure for the Displacement of Citrate-Caps on the Gold Nanospheres III-39 (4.5 nm as mean diameter) with Glycoconjugates is as follows: To a solution of glycoconjugates [3.0 mL, 5.4 mM in HEPES buffer (20 mM, pH = 7.4)] was added a suspension of citrate-capped gold nanospheres **139** (10 mL). The resulting mixture was stirred at room temperature for 2 days. The particle suspension was then purified by centrifugal filtration (Centriplus YM-30, MWCO = 30kD, repeated two times with pure water) and a size exclusive column chromatography (GE Healthcare, PD-10, Sephadex-G25 medium). Finally, carbohydrate-functionalized gold nanospheres were diluted with pure water with a total volume of 10 mL and stored at 4 ^{o}C for the lectin binding study.

Glucose-AuNSs 144 (4.5 nm, mean diameter) were prepared using citrate-capped gold nanospheres (10 mL) and glucosyl thioctanamide **78** (10 mL, 5.4 mM): IR (drop-casting on CaF_2, cm^{-1}) 3332 (br), 2922 (s), 1661 (m, amide I band), 1540 (m, amide II band), 1248 (m).

Lactose-AuNSs 145 (4.5 nm, mean diameter) were prepared using citrate-capped gold nanospheres (10 mL) and lactosyl thioctanamide **81** (10 mL, 5.4 mM): IR (drop-casting on CaF_2, cm^{-1}) 3334 (br), 2924 (s), 1660 (m, amide I band), 1543 (m, amide II band), 1375 (w).

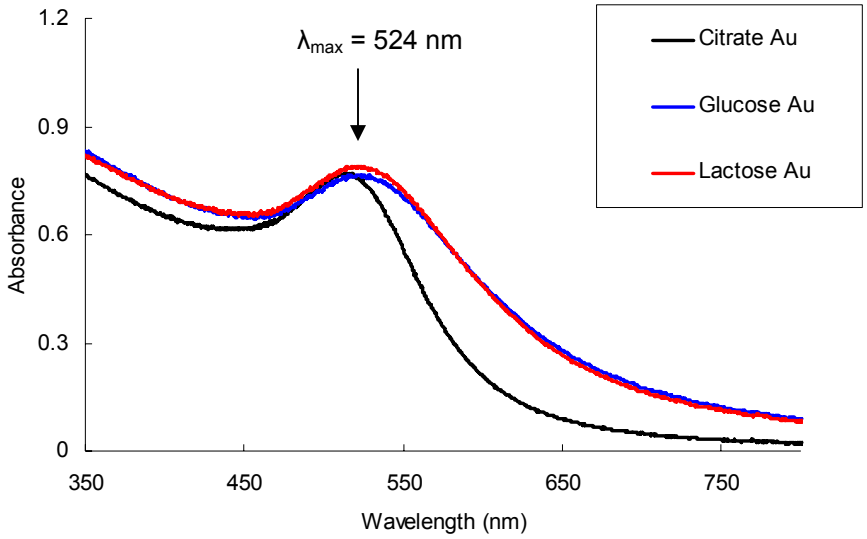

Figure 35. UV-visible absorption spectra of citrate-capped AuNSs, glucose-AuNPs **144**, and lactose-AuNSs **145**.

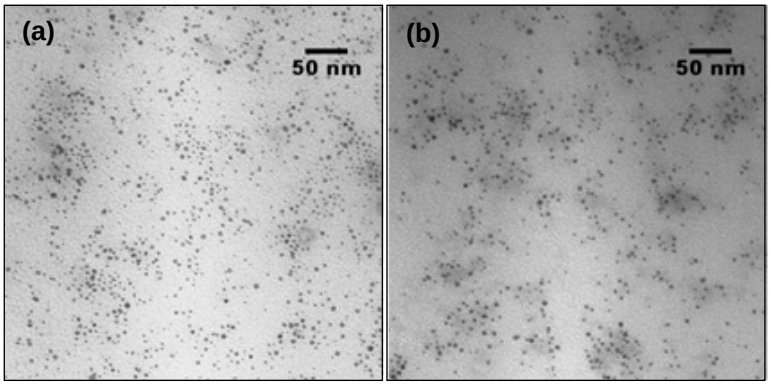

Figure 36. TEM images of (a) glucose-AuNPs **144** and (b) lactose-AuNSs **145**.

Agglutination Assay

Concanavalin A (Con A, Type V, lyophilized power), peanut agglutinin (PNA, lyophilized power), HEPES, and all other reagents were obtained from Sigma. For the preparation of lectin stock solution, the lectin was dissolved in HEPES-buffered saline ([HEPES 10 mM, NaCl 150 mM, $CaCl_2$ 1 mM, $MnCl_2$ 1 mM, and $MgCl_2$ 1 mM adjusted to pH 7.4]), incubated at room temperature overnight, and then syringe-filtered (0.22 μm). The concentration of the stock solution was determined from the absorbance at 280 nm (A_{280} = 1.37 × [mg/mL Con A],[144] A_{280} = 0.96 × [mg/mL PNA][145]). The solution was then diluted to given concentrations (based on Con A tetramer at 104 kDa, PNA tetramer at 110 kDa). The suspension of gold nanospheres (glucose-AuNSs **144** and lactose-AuNSs **145**) was exchanged from water to HEPES-buffered saline by centrifugal filtration (Centriplus YM-30, MWCO = 30kD with a total volume of 10 mL. ***For the specific binding assay:*** the suspension of carbohydrate-functionalized gold nanospheres (0.5 mL) was added to the lectin solution (0.5 mL at 0, 2, 4, 6, 8, and 10 μM, respectively). This assures that the pH and ionic strength are the same in all experiments and only the lectin concentration changes. The samples were incubated at room temperature for 40 min, and UV-visible absoption spectra of each sample solution were recorded. ***For the TEM experiment***: each suspension of gold nanospheres (0.5 mL, **144** or **145**) was mixed with a corresponding lectin solution (0.5 mL, 1.0 μM). After incubation at room temperature for 20 min, 5 μL took out of each mixture, loaded on TEM grid, and dried for measurement.

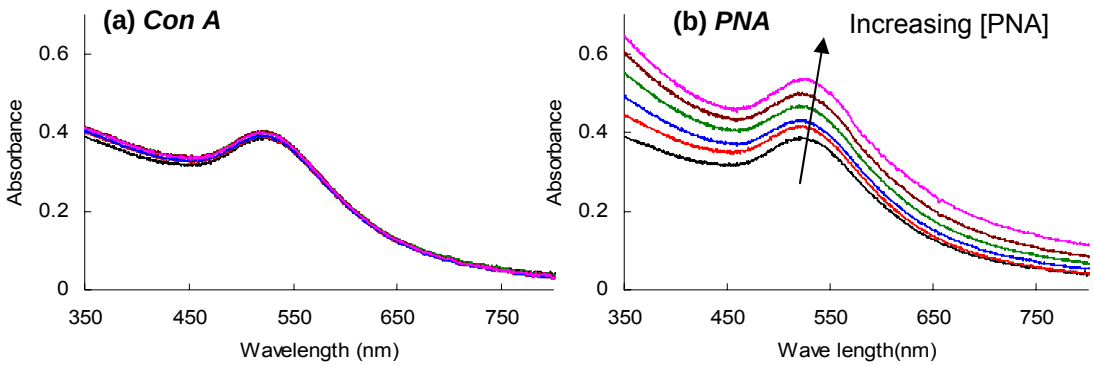

Figure 37. Changes in the UV-visible spectra of lactose-AuNSs **145** on addition of different concentration of (a) Con A and (b) PNA. From bottom to top, 0, 0.1, 0.2, 0.3, 0.4, and 0.5 μM of lectins. Spectra were obtained 40 min after addition of lectins.

Chapter 4: Preparation and Characterization of Carbohydrate-Functionalized Surfactant Vesicles for the Targeted Delivery of Drugs

This chapter is related to the article published in Soft Matter ***2008****, 4, 1916-1921.*

INTRODUCTION

In the clinical use, it is ideal that a drug has a high therapeutic index, which is the ratio of the drug's efficacy over the its toxicity (side effects). However, many drugs, particularly chemotherapeutic drugs, have low therapeutic indices due to their side effects. One of the means being explored to achieve the improvement of therapeutic indices of drugs is targeted delivery, where drugs are delivered to selected cells, effectively reducing their toxic effects to normal cells. For this purpose, phospholipid-based vesicles, *i.e.* liposomes, are full of promise due to their huge inside cavity in which toxic drugs can be entrapped and delivered to the selected cells.

Liposomes were discovered by Bangham and co-workers roughly 40 years ago[146] and have been evolved to increase the circulation time by coating a protective layer such as polyethylene glycol (PEG) over the liposome surface.[37,147] Targeting of liposomes *in vivo* has been accomplished by modifying the bilayer surface with targeting agents such as antibodies, folates, transferrins, carbohydrates, or arginine-glycine-aspartic acid (RGD) analogs, thereby directing the drug toward a specific tissue type.[36-38,147,148-150] Depending on the permeability and stability of the liposome *in vivo*, the drug solute may be released slowly and continually or it may be released rapidly in response to a specific stimulus, which allows ‘‘controlled-release’’ of a drug.[151] Liposomal formulations approved for clinical use include Doxil, DepoCyt and DaunoXome for cancer chemotherapeutic drugs, DepoDur for morphine and

Ambisome for antifungal agent.[37,152]

In spite of their excellent performance, a major drawback of liposomal formulations is the inherent instability, expense, and difficulty of preparation associated with phospholipid-based vesicles. Liposomes formed by sonication or extrusion are essentially kinetically-trapped, nonequilibrium structures, that tend to fuse or rupture to form lamellar phases. In the fusion process, the contents of the phospholipid vesicles are released. Typically, this fusion process and premature release of the payload can be avoided by changing bilayer composition.[153-155]

A simple attractive alternative to phospholipid vesicles was offered by Kaler and co-workers in 1989.[156] In this system (Figure 38), surfactant vesicles are spontaneously produced by simply mixing a cationic surfactant (CTAT: cetyltrimethylammonium tosylate) and an anionic surfactant (SDBS: sodium dodecylbenzenesulfonate) with water in the right proportion.[157-159] These vesicles are approximately 120 nm in mean diameter with bilayer thickness of 2.5 nm.[160]

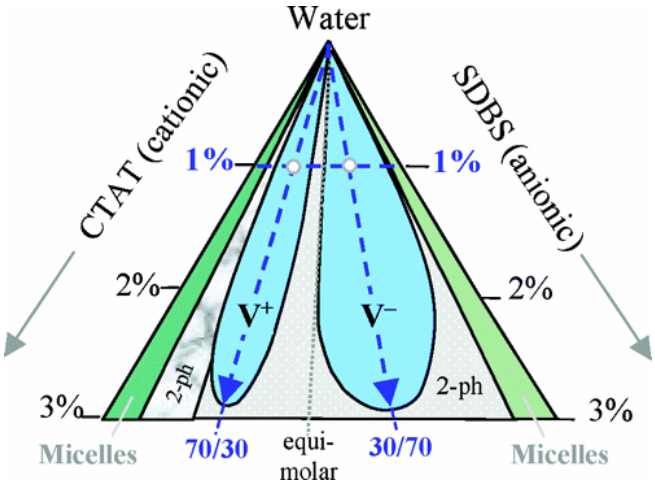

Figure 38. Phase diagram of CTAT/SDBS/H_2O system at 25 ^oC. Vesicles are present in the two lobes, denoted by V^+ for CTAT-rich vesicles and V^- for SDBS-rich vesicles. The bottom axis is weight ratio of two surfactants and the side axes indicate a total concentration (wt %) of the two surfactants in H_2O. Adapted from ref. 161.

In order to prepare 1 wt % of SDBS-rich vesicles (Scheme 23), for example, each surfactant (30 mg of CTAT and 70 mg of SDBS) is weighed and mixed with 9.9 mL of H_2O, followed by gentle stirring at room temperatuer for 30 min. Finally, the resulting mixture allows to equilibrate at room temperature for at least 48 h to generate thermodynamically stable surfactant vesicles.

Scheme 23

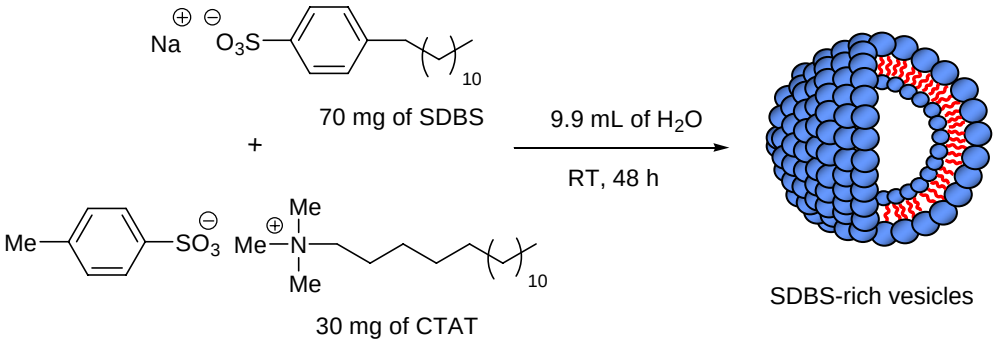

Surfactant vesicles have several advantages over liposomes including lower cost, ease of preparation and stability. Vesicle formation under these conditions is spontaneous and fairly rapid and yields vesicles that are thermodynamically stable. Furthermore, the required materials for vesicle formation are readily available surfactants that are cheaper than purified or synthetic phospholipids. It is also possible to prepare vesicles that present different surface charge by changing the ratio of CTAT/SDBS (Figure 38).

The surface functionalization of vesicles produced by the CTAT/SDBS system was reported by Walker and Zasadzinski.[162] They prepared biotin-functionalized surfactant vesicles by mixing CTAT, SDBS, and phospholipid-tethered biotin. The addition of the phospholipid-tethered biotin at low concentration (0.2 mol % of total surfactant) did not disrupt formation of vesicles. Upon addition of streptavidin as a

cross linking receptor, biotin-functionalized vesicles were aggregated.

English and co-workers demonstrated the high efficiency of surfactant vesicles for the capture and long-term storage of charged organic solutes, compared to those of phospholipid vesicles.[161,163] The high carrying capacity of the surfactant vesicles is due to strong electrostatic interactions between the charged vesicle bilayer and the organic solute. The ability of long-term storage is due to the superior stability of surfactant vesicles. For example, CTAT-rich vesicles presenting cationic bilayers captured the anionic solute carboxyfluorescein with high efficiency (21 %) and retained the solute for long periods of time (half-life, $t_{1/2}$ = 84 days). However, phospholipid-based vesicles showed only 1.6 % of capturing efficiency and 2 days (half-life) of retention ability.

The robust nature of vesicles produced by the CTAT/SDBS system was also demonstrated by Kaler and co-workers.[164] They utilized CTAT-rich vesicles as a template to prepare silica hollow spheres. The silica coated vesicles were generated by addition of tetramethoxysilane into the vesicular templates, and then the core vesicles were dissolved in methanol to create hollow structures. During the deposition of silica precusor on the surface of surfactant vesicles, the vesicular structure was retained without disruption.

Raghavan and co-workers reported the transformation of CTAT-rich vesicles into an elastic gel by adding hydrophobically modified chitosan (polysaccharide).[160] In a three-dimensional network (an elastic gel), vesicles and chitosan were connected to each other by insertion of hydrophobic chains in chitosan into vesicle bilayers. Interestingly, the surfactant vesicles remained intact within the networks.

Research in the DeShong group has been focused on the development of nanovehicles for the targeted delivery of drugs utilizing carbohydrate-receptor interactions. The vesicles formed from CTAT/SDBS surfactants are very attractive for the drug delivery because of their hollow structure, size (ca. 120 nm in diameter),[147] stability, and capturing ability. As shown previously in studies using hydrophobically modified chitosan to form a cross-linked vesicle gel,[160] it is possible to functionalize their surface with carbohydrates by simple hydrophobic insertion of long hydrocarbon-modified carbohydrates. Anionic surfactant vesicles formed from SDBS and CTAT with a 3 : 1 molar excess of SDBS would be particularly useful for the selective cellular targeting since non-specific electrostatic interactions of the anionic vesicle with negatively charged cell surface can be avoided.[165]

The goal of research in this section was to prepare carbohydrate-functionalized surfactant vesicles and investigate the bioavailability of carbohydrates on the vesicle surface, as an initial step for the construction of a targeted delivery system utilizing surfactant vesicles.

RESULTS AND DISCUSSION

For these studies, the hydrocarbon-modified glycoconjugates ranging from monosaccharide to trisaccharide were synthesized (Figure 39) as described in Chapter 2.

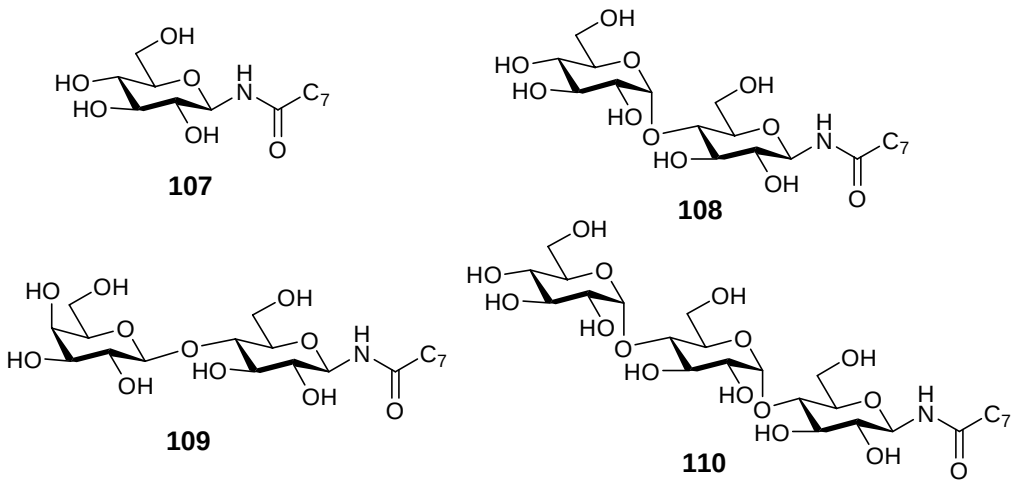

Figure 39. Structures of N-linked glycoconjugates for the surface functionalization of surfactant vesicles: C_8-glucose **107**, C_8-maltose **108**, C_8-lactose **109**, and C_8-maltotriose **110**.

In order to confirm that C_8-glycoconjugates can be incorporated during vesicle formation, the SDBS-rich vesicles consisting of 1 wt % total surfactant with a 7:3 w/w of SDBS to CTAT were prepared in the presence of C_8-glycoconjugates (1 mM in H_2O) (Figure 40). To evaluate the amount of glycoconjugate that associated with the vesicle, size exclusion chromatography (SEC) was used to separate the vesicles from excess conjugate. Once separated, the presence of vesicles and the amount of carbohydrate in the vesicle-containing fractions were determined by dynamic light scattering (DLS) and UV-visible spectroscopy,[166] respectively. The results are summarized in Table 8 and Figure 41.

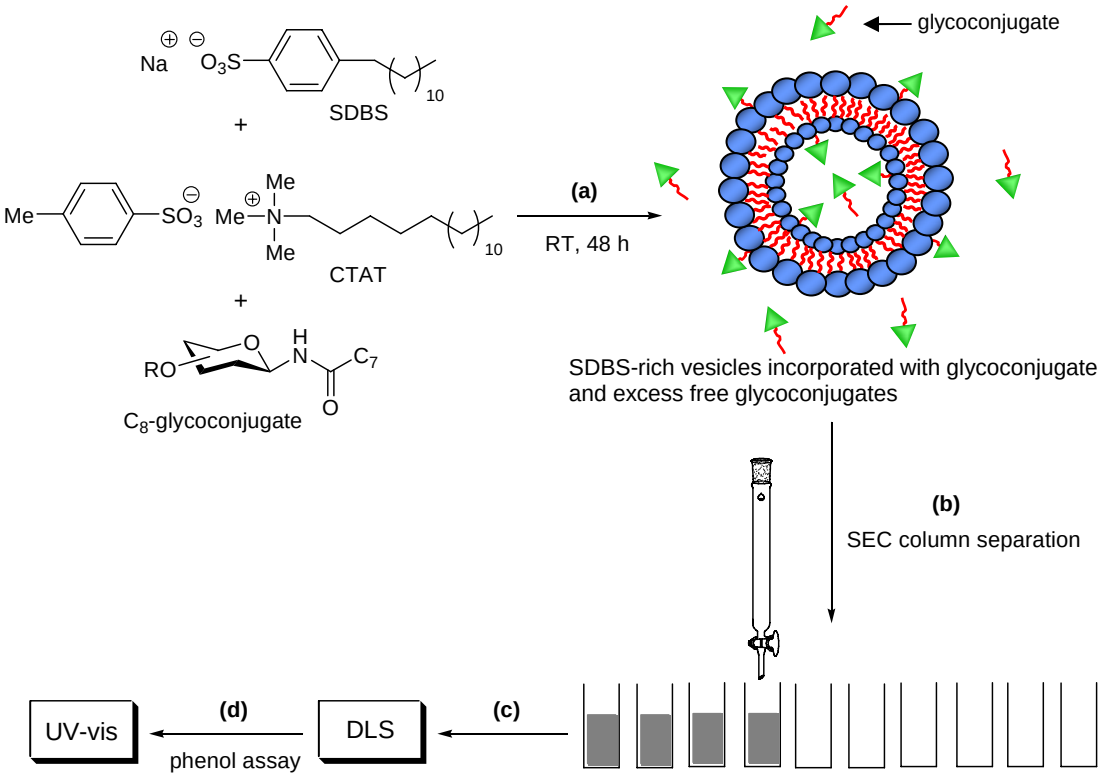

Figure 40. Schematic illustration of the procedure for (a) the preparation of SDBS-rich vesicles, (b) separation of vesicles from the excess glycoconjugates by size exclusion chromatography (SEC), (c) confirmation of vesicle sizes by dynamic light scattering, and (d) determination of carbohydrate contents by UV-visible spectroscopy following phenol-sulfuric acid assay.

Figure 41 shows the results for the glucose and lactose conjugates in SDBS-rich vesicles. In all cases 18-25% of the conjugate eluted with the vesicle fractions. The incorporation values for all conjugates in SDBS-rich vesicles are shown in Table 8. At the incorporation levels summarized in Table 8, the ratio of carbohydrate conjugate to surfactant is approximately 1 : 100. DLS measurements (Table 1) showed that the vesicle sizes were not affected by inclusion of the glycoconjugate at these levels in SDBS-rich samples and remained intact before and after SEC, suggesting the stability of SDBS-rich vesicles.

Table 8. Glycoconjugate vesicle incorporation and DLS results.

Glycoconjugate	Incorporation (%)[a]	Vesicle Radius (nm)[b]	
		Before SEC	After SEC
Bare vesicles	_	70	71
C_8-glucose	18	69	69
C_8-lactose	23	69	72
C_8-maltose	25	67	74
C_8-maltotriose	19	68	72

[a] Incorporation percentage is the fraction of a 1 mM solution of glycoconjugate that elutes with vesicles during SEC. [b] Hydrodynamic radii were determined by DLS before and after SEC. See the experimental section for details.

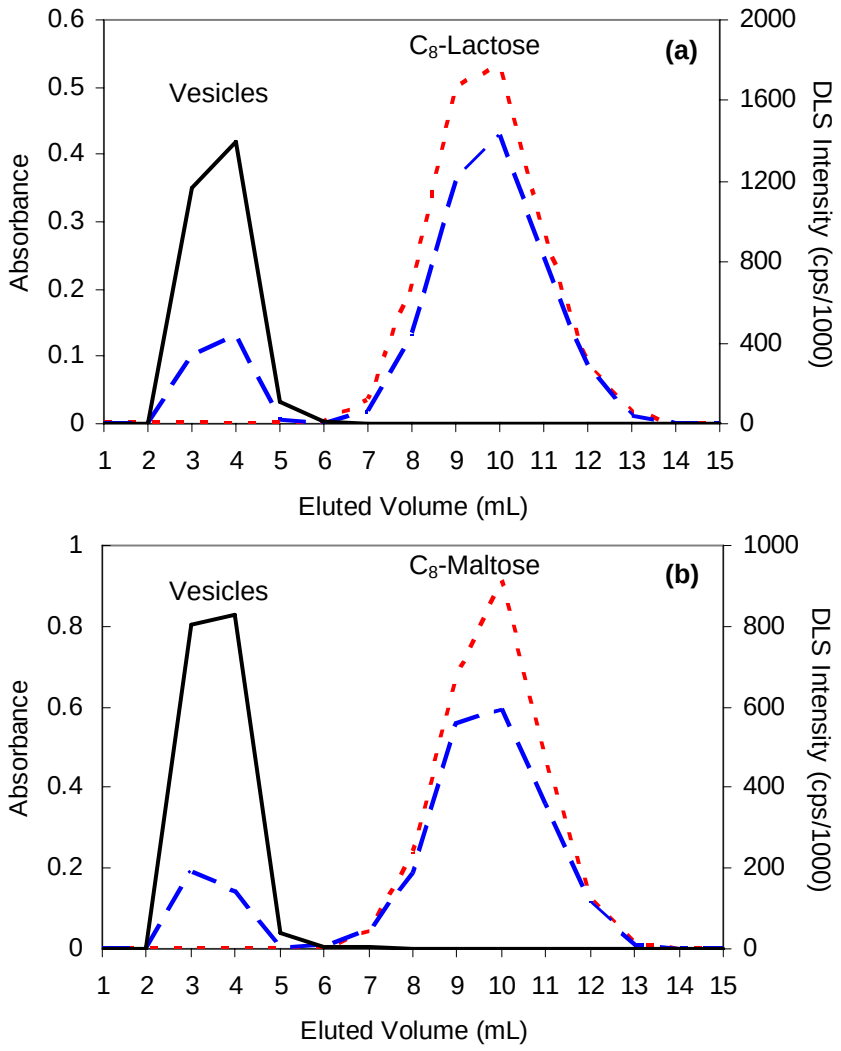

Figure 41. Results from SEC of vesicles with various glycoconjugates: (A) SDBS-rich vesicles prepared with C_8-lactose; (B) SDBS-rich vesicles prepared with C_8-maltose. SEC fractions were evaluated with DLS to identify the vesicle-containing fractions (solid line). Fractions containing carbohydrates were identified with colorimetric detection (dashed line).[166] Samples containing only glycoconjugate (no vesicles) were evaluated with SEC to determine the elution properties of the free compound (dotted line). The apparent incorporation rates (ρ) correspond to the differences in peak areas of the conjugates with and without vesicles present (i.e. dotted line minus dashed line). See the experimental section for details of this analysis.

The task remaining was to confirm whether the carbohydrates introduced into the vesicle are located at the exterior of surfactant vesicles or embedded in the interior of

vesicles. Although the carbohydrates are presented on the surface of vesicles, it is also questionable whether they can serve as targeting entities.

Lectins have high binding specificity for their carbohydrate ligands and are widely distributed in nature, including microorganisms, plants and animals. Lectins presented on the cell surface play roles as receptors to mediate cell-cell interactions by the recognition of carbohydrates on apposing cells.[133,134] A lectin, concanavalin A (Con A) binds selectively to the monosaccharides mannose and glucose and to polysaccharides with terminal glucose or mannose residues.[135,136] Another lectin, peanut agglutinin (PNA) binds selectively to the monosaccharide galactose and to oligosaccharides with terminal galactose residues.[137,138] Both of them are a homotetramer at physiological pH, and each monomer possesses one saccharide binding site.[139-141] Thus, it is anticipated that they would bind multiple carbohydrates and result in aggregation, followed by precipitation if there are corresponding carbohydrate-bearing vesicles (Scheme 24).

Scheme 24

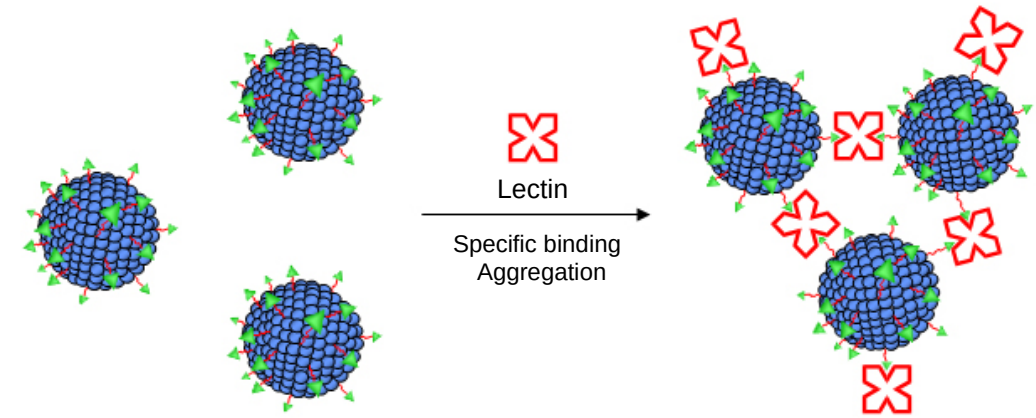

Accordingly, attention turned to the binding assay using lectins to probe for the presence of surface carbohydrate residues. Monitoring lectin-induced turbidity provided a

convenient method to determine the bioavailability of synthetic mannose or glucose-functionalized glycoconjugates.[167-169]

Figure 42a summarizes the results from the Con A aggregation experiments. Bare vesicles and vesicles containing lactosyl conjugate **109** showed no increase in turbidity when titrated with Con A. Conversely, vesicles carrying the glucosyl conjugate **107** had a distinct increase in turbidity with increasing additions of Con A above 2.0 μM. The increase in turbidity was readily visible by eye and is due to aggregation of vesicles that occurs when a Con A tetramer binds one or more glucose residues on different vesicles (Scheme 24). Figure 42b shows an analogous set of experiments using the lectin peanut agglutinin (PNA). As with Con A, the solution turbidity for the three vesicle samples was monitored with increasing PNA concentration. In the case of PNA, an increase in turbidity was observed only in the presence of lactose-functionalized vesicles. Binding of PNA to the terminal galactose of the lactosyl coconjugate induces agglutination in the lactose-bearing vesicles. In both sets of experiments, control samples containing only the C_8-glucosyl conjugate **107** or C_8-lactosyl conjugate **109** gave no change in turbidity with addition of lectins (data not shown). The results outlined in Figure 42 show that amphiphilic glycoconjugates can be used to functionalize surfactant vesicles for recognition by cell surface receptors and represent a promising first step toward targeted delivery using carbohydrate-functionalized surfactant vesicles.

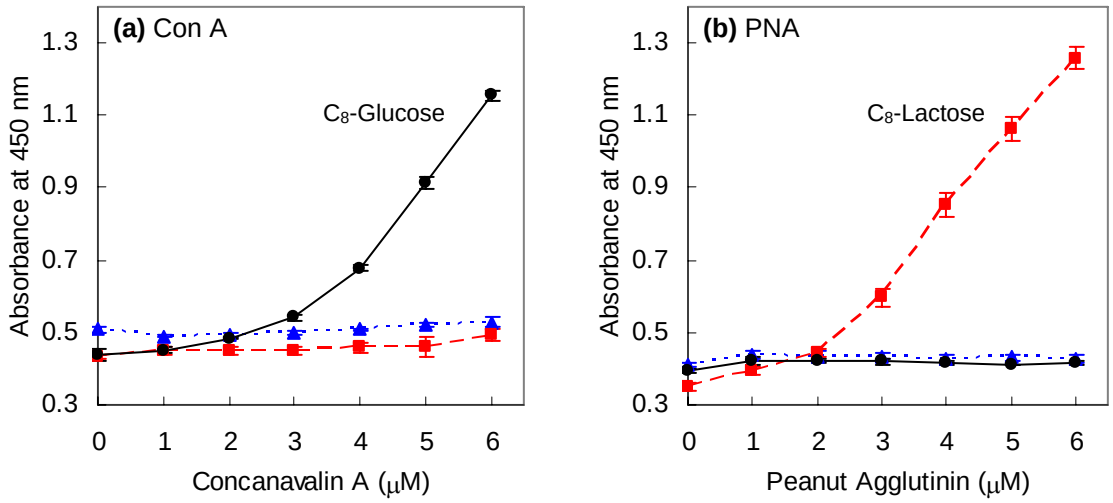

Figure 42. Results from lectin-induced agglutination studies with carbohydrate-functionalized surfactant vesicles. Turbidity was monitored at 450 nm as a function of lectin concentration for samples containing glucose-functionalized vesicles (●), lactose-functionalized vesicles (■) and bare vesicles (▲). Curves shown are the average of three assays. (a) Titration results using Con A. (b) Titration results using PNA. Turbidity was measured 60 min after addition of lectins.

In Figure 42, turbidity increases slightly more rapidly with PNA binding to lactose-functionalized vesicles than with Con A binding to glucose-functionalized vesicles. This difference in agglutination is rationalized by assuming increased accessibility at the bilayer interface of the terminal galactose in the disaccharide lactose relative to the monosaccharide glucose. Others have demonstrated the binding of Con A to glycolipids embedded in phospholipid vesicle membranes and have shown that the binding of Con A to the mannose residues on the liposome surface depends on the length of a water soluble spacer group between the alkyl chains and the carbohydrate head group.[170] To explore the effect of oligosaccharide length on lectin-induced agglutination, we utilized vesicles functionalized with three different glycoconjugates whose terminal residue is glucose: C_8-glucose **107**, C_8-maltose **108** and C_8-maltotriose **110** (Figure 39) and measured their aggregation as a function of

Con A concentration. Figure 43a summarizes the results from these experiments. The vesicles functionalized with maltose conjugate **108**, a disaccharide, shows increased turbidity relative to the vesicles functionalized with glucose conjugate **107**, the monosaccharide analog, indicating stronger binding by the lectin.

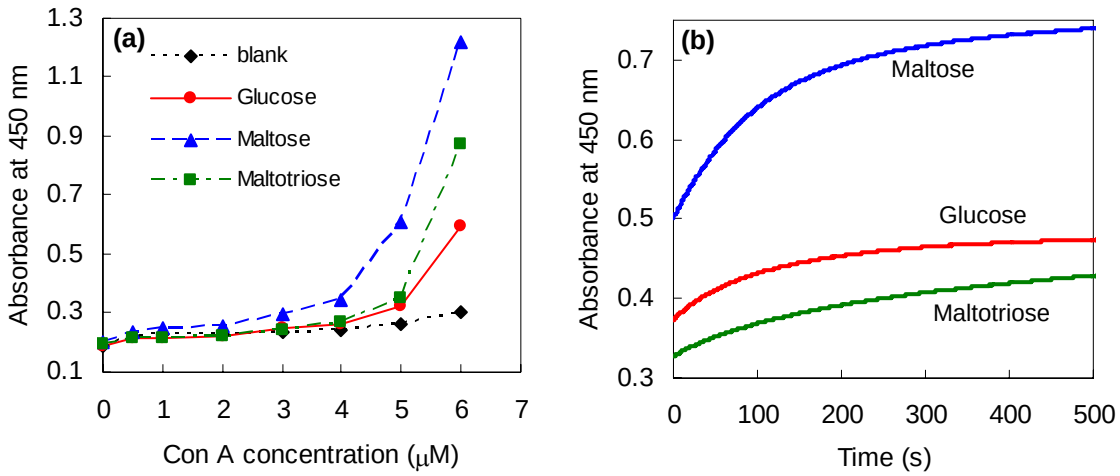

Figure 43. Effect of carbohydrate length on Con A-induced agglutination. (a) Final trubidity as a function of Con A concentration. Turbidity was measured 60 min after addition of Con A (b) Turbidity as a function of time with [Con A] = 6.0 μM.

Surprisingly, the vesicles functionalized with maltotriose conjugate, a trisaccharide, did not induce aggregation as effectively as either the mono- or disaccharide. These results suggest that carbohydrate length is not the only governing factor in binding affinity. A plausible explanation for the diminished binding between Con A and maltotriose relative to the other conjugates is that the conformation of the trisaccharide may diminish the ability of Con A to access the terminal glucose. To further verify the observed trend, the kinetics of binding were measured (Figure 43b). The initial slope of the maltose-functionalized vesicles in Figure 43b showed a significant increase in the turbidity compared to those of glucose- and maltotriose-functionalized vesicles. These results from maltose and lactose suggest that a

disaccharide improves the accessibility of the terminal sugar at the bilayer interface. This is likely due to the increased separation between the ligand and the interface. However, this trend did not hold with the trisaccharide maltotriose and may indicate that the trisaccharide has sufficient flexibility to adopt a conformation which lessens the accessibility of the terminal sugar.

A detailed study will be required to fully elucidate the important factors and effects that ultimately determine binding affinity of carbohydrate-functionalized vesicles.

CONCLUSIONS AND OUTLOOK

We have demonstrated that the surface of SDBS-rich surfactant vesicles can be functionalized with carbohydrates linked to a short alkyl chain. The carbohydrates bound on the surface of surfactant vesicles preserved their function for the binding of receptors. These results represent an important first step in evaluating the viability of surfactant-based vesicles for use as drug delivery vehicles. In addition, carbohydrate-functionalized surfactant vesicles (SDBS-rich) hold promise as diagnostic agents for *in vitro* investigation of cell surface receptors and as tools for glycobiology.

However, a number of important questions remain unanswered regarding the suitability of carbohydrate-functionalized surfactant vesicles for drug delivery. For instance, the knowledge of toxicology for surfactant-based vesicles *in vivo* is limited since only a single study has been reported.[171] Kuo and co-workers showed that the toxicity of surfactant vesicles formed from a mixture of anionic surfactant (SDS: sodium dodecylsulfate) and cationic surfactant (HTMAB: hexadecyltrimethylammonium bromide) depends on the concentration of vesicles. At the concentration of surfactant

vesicles lower than 9 μM, the murin macrophage-like cell line, RAW 264.7, appear to be nontoxic. The cytotoxicity study of vesicles formed from CTAT/SDBS system is currently underway with collaboration of the Fisher group (Department of Bioengineering, UMCP). The initial results showed that the majority of chondrocyte cells are survived with SDBS-rich vesicles at the concentration of vesicles lower than 1.0 μg/mL. However, CTAT-rich vesicles are highly toxic to the cells at the same concentration, suggesting that SDBS-rich vesicles are more suitable as drug delivery vehicles. In addition to the further evaluation of their cytotoxicity, the stability of surfactant vesicles *in vivo* should be explored in order to prevent premature release of drug.

EXPERIMENTAL SECTION

General. All reagents and solvents were purchased from commercial suppliers and used without further purification unless noted otherwise. The detailed experimental procedures for the synthesis and characterization of glycoconjugates are provided in the Experimental Section of Chapter 2.

Vesicle Preparation. The surfactants cetyltrimethylammonium tosylate (CTAT) and sodium dodecylbenzenesulfonate (SDBS) were obtained from Aldrich Chemicals. CTAT was purified by recrystallization (ethanol/acetone). Millipore water (18 MΩ) was used as a solvent for sample preparation and purification in all cases. Vesicles were prepared by mixing the two surfactants with 1 mM of glycoconjugate in water (1 wt % of total surfactant), followed by gentle stirring for 30 min. The samples were then allowed to

equilibrate at room temperature for at least 48 h. A mole ratio of 3 : 1 SDBS to CTAT was used throughout. Dynamic light scattering (DLS) was used to confirm vesicle formation, and size exclusion chromatography (SEC) was used to purify vesicles. A column (length 5.5 cm; diameter 1.5 cm) packed with Sephadex G-100 (Sigma) was used.

Dynamic Light Scattering (DLS). The mean size and size-dispersion of vesicles in solution was analyzed using a Photocor-FC light scattering instrument equipped with a 5 mW laser light source at 633 nm. The scattering angle was 90^{o} and all measurements were performed at 25 ºC. A logarithmic correlator was used to obtain the autocorrelation function, which was analyzed by the method of cumulants to yield a hydrodynamic radius.

Colorimetric Detection of Glycoconjugates. For glycoconjugate incorporation, vesicle samples were prepared using aqueous solutions containing 1.0 mM glycoconjugates. SEC was used to separate vesicle-incorporated glycoconjugate from free glycoconjugate in solution. The glycoconjugate content was then determined spectroscopically[166] using the following procedure: the vesicle solution (1.0 mL) was eluted through the SEC column (fractions of 1.0 mL) and the vesicle containing fractions were identified by DLS. A 0.5 mL portion of each fraction was transferred into a test tube, 0.25 mL of aqueous phenol solution (0.53 M in water) was added, followed by 1.25 mL of concentrated sulfuric acid (in order to obtain reproducible results, the stream of sulfuric acid was introduced into the liquid surface rather than against the side of the test tube). After 10 min, the solution was

vortexed and then allowed to rest at room temperature for 1 h. At this point, any fractions containing carbohydrates showed a light-yellow coloring. Next, 0.5 mL of ethanol was added, mixed well, and after 10 min the absorbance was measured (Ocean Optics USB 2000 Spectrometer). The absorbance values were plotted as a function of eluted volume as shown in Figure 4. DLS was conducted on each fraction prior to the colorimetric assay and the vesicle containing fractions were identified by the peak in DLS intensity near 3.0 mL of eluted volume in Figure 4. The corresponding absorbance intensity observed in the vesicle DLS band was due to the presence of glycoconjugate traveling in the vesicle band and therefore incorporated in the vesicle. In determining the amount of incorporated glycoconjugate, it was found that the most reliable method was to measure the amount of free glycoconjugate that eluted and compare this value with the amount of glycoconjugate that eluted in the absence of vesicles. This approach corresponds to comparing the peak areas of the dashed and dotted lines between 6.0 and 13.0 mL in the panels of Figure 4. This method was used to avoid artifacts that occur during the colorimetric analysis of vesicle-containing fractions due to the presence of surfactants. From our results we calculated an apparent incorporation rate (ρ) as defined by:

$$\rho = 1 - \frac{\sum OD_v}{\sum OD_i} \qquad (1)$$

where *OD* is optical density of absorbance at a given wavelength (491 nm for glucose conjugate, 492 nm for lactose and maltose conjugate, and 493 nm for maltotriose conjugate). The *OD* values for fractions containing free glycoconjugate separated from the vesicle sample (dashed lines in Figure 4) are denoted by v and i denotes values obtained from a solution of free glycoconjugates (1 mM, 1 mL) in the SEC

column (dotted line in Figure 4).

Agglutination Assay. Concanavalin A (Con A, Type V, lyophilized power), peanut agglutinin (PNA, lyophilized power), HEPES, and all other reagents were obtained from Sigma. For the preparation of lectin stock solution, the lectin was dissolved in HEPES-buffered saline ([HEPES 10 mM, NaCl 150 mM, $CaCl_2$ 1 mM, and $MnCl_2$ 1 mM adjusted to pH 7.4 for Con A], [HEPES 10 mM, NaCl 150 mM, $CaCl_2$ 1 mM, $MnCl_2$ 1 mM, and $MgCl_2$ 1 mM adjusted to pH 7.4 for PNA]), incubated at room temperature overnight, and then syringe-filtered (0.22 μm). The concentration of the stock solution was determined from the absorbance at 280 nm (A_{280} = 1.37 × [mg/mL Con A],[144] A_{280} = 0.96 × [mg/mL PNA][145]). The solution was then diluted to given concentrations (based on Con A tetramer at 104 kDa, PNA tetramer at 110 kDa). All the vesicle samples prepared with 1.0 mM glycoconjugates were purified by SEC (1.0 mL of vesicle solution was eluted through the column and then collected with final volume of 2.0 mL). ***For the specific binding assay*:** vesicle solution (150 μL) was added to the lectin solution (150 μL at 0, 2, 4, 6, 8, 10, and 12 μM, respectively). This assures that the pH and ionic strength are the same in all experiments and only the lectin concentration changes. To determine the degree of agglutination, the samples were incubated at room temperature for 60 min and turbidity was recorded at 450 nm. ***For the carbohydrate length dependent assay*:** turbidity measurements were performed by the same manner described above except that the vesicle solution was diluted twice with water after SEC purification. ***To monitor agglutination kinetics*:** the samples were mixed for 5 s and the absorption at 450 nm was monitored with 1 s intervals at 25 ^{o}C.

Appendix

Synthesis and Structural Characterization of Glucopyranosylamide Films on Gold

Langmuir **2007,** *23,* 700-707

Mridula Kadalbajoo, Juhee Park, Aric Opdahl, Hiromi Suda, Carolyn A. Kitchens, Jayne C. Garno, James D. Batteas, Michael J. Tarlov, and Philip DeShong

Department of Chemistry and Biochemistry, University of Maryland, College Park, Maryland 20742, and National Institute of Standards and Technology, Gaithersburg, Maryland 20899

ABSTRACT

Self-assembled monolayers (SAMs) of glucose derivatives on gold have been prepared from α- and β-glucopyranosylamide derivatives. The glucosyl conjugates were synthesized stereoselectively via the in situ generation of glucosyl isoxazolines followed by treatment with thiopyridyl esters. The resulting film structures were characterized by atomic force microscopy, reflection Fourier transform infrared spectroscopy, and X-ray photoelectron spectroscopy. The experimental data indicated that α- or β-linked glucopyranosylamide derivatives with free hydroxyl groups attach to gold via the thiol linker. Both derivatives form monolayer films with high packing densities - comparable to those typically observed for alkanethiol monolayers on gold. Acetate analogues of these conjugates do not form SAMs on gold; they form multilayered films under identical deposition conditions.

INTRODUCTION

Self-assembled monolayers (SAMs) derived from biomolecules have significant potential in bioanalytical analysis if their assembly can be controlled to yield

reproducible films with high biological activities. SAMs of *n*-alkanethiols on gold are the archetypal system for studying physical and chemical properties of organic surfaces because these systems yield monolayers that can be highly crystalline and form well-defined structures.[1] The surface characteristics of monolayers of complex thiol-derivatized bioconjugates (DNA, proteins, carbohydrates) on gold and other noble metal surfaces, however, in comparison to simple alkanethiol derivatives, are poorly understood.[2] It should not be assumed that thiol attachment of biomolecules will result in end-tethering of these species to the surface whereby they are properly oriented and fully accessible for binding to their conjugate ligands (i.e. receptors, enzymes, etc.) at the sensor interface (Figure 1). For example, it is well-established that the assembly of thiol-derivatized DNA SAMs on gold is strongly influenced by the interaction of nucleotides with the gold surface and that the adsorption of single-stranded DNA on gold is strong enough to prevent hybridization with complementary DNA. In this case, the surface must be treated with a second thiol molecule to liberate adsorbed strands and to passivate the surface against nonspecific adsorption of DNA targets.[3] For the development of devices that depend on the binding of biomolecules to surfaces, it is crucial that these films can be formed reproducibly and that their orientation in the film can be characterized unambiguously. Accordingly, we have undertaken a study to characterize the SAMs resulting from the attachment of carbohydrate bioconjugates to gold surfaces. The goal of this study was (1) to determine the orientation of the bioconjugates to the surface (Figure 1), (2) to determine the density of SAM coverage, and (3) to measure whether the surface coverage is sensitive to the stereochemistry of the biomolecule attached.

Carbohydrates are known to be involved in a variety of cell-cell mediated processes

including recognition, regulation of cell growth, infectivity (of bacteria), and the immune response.[4] We are developing biosensors based on the rapid and specific recognition of cell surface oligosaccharides, and toward this goal, it is critical that the oligosaccharide be extended from the surface if a viable specific recognition event is to occur.

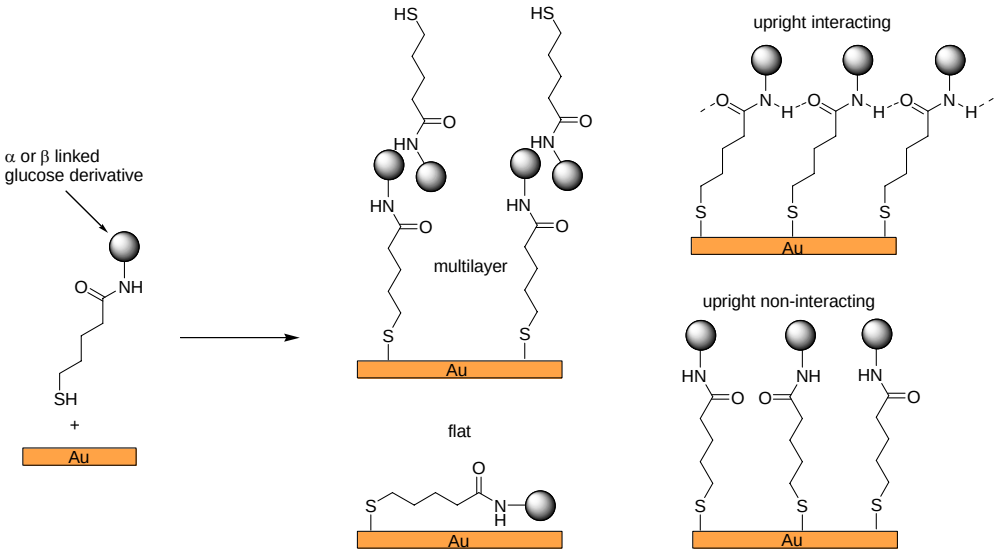

Figure 1. Possible conformations of thiol-modified glucopyranosyls adsorbed on gold.

Although carbohydrate-based SAMs have been prepared by others,[5] the surface characteristics of the SAMs (ie., orientation and surface coverage) of these groups have not been determined in most instances.[5a] In this study, we investigate a series of related sugar derivatives bound to gold utilizing a full complement of surface analytical techniques. Accordingly, our groups have studied the formation of glucopyranosyl-based SAMs by the attachment of thiol-modified glucosylamide conjugates to gold surfaces as the prototypical oligosaccharide SAM. In this paper we report the stereoselective synthesis of a series of glycosylamide conjugates, attachment of these conjugates to gold surfaces, and characterization of the resulting assembled molecular films by Fourier-

transform infrared FTIR and X-ray photoelectron (XPS) spectroscopies, and by atomic force microscopy (AFM) measurements under differing deposition conditions. The time course experiments reported in this paper are particularly significant because they clearly demonstrate that films of different surface coverage and morphology can be obtained by altering either the structure of the glucosyl conjugate or the deposition conditions. In addition, as noted above, the resulting glycoconjugates have the potential to adsorb to the surface in a number of conformations (Figure 1), many of which may be unsuitable for diagnostic applications. However, the evidence from these studies demonstrates that these conjugates can be reproducibly assembled on gold surfaces at relatively high coverages and attach in an upright fashion via the thiol linker, thus presenting the carbohydrate to the solvent media.

RESULT AND DISCUSSION

Synthesis of Glucopyranosyl Conjugates. Glucopyranosylamide conjugates were prepared using the methodology developed by Damkaci and DeShong for the stereoselective synthesis of N-linked glycopeptide derivatives.[6] The key step in this process is the coupling of a glucopyranosyl azide to an acid derivative to provide an N-linked glucopyranosylamide derivative (Scheme 1). Two methods for synthesis of glucopyranosylamide conjugates were developed. In the first method, β-glucopyranosyl azide **1** was allowed to react with phosphine, followed by coupling with acid chloride **2** to provide either α-glucopyranosylamide **3** or β-glucopyranosylamide **6**, respectively, depending on the conditions utilized in the coupling reaction. As shown previously, the α -stereochemistry of the amide linkage resulted from an equilibration of the

phosphorimine intermediate.[6] Displacement of the bromide with thioacetate, followed by removal of the acetate protecting groups with sodium methoxide in methanol and air oxidation afforded α-glucopyranosylamide disulfide **5** (α-glu-S)$_2$ or β-glucopyranosylamide disulfide **8** (β-glu-S)$_2$, respectively. Note that these conditions were selective for ester removal and did not result in hydrolysis of the amide functionality.

Glucopyranosylamide conjugates of lipoic acid (**10**, **11**, **13**, **14**) were synthesized by coupling azide **1** with the thiopyridyl ester **9** or thioctic acid **12** to afford either the α- or β-products, respectively, depending on the phosphine employed in the condensation.[7]

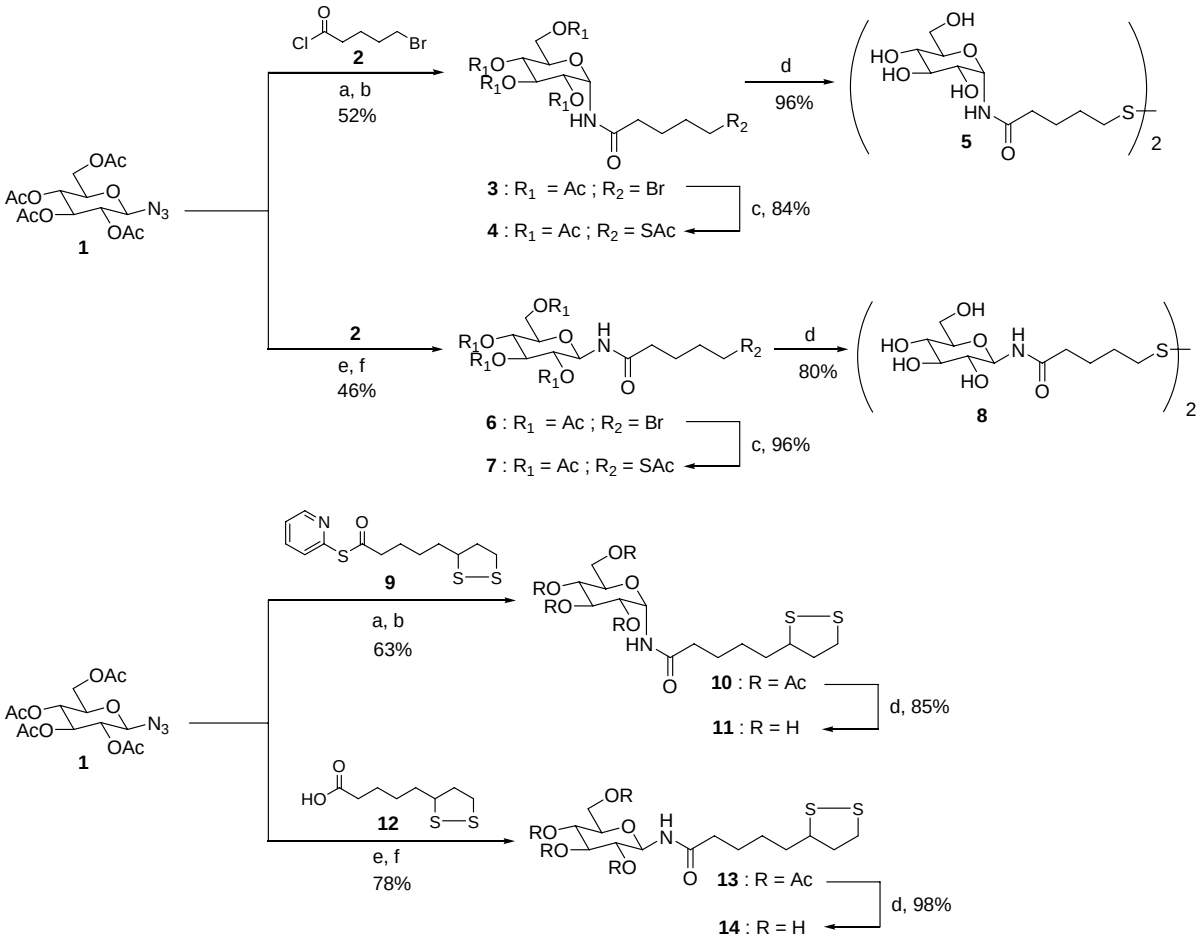

Scheme 1. Synthesis of glucopyranosylamide conjugates. Keys: (a) PPh_3, 1,2-dichloroethane, 95 °C, 16 h. (b) coupling partner, 24 h. (c) KSAc, DMF, RT, 20 h. (d) NaOMe, MeOH, RT. (e) PMe_3, DIEA, 1,2-dichloroethane, RT, 30 m. (f) coupling partner, RT, 24 h.

This strategy for preparing oligosaccharide conjugates has several inherent advantages over the alternative approaches, the majority of which depend on attachment to a poly(ethylene glycol) (PEG) analogue to tether the saccharide moiety to the surface.[8] First, as noted in Scheme 1, it is possible to prepare either the α- or β-linkage at the anomeric center by choosing the appropriate combination of phosphine and reaction conditions, and as shown below, these stereoisomeric bioconjugates give SAMs with different surface characteristics. Second, it is possible to synthesize glycosylamide conjugates from the intact oligosaccharide derivatives, thus avoiding the need to develop a multistep synthesis of a complex oligosaccharide if it is available from natural sources (vide infra). Although only the monosaccharide conjugates are reported in this paper, we have reported the application of this methodology to the synthesis of oligosaccharide derivatives previously.[6,7] More important, the resulting glucopyranosylamide conjugates have proven to be particularly robust to a wide variety of chemical and biological reaction conditions. For example, prolonged exposure of glucopyranosylamide conjugates to either strongly acidic or basic conditions did not result in significant loss of material due to hydrolysis of the amide linkage. This high chemical stability means that a wide variety of hydroxyl protecting groups can be employed for selective protection/deprotection of carbohydrates without inducing cleavage of the glucopyranosylamide linkage.

Polycrystalline gold films (200 Au; 20 nm Cr) on single-crystal Si (100) wafers were used as substrates for the FTIR and XPS experiments. The gold films were cleaned using a “piranha solution” consisting of 70 % H_2SO_4 and 30 % H_2O_2 (30 % H_2O_2 in H_2O) and rinsed thoroughly with deionized water (18.3 MΩ) immediately prior to adsorption

of glycosyl derivative. Piranha solution must be used with care: it is extremely oxidizing, reacts violently with organics, and should be stored in loosely covered containers to avoid pressure buildup. Gold-coated mica (Molecular Imaging) was used as a substrate for AFM experiments and used as-received. Deposition conditions for all glucopyranosylamide films were 1 mM (2 mL) glucopyranosylamide derivative in ethanolic solutions for 20 hours. Before analysis, each sample was extensively rinsed with ethanol to remove loosely bound material and blown dry under flowing nitrogen.

Scanning probe microscopy of glycosylamide gold films. The atomic force microscopy (AFM) determined morphologies of a representative set of the glucose SAMs on gold (compounds **5**, **10** and **11**) are presented in Figures 2 and 3 (2 hour and 20 hour incubation times, respectively). For compounds **5** and **11**, after 2 hours of deposition, monolayers were observed (as determined by nanografting experiments) with approximately 10 % and 25 % of a bilayer present, respectively (Figure 2) based on the areal density of the protruding features on the monolayers.

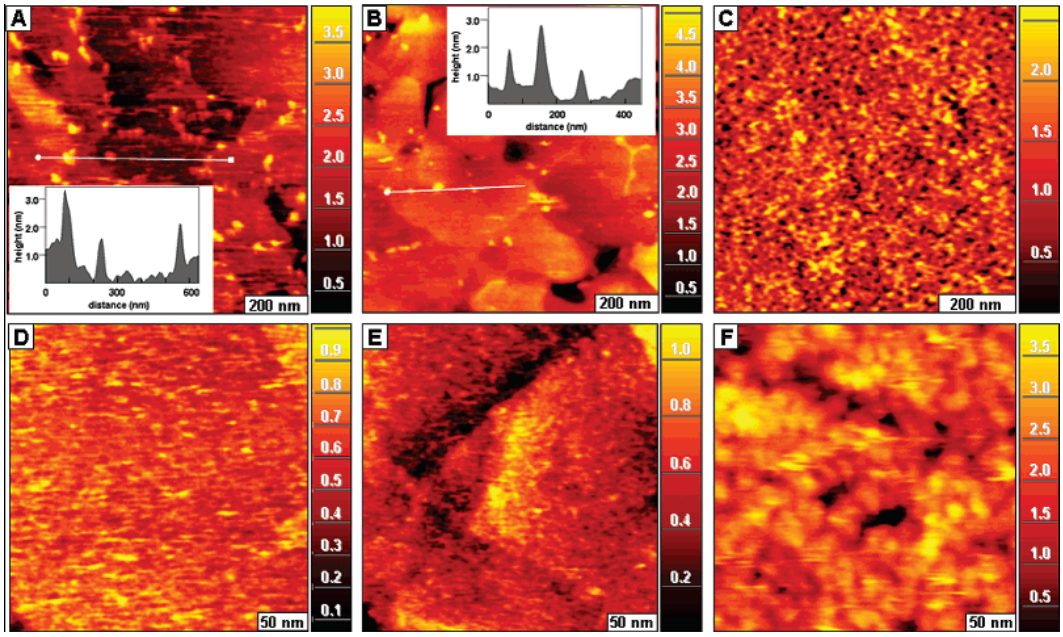

Figure 2. Comparison of sugar SAMs derived from disulfides after a 2 h immobilization period. AFM topographic images (1 μm × 1 μm) for [A] compound **11**; [B] compound **5**; [C] compound **10** and (300 nm × 300 nm) for [D] compound **11**; [E] compound **5**; [F] compound **10**. The cursor traces inset in A and B illustrate that a small amount of a bilayer is formed with features on the order of ~1.5 nm above the monolayer.

We attribute these features to a biliayer structure as the features protrude from the surface by ~1.5 nm, consistent with the molecular length of the molecules of ~1.3 - 1.4 nm. The bilayers are presumably held in place by hydrogen bonding between the glucose headgroups and under increased load and prolonged scanning may be swept away while imaging in ethanol. From nanografting of dodecanethiol and hexadecanethiol into the films derived from disulfides **5** and **11**, respectively, the monolayer thicknesses were estimated to be ≈1 nm for each. For the acetylated disulfide **10**, however, monolayer formation was never observed under the identical deposition conditions. Acetylated disulfide **10** was found to form only multilayered films with thickness on the order of 4 - 5 nm. Moreover, rather than the molecularly smooth films which were observed for the disulfides **5** and **11**, acetylated disulfide **10** formed nanoscale clusters on the order of ≈5

nm, suggesting that the acetate disulfide readily aggregates either before or during deposition.

For deposition of each of these compounds after 20 h (Figure 3), the glucose monothiol and disulfide films show clean, smooth films on the Au surface with little to no evidence of a bilayer, while the acetate disulfide film is unchanged in its observed morphology and film thickness. The reduction in the formation of the bilayer over time may be due to an increase in packing density of the films. Our hypothesis is that as defects in the bilayer (2 h incubation) are filled, the bilayer disappears. This hypothesis is supported by the AFM images of the surface after 2 h vs 20 h incubation.Nomolecularly resolved ordered structures were observed in the case of any of the above molecules. AFM images of the β-glucopyranosylamide disulfide **14** (data not shown) also show smooth monolayers analogous to its α-anomeric congener.

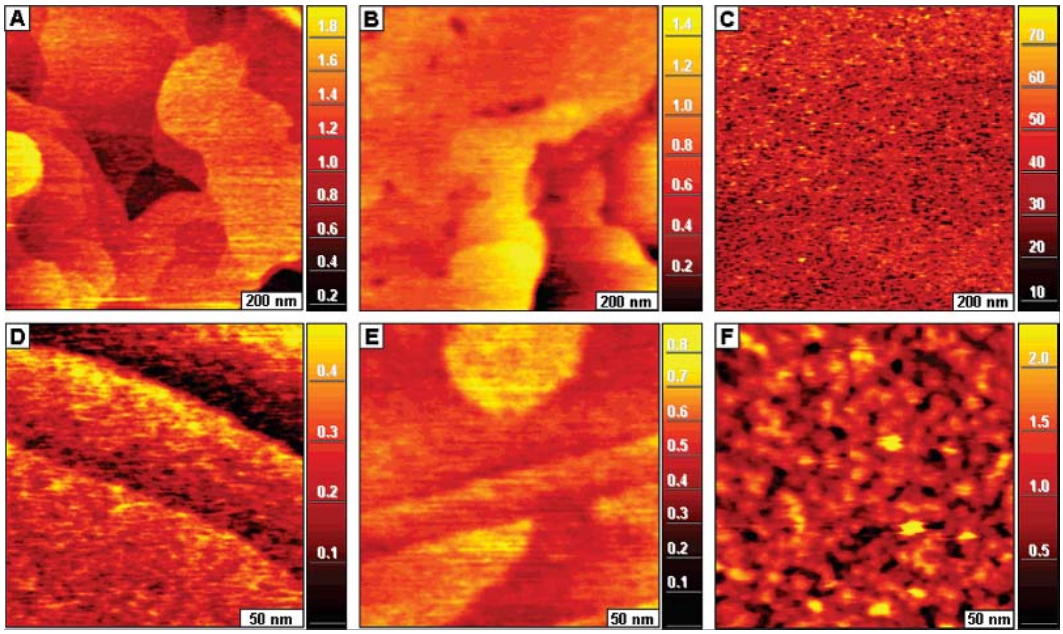

Figure 3. Comparison of sugar SAMs derived from disulfides after a 20 h immobilization period. AFM topographic images (1 μm × 1 μm) for [A] compound **11**; [B] compound **5**; [C] compound **10** and (300 nm × 300 nm) for [D] compound **11**; [E] compound **5**; [F] compound **10**.

Reflectance FTIR of Glucosylamide Gold Films. FTIR spectra obtained from α-glucopyranosylamide disulfide **5**, β-glucopyranosylamide disulfide **8**, and acetylated disulfide **10** adsorbed on gold are shown in Figure 4. All of the spectra contain features at ≈1650 and ≈1560 cm^{-1}, which we attribute to the amide I and amide II bands from the amide group, respectively. Several modes are present between 1200 and 1000 cm^{-1}. We attribute these features to C-O stretches arising from the glucose component. Spectra obtained from the acetylated disulfide **10** contain a strong carbonyl feature arising from the ester functionalities at ≈1765 cm^{-1} as anticipated.

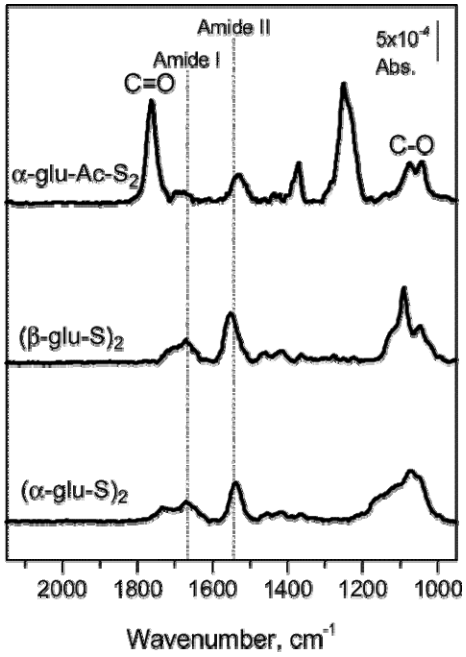

Figure 4. Reflectance FTIR spectra obtained from SAMs prepared from compound **5** (α-glu-$S)_2$, compound **8** (β-glu-$S)_2$, and acetylated disulfide **10** (α-glu-Ac-$S)_2$ adsorbed on gold, 20 hour immobilization period.

The absorbances measured for the amide I feature are relatively weak and are similar for all of the samples studied. The primary component of this feature is the carbonyl vibration. The small absorbance measured for this feature suggests that the amide

carbonyl may be aligned coplanar with the gold substrate.[9] It has been proposed that immobilized molecules containing this functionality can hydrogen bond with adjacent molecules. The positions of the amide I and amide II features have been used to ascertain the degree of hydrogen bonding between adjacent molecules. For the amide II feature, a shift from ≈1520 to ≈1560 cm^{-1} has been interpreted as indicating a higher degree of hydrogen bonding.[10] That the amide II feature is similarly shifted to ≈1560 cm^{-1} in these glucosylated films shift suggests that these films may be similarly stabilized through the hydrogen bonding. Additional hydrogen bonding interactions between the adjacent sugar moieties may further stabilize films. Similar spectra were obtained from thiol-modified disaccharides.

XPS of Glucosylated Gold Films. XPS was used to ascertain the composition, mode of binding to the surface, and surface density of glucopyranosylamides monolayers self-assembled on gold. SAMs of α-glucopyranosylamide disulfide **5** (a-glu-$S)_2$, β-glucopyranosylamide disulfide **8** (β-glu-$S)_2$, and *n*-dodecanethiol (C_{12}-SH) were characterized using XPS. The C_{12}-SH SAM was selected as a reference sample for comparing data acquired from the thiol-derivatized glucosylamide SAMs because C_{12}-SH contains approximately the same number of C atoms (12) as that in the (α-glu-$S)_2$ and (β-glu-$S)_2$ molecules (11). Wide binding energy (BE) XPS spectra of the glucopyranosylamide SAMs samples contained only features assignable to gold (Au), nitrogen (N), carbon (C), oxygen (O), and sulfur (S). The C_{12}-SH sample only contained features assignable to C and S.

Representative high-resolution spectra of the S 2p, C 1s, and N 1s regions acquired from the three SAMs are displayed in Figure 5.

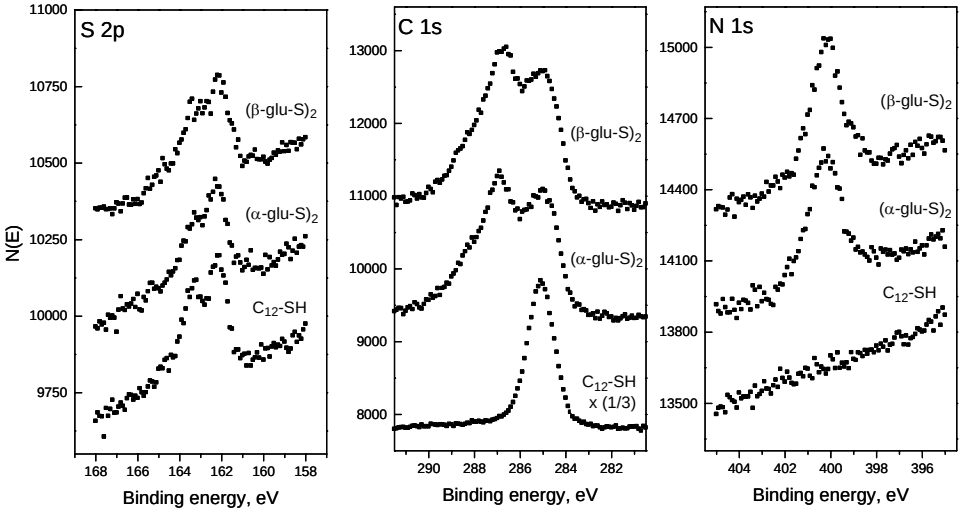

Figure 5. XPS S 2p, C 1s, and N 1s spectra obtained from compound **5** (α-glu-S)$_2$, compound **8** (β-glu-S)$_2$, and dodecanethiol (C_{12}-SH) adsorbed on gold, 20 h immobilization period.

The C12-SH SAM exhibits a S 2p doublet spectrum with a BE of the primary peak at 162.2 eV consistent with reported S 2p BE values for *n*-alkylthiolates on gold. The S 2p spectra acquired from (α-glu-S)$_2$ and (β-glu-S)$_2$ SAMs are nearly identical in BE and shape, suggesting that the glucopyranosylamide molecules are bound as thiolates to the gold surface. In addition, the uncorrected S 2p/Au 4f peak area ratios (see Table 1) obtained from the (α-glu-S)$_2$ (0.0036) and (β-glu-S)$_2$ (0.0042) SAMs are less than that obtained from the C_{12}-SH SAM (0.0045), suggesting that the surface coverage of the α-glucose monolayers is nearly 20% less than that the *n*-alkanethiol SAMs on gold, while the β-glucose SAMs, despite the sterically demanding glucose headgroup, have ratios similar to that of the alkanethiol standards. The efficient packing of the β-glucopyranosyl side chains is consistent with the observed hydrogen bonding in the (β-glu-S)$_2$

monolayers, which enhances packing of molecules on the surface.

Table 1. Uncorrected XPS Peak Area Ratios for C_{12}-SH, **5** (α-glu-S)$_2$, and **8** (β-glu-S)$_2$ SAMs on Gold.[a]

	S 2p / Au 4f	C 1s / Au 4f	N 1s / Au 4f
C_{12}-SH	0.0045	0.050	–
5 (α-glu-S)$_2$	0.0036	0.041	0.067
8 (β-glu-S)$_2$	0.0042	0.048	0.072

[a] Ratios represent the average of two samples.

The C 1s spectra are also consistent with the formation of glucopyranosylamide SAMs on gold. The C 1s region of the C_{12}-SH SAM exhibits a symmetric peak centered at 285.0 eV characteristic of carbon existing as CH_2 groups. In contrast, the C 1s spectra of both glucopyranosylamide SAMs, while similar to each other as expected, exhibit a more complex spectral envelope compared to the C_{12}-SH SAM. We assign the peak centered at ≈285.0 eV to the CH_2 linker groups of the glucopyranosylamide molecules. The peak centered at ≈286.7 eV is most likely associated with carbons singly bonded to oxygen in the glucosyl moiety. There appear to be 1 - 2 other weaker, higher-BE components that contribute to the spectral envelope that we tentatively assign to the amide group carbon and the number 1 carbon of the glycosyl ring that is bound to both oxygen and nitrogen. In addition, the C 1s/Au 4f peak area ratios for the glucopyranosylamide SAMs are similar to that of the C_{12}-SH SAM (see Table 1), consistent with the conclusion that the coverage of the glucopyranosylamide SAMs is close to that of *n*-alkanethiols on gold.

The N 1s regions of both the **5** (α-glu-S)$_2$ and **8** (β-glu-S)$_2$ SAMs exhibit a symmetric peak centered at 400.0 eV, consistent with nitrogen existing as an amide functionality. Finally, we note that given the consistently higher S 2p/Au 4f, C 1s/Au 4f, and N 1s/Au

4f peak area ratios for the **8** (β-glu-S)$_2$ SAMs compared to the **5** (α-glu-S)$_2$ SAMs, it is tempting to conclude that the **8** (β-glu-S)$_2$ molecules pack at slightly higher densities.

CONCLUSIONS

Glucopyranosylamide conjugates were prepared by coupling of glucopyranosyl azide derivatives, and the coupling reaction can be tailored to provide either the α- or β-anomer of the corresponding conjugate (Scheme 1). Gold surfaces were exposed to ethanol solutions containing glucopyranosylamide disulfide derivatives to provide SAMs and multilayered structures which were characterized by AFM, FTIR, and XPS analysis. AFM analysis showed that both α- or β-anomers of hydroxylated conjugates formed dense adsorbed layers with monolayer thickness. Acetylated conjugates, on the other hand, formed clusters on the surface. XPS analysis suggested that the SAMs derived from hydroxylated conjugates attach to gold in an upright fashion via the thiol linker (see Figure 1) and have packing density approaching that commonly observed for alkanethiol monolayers. FTIR spectra suggested that one possible mechanism for the high packing densities observed may be hydrogen bonding between amide groups on adjacent immobilized molecules. Now that saccharide-derived SAMs have been produced and fully characterized, we shall investigate the specific binding capacity of saccharide-derived SAMs with enzymes (lectins) and cells as models for biological recognition events. Initial studies of selective binding of concanavalin A to nanopatterned features of compound **11** are quite promising (see Supporting Information). The complete results of these studies will be reported in due course.

EXPERIMENTAL SECTION

General. Certain commercial equipment, instruments, or materials are identified in this article to adequately specify the experimental procedure. In no case does such identification imply recommendation or endorsement by the National Institute of Standards and Technology, nor does it imply that the materials or equipment identified are necessarily the best available for the purpose.

Polycrystalline gold films (200 Au; 20 nm Cr) on single-crystal Si (100) wafers were used as substrates for the FTIR and XPS experiments. The gold films were cleaned using a "piranha solution" consisting of 70 % H_2SO_4 and 30 % H_2O_2 (30 % H_2O_2 in H_2O) and rinsed thoroughly with deionized water (18.3 MΩ) immediately prior to adsorption of glycosyl derivative. Piranha solution must be used with care: it is extremely oxidizing, reacts violently with organics, and should be stored in loosely covered containers to avoid pressure buildup. Gold-coated mica (Molecular Imaging) was used as a substrate for AFM experiments and used as-received. Deposition conditions for all glucopyranosylamide films were 1 mM (2 mL) glucopyranosylamide derivative in ethanolic solutions for 20 hours. Before analysis, each sample was extensively rinsed with ethanol to remove loosely bound material and blown dry under flowing nitrogen.

Scanning Probe Microscopy. AFM images were acquired using a commercial instrument with a deflection-type scanning head (Molecular Imaging, PicoSPM, Phoenix, AZ), controlled by an SPM1000 feedback electronics Revision 8 (RHK Technology Inc., Troy, MI). The scanner was calibrated using the crystalline surfaces of both mica (0001) and Au (111) to establish lateral dimensions, with lattice constants of 0.56 nm and 0.288 nm, respectively. The z-scale was calibrated using monatomic Au (111) steps (0.235 nm)

and verified using the known thicknesses of n-alkanethiol SAMs. Contact-mode images were acquired under ethanol using Si_3N_4 microlevers (VeecoProbes, Santa Barbara, CA) with a nominal force constant of $\approx$0.5 N/m.

To estimate film thicknesses, nanografting was employed to examine the comparative heights of the SAMs to grafted patterns of dodecanethiol and hexadecanethiol in the SAM layers. Nanografting combines adsorbate displacement with the self-assembly of thiols on gold.[11] Fabrication is accomplished while scanning by exerting pressure on an AFM tip, thus pushing through the matrix molecules to contact the underlying gold surface. The pressure of the AFM tip is used to displace or scrape away selected areas of the matrix SAM, following the scanning track of the tip. For nanografting, the imaging media contains a different thiol molecule than the matrix. As the AFM tip scans at high force over nano-sized areas, matrix molecules are removed and replaced by new molecules from solution. Nanografted structures can then be imaged using the same tip at low force. The AFM controller was interfaced with a programmable vector scanning module (VSCAN, RHK Technology, Inc.) to enable automated scanning probe lithography.[12] Sets of programmed motions were written and compiled into lithography scripts, to create designed surface arrangements of nanopatterns.

FT-IR Measurements. FT-IR absorption spectra were measured in a Digilab FTS 7000 series spectrometer with a wire grid infrared polarizer (p-polarized) and a Vee Max variable-angle specular reflectance accessory (reflectance angle 75˚). Spectra (2000 cm^{-1} - 900 cm^{-1}) were collected using a cryogenic mercury cadmium telluride detector in a nitrogen-purged environment.

XPS Measurements. The X-ray photoelectron measurements were performed using a Kratos Axis 165 spectrometer at a vacuum of 4×10^{-10} Torr with monochromatic AlKα radiation. The X-ray power used for the measurements was 144 W. The samples were introduced into the vacuum chamber using a conductive carbon tape. A wide scan survey and various slots of regions (Au 4f, S 2p, N 1s, O 1s and C 1s) were measured. All measurements were performed in hybrid mode using both electrostatic and magnetic lenses, with a step size of 0.1 eV and sweep time of 60 s. All individual region spectra were recorded in the FAT analyzer mode with pass energy of 80 eV, and an average of 10 scans. The energy resolution during acquisition of single region-scan was about 1.0 eV. Charge neutralizer was off during the measurements and binding energy calibration was done with respect to Au 4f at 84.0 eV.

References for Appendix

1. (a) Porter, M. D.; Bright, T. B.; Allara, D. L.; Chidsey, C. E. D. *J. Am. Chem. Soc.* **1987**, *109*, 3559-3568. (b) Troughton, E. B.; Bain, C. D.; Whitesides, G. M.; Nuzzo, R. G.; Allara, D. L.; Porter, M. D. *Langmuir* **1988**, *4*, 365-385. (c) Bain, C. D,; Troughton, E. B.; Tao, Y.-T.; Evall, J.; Whitesides, G. M.; Nuzzo, R. G. *J. Am. Chem. Soc*. **1989**, *111*, 321-335. (d) Laibinis, P. E.; Whitesides, G. M.; Allara, D. L.; Tao, Y.-T.; Parikh, A. N.; Nuzzo, R. G. *J. Am. Chem. Soc*. **1991**, *113*, 7152-7161. (e) Love, J. C.; Estroff, L. A.; Kriebel, J. K.; Nuzzo, R. G.; Whitesides, G. M. *Chem. Rev*. **2005**, *105*, 1103-1170.

2. Fritz, M. C.; Hahner, G.; Spencer, N. D.; Burli, R.; Vasella, A. *Langmuir* **1996**, *12*, 6074-6082.

3. Petrovykh, D. Y.; Kimura-Suda, H.; Tarlov, M. J.; Whitman, L. J. *Langmuir* **2004**, *20*,

429-440.

4. Miller, D. J.; Macek, M. B.; Shur, B. D. *Nature* **1992**, *357*, 589-593.

5. For a paper on surface characterization of a carbohydrate SAM, see (a) Zhang, Y.; Luo, S.; Tang, Y.; Yu, L.; Hou, K.-Y.; Cheng, J.-P.; Peng, G. *Anal. Chem*. **2006**, *78*, 2001-2008. For reviews of carbohydrate SAMs in binding studies, see (b) Langenham, J. M.; Thorson, J. S. *Curr. Org. Syn*. **2005**, *2*, 59-81. (c) Ratner, D. M.; Adams, E. W.; Disney, M. D.; Seeberger, P. H. *ChemBioChem*. **2004**, *5*, 1375-1383. (d) Houseman, B. T.; Mrksich, M. *Top. Curr. Chem.* **2002**, *218*, 1-44. For additional papers relating to carbohydrate SAMs, see (e) Zhi, Z.-L.; Powell, A.K.; Turnbull, J. E. *Anal. Chem*. **2006**, *78*, 4786-4793. (f) Shin, I.; Park, S.; Lee, M.-R. *Chem. Eur. J.*, **2005**, *11*, 2894-2901. (g) Yonzon, C. R.; Jeoung, E.; Zou, S.; Schatz, G. C.; Mrksich, M.; Van Buyne, R. P. *J. Am. Chem. Soc.* **2004**, *126*, 12669-12676. (h) Ratner, D. M.; Adams, E. W.; Su, J.; O'Keefe, B. R.; Mrksich, M..; Seeberger, P. H. *ChemBioChem*. **2004**, *5*, 379-382. (i) Orner, B. P.; Derda, R.; Lewis, R. L.; Thomson, J. A.; Kiessling, L. L. *J. Am. Chem. Soc.* **2004**, *126*, 10808-10809. (j) Houseman, B. T.; Mrksich, M. *Chem. Biol*. **2002**, *9*, 443-454. (k) Houseman, B. T.; Gawalt, E. S.; Mrksich, M. *Langmuir* **2003**, *19*, 1522-1531. For a description of a carbohydrate SAM on silica, see (l) de Smet, L. C. P. M.; Stork, G. A.; Hurenkamp, G. H. F.; Sun, Q.-Y.; Topai, H.; Vronen, P. J. E.; Sieval, A. B.; Wright, A.; Visser, G. M.; Zuilhof, H.; Sucholter, E. J. R. *J. Am. Chem. Soc.* **2003**, *125*, 13916-13917.

6. Damkaci, F.; DeShong, P. *J. Am. Chem. Soc*. **2003**, *125*, 4408-4409.

7. Damkaci, F.; Park, J.; DeShong, P. Unpublished results. Damkaci, F. Ph.D. Thesis, University of Maryland, 2004.

8. Park, W. K. C.; Auer, M.; Jaksche, H.; Wong, C.-H. *J. Am. Chem. Soc.* **1996**, *118*, 10150-10155.

9. Sheppard, N.; Erkelens, J. *Appl. Spectroscopy* **1984**, *38*, 471-485.

10. Valiokas, R.; Ostblom, M.; Svedhem, S.; Svensson, S. C. T.; Liedberg, B. *J. Phys. Chem. B* **2002**, *106*, 10401-10409.

11. Liu, G.-Y.; Xu, S.; Qian, Y. *Acc. Chem. Res.* **2000**, *33*, 457-466.

12. Cruchon-Dupeyrat, S.; Porthun, S.; Liu, G.-Y. *Appl. Surf. Sci.* **2001**, *175-176*, 636-642.

REFERENCES

(1) Nelson, D. L.; Cox, M. M. *Lehninger Principles of Biochemistry*, 4th ed.; W. H. Freeman: New York, 2005; Chapter 7.

(2) Taylor, M. E.; Drickamer, K. *Introduction to Glycobiology*, 2nd ed.; Oxford University Press, New York, 2006.

(3) Brook, S. A.; Dwek, M. V.; Schumacher, U. *Functional and Molecular Glycobiology*; Bios: Oxford, 2002.

(4) Helenius, A.; Smith, A. E. *Science* **2004**, *304*, 237-242.

(5) Varki, A. *Nature* **2007**, *446*, 1023-1029.

(6) Wu, L.; KewalRamani, V. N. *Nature Rev. Immunol*. **2006**, *6*, 859-868.

(7) Feinberg, H.; Mitchell, D. A.; Drickamer, K.; Weis, W. I. *Science* **2001**, *294*, 2163-2166.

(8) Arnold, J. N.; Wormald, M. R.; Sim, R. B.; Rudd, P. M.; Dwek, R. A. *Annu. Rev. Immunol*. **2007**, *25*, 21-50.

(9) Scanlan, C. N.; Burton, D. R.; Dwek, R. A. *Proc. Natl. Acad. Sci. U.S.A.* **2008**, *105*, 4081-4082.

(10) Burton, D. R.; Dwek, R. A. *Science* **2006**, *313*, 627-628.

(11) Kobayashi, H.; Boelte, K. C.; Lin, P. C. *Curr. Med. Chem*. **2007**, *14*, 377-386.

(12) Salmi, M.; Jalkanen, S. *Immuno. Rev*. **2005**, *206*, 100-113.

(13) Dube, D. H.; Bertozzi, C. R. *Nature Rev. Drug Disc*. **2005**, *4*, 477-488.

(14) Fuster, M. M.; Esko, J. D. *Nature Rev. Cancer* **2005**, *5*, 526-542.

(15) Hanson, S.; Best, M.; Bryan, M. C.; Wong, C.-H. *Trends Biochem. Sci*. **2004**, *29*, 656-663.

(16) Bertozzi, C. R.; Kiessling, L. L. *Science* **2001**, *291*, 2357-2364.

(17) Seeberger, P. H.; Werz, D. B. *Nature* **2007**, *446*, 1046-1051.

(18) Blixt, O.; Norberg, T. *J. Ogr. Chem*. **1998**, *63*, 2705-2710.

(19) Nishiguchi, S.; Yamada, K.; Fuji, Y.; Shibatani, S.; Toda, A.; Nishimura, S.-I. *Chem. Commun*. **2001**, 1944-1945.

(20) Zhang, Z.; Ollmann, I. R.; Ye, X.-S.; Wischnat, R. W.; Baasov, T.; Wong, C.-H. *J. Am. Chem. Soc.* **1999**, *121*, 734-753.

(21) Burkhart, F.; Zhang, Z.; Wacowich-Sgarbi, S.; Wong, C.-H. *Angew. Chem., Int. Ed.* **2001**, *40*, 1274-1277.

(22) Mong, T. K.-K.; Lee, H.-K.; Duron, S. G.; Wong, C.-H. *Proc. Natl. Acad. Sci. U.S.A.* **2003**, 100, 797-802.

(23) Polat, T.; Wong. C.-H. *J. Am. Chem. Soc.* **2007**, *129*, 12795-12800.

(24) Plante, O. J.; Palmacci, E. R.; Seeberger, P. H. *Science* **2001**, *291*, 1523-1527.

(25) Castagner, B.; Seeberger, P. H. *Top. Curr. Chem*. **2007**, *278*, 289-309.

(26) Mammen, M.; Choi, S.-K.; Whitesides, G. M. *Angew. Chem., Int. Ed.* **1998**, *37*, 2754-2794.

(27) Larsen, K.; Thygesen, M. B.; Guillaumie, F.; Willats, W. G. T.; Jensen, K. J. *Carbohydr. Res*. **2006**, *341*, 1209-1234.

(28) Ratner, D. M.; Adams, E. W.; Disney, M. D.; Seeberger, P. H. *ChemBioChem* **2004**, *5*, 1375-1383.

(29) de la Fuente, J. M.; Penades, S. *Biochim. Biophys. Acta* **2006**, *1760*, 636-651.

(30) Conlan, J. W.; Shen, H.; Webb, A.; Perry, M. B. *Vaccine* **2002**, *20*, 3465-3471.

(31) Galonic, D. P.; Gin, D. Y. *Nature* **2007**, *446*, 1000-1007.

(32) Lees, A.; Sen, G.; LopezAcosta, A. *Vaccine* **2006**, *24*, 716-729.

(33) Manimala, J. C.; Roach, T. A.; Li, Z.; Gildersleeve, J. C. *Glycobiology* **2007**, *17*, 17C-23C.

(34) Smith, E. A.; Thomas, W. D.; Kiessling, L. L.; Corn, R. M. *J. Am. Chem. Soc*. **2003**, *125*, 6140-6148.

(35) Houseman, B. T.; Mrksich, M. *Chem. Biol*. **2002**, *9*, 443-454.

(36) Hashida, M.; Nishikawa, M.; Yamashita, F.; Takakura, Y. *Adv. Drug Deliv. Rev.* **2001**, *52*, 187-196.

(37) Torchilin, V. P. *Nature Rev. Drug Disc*. **2005**, *4*, 145-160.

(38) Nishikawa, M.; Kawakami, S.; Yamashita, F.; Hashida, M. *Methods Enzymol*. **2003**, *373*, 384-399.

(39) Park, S.; Lee, M.-R.; Shin, I. *Chem. Soc. Rev*. **2008**, *37*, 1579-1591.

(40) Horlacher, T.; Seeberger, P. H. *Chem. Soc. Rev*. **2008**, *37*, 1414-1422.

(41) Paulson, J. C.; Blixt, O.; Collins, B. E. *Nature Chem. Biol*. **2006**, *2*, 238-248.

(42) Schmidt, R. R.; Jung, K.-H. In *Preparative Carbohydrate Chemistry*; Hanessian, S., Ed.; Marcel Dekker: New York, 1997; Chapter 12.

(43) Nicolaou, K. C.; Mitchell, H. J. *Angew. Chem., Int. Ed.* **2001**, *40*, 1576-1624.

(44) Nicolaou, K. C.; Ueno, H. In *Preparative Carbohydrate Chemistry*; Hanessian, S., Ed.; Marcel Dekker: New York, 1997; Chapter 13.

(45) Schmidt, R. R. *Angew. Chem., Int. Ed.* **1986**, *25*, 212-235.

(46) Liu, Y.; Feizi, T.; Campanero-Rhodes, M. A.; Childs, R. A.; Zhang, Y.; Mulloy, B.; Evans, P. G.; Osborn, H. M. I.; Otto, D.; Crocker, P. R.; Chai, W. *Chem. Biol*. **2007**, *14*, 847-859.

(47) Lee, M.-R.; Shin, I. *Org. Lett*. **2005**, *7*, 4269-4272.

(48) Auge, J.; Lubin-Germain, N. *J. Carbohydr. Chem*. **2000**, *19*, 379-392.

(49) Flinn, N. S.; Quibell, M.; Monk, T. P.; Ramjee, M. K.; Urch, C. J. *Bioconjugate Chem*. **2005**, *16*, 722-728.

(50) Bendiak, B. *Carbohydr. Res*. **1997**, *304*, 85-90.

(51) Hatanaka, Y.; Kempin, U.; Park, J.-J. *J. Org. Chem*. **2000**, *65*, 5639-5643.

(52) Lees, A.; Sen, G.; LopezAcosta, A. *Vaccine* **2006**, *24*, 716-729.

(53) Likhosherstov, L. M.; Novikova, O. S.; Derevitskaja, V. A.; Kochetkov, N. K. *Carbohydr. Res*. **1986**, *146*, C1-C5.

(54) Vetter, D.; Gallop, M. A. *Bioconjugate Chem*. **1995**, *6*, 316-318.

(55) Vetter, D.; Tate, E. M.; Gallop, M. A. *Bioconjugate Chem*. **1995**, *6*, 319-322.

(56) Oberg, C. T.; Carlsson, S.; Fillion, E.; Leffler, H.; Nilsson, U. J. *Bioconjugate Chem*. **2003**, *14*, 1289-1297.

(57) Wang, D.; Liu, S.; Trummer, B. J.; Deng, C.; Wang, A. *Nature Biotechnol*. **2002**, *20*, 275-281.

(58) Fukui, S.; Feizi, T.; Galustian, C.; Lawson, A. M.; Chai, W. *Nature Biotechnol*. **2002**, *20*, 1011-1017.

(59) Bryan, M. C.; Plettenburg, O.; Sears, P.; Rabuka, D.; Wacowich-Sgarbi, S.; Wong, C.-H. *Chem. Biol*. **2002**, *9*, 713-720.

(60) Ko, K.-S.; Jaipuri, F. A.; Pohl, N. L. *J. Am. Chem. Soc*. **2005**, *127*, 13162-13163.

(61) Chen, G.-S.; Pohl, N. L. *Org. Lett*. **2008**, *10*, 785-788.

(62) Zhang, W. *Chem. Rev*. **2004**, *104*, 2531-2556.

(63) Love, J. C.; Estroff, L. A.; Kriebel, J. K.; Nuzzo, R. G.; Whitesides, G. M. *Chem.*

Rev. **2005**, *105*, 1103-1169.

(64) Mrksich, M. *Chem. Soc. Rev*. **2000**, *29*, 267-273.

(65) Revell, D. J.; Knight, J. R.; Blyth, D. J.; Haines, A. H.; Russell, D. A. *Langmuir* **1998**, *14*, 4517-4524.

(66) Svedhem, S.; Ohberg, L.; Borrelli, S.; Valiokas, R.; Andersson, M.; Oscarson, S.; Svensson, S. C. T.; Liedberg, B.; Konradsson, P. *Langmuir* **2002**, *18*, 2848-2858.

(67) Tromas, C.; Eaton, P.; Mimault, J.; Rojo, J.; Penades, S. *Langmuir* **2005**, *21*, 6142-6144.

(68) Zhi, Z.-L.; Powell, A. K.; Turnbull, J. E. *Anal. Chem*. **2006**, *78*, 4786-4793.

(69) Zhou, X.; Zhou, J. *Biosens. Bioelectron*. **2006**, *21*, 1451-1458.

(70) Angeloni, S.; Ridet, J. L.; Kusy, N.; Gao, H.; Crevoisier, F.; Guinchard, S.; Kochhar, S.; Sigrist, H.; Sprenger, N. *Glycobiology* **2005**, *15*, 31-41.

(71) Blencowe, A.; Hayes, W. *Soft Matter* **2005**, *1*, 178-205.

(72) Sigrist, H.; Collioud, A.; Clemence, J. F.; Gao, H.; Luginbul, R.; Sanger, M.; Sundarababu, G. *Optical Engin*. **1995**, *34*, 2339-2348.

(73) Galanina, O. E.; Mecklenburg, M.; Nifantiev, N. E.; Pazynina, G. V.; Bovin, N. V. *Lab Chip* **2003**, *3*, 260-265.

(74) Alvarez, R. A.; Blixt, O. *Methods Enzymol*. **2006**, *415*, 292-310.

(75) Park, S.; Shin, I. *Angew. Chem., Int. Ed.* **2002**, *41*, 3180-3182.

(76) Park, S.; Lee, M.-R.; Pyo, S. J.; Shin, I. *J. Am. Chem. Soc*. **2004**, *126*, 4812-4819.

(77) Houseman, B. T.; Gawalt, E. S.; Mrksich, M. *Langmuir* **2003**, *19*, 1522-1531.

(78) Yonzon, C. R.; Jeoung, E.; Zou, S.; Schatz, G. C.; Mrksich, M.; Van Duyne, R. P. *J. Am. Chem. Soc*. **2004**, *126*, 12669-12676.

(79) Houseman, B. T.; Mrksich, M. *Chem. Biol*. **2002**, *9*, 443-454.

(80) Fazio, F.; Bryan, M. C.; Blixt, O.; Paulson, J. C.; Wong, C.-H. *J. Am. Chem. Soc*. **2002**, *124*, 14397-14402.

(81) Sun, X.-L.; Stabler, C. L.; Cazalis, C. S.; Chaikof, E. L. *Bioconjugate Chem*. **2006**, *17*, 52-57.

(82) Zhang, Y.; Luo, S.; Tang, Y.; Yu, Lei.; Hou, K.-Y.; Cheng, J. P. Zeng, X.; Wang, P. G. *Anal. Chem*. **2006**, *78*, 2001-2008.

(83) Damkaci, F.; DeShong, P. *J. Am. Chem. Soc*. **2003**, *125*, 4408-4409.

(84) Damkaci, F. *Methods for Stereoselective Synthesis of Glycopyranosylamide Linkage*; PhD Dissertation, University of Maryland: College Park, 2004.

(85) Tian, W. Q.; Wang, Y. A. *J. Org. Chem*. **2004**, *69*, 4299-4308.

(86) Garcia, B.; Salome, M.; Lemelle, L.; Bridot, J.-L.; Gillet, P.; Perriat, P.; Roux, S.; Tillement, O. *Chem. Commun*. **2005**, 369-371.

(87) Karamanska, R.; Mukhopadhyay, B.; Russell, D. A.; Field, R. A. *Chem. Commun*. **2005**, 3334-3336.

(88) Endo, T.; Ikenaga, S.; Mukaiyama, T. *Bull. Chem. Soc. Jpn*. **1970**, *43*, 2632-2633.

(89) Merchant, R.; Wickert, J. N.; Marvel, C. S. *J. Am. Chem. Soc.* **1927**, *49*, 1828-1831.

(90) Field, L. D.; Ward, A. J. *J. Organomet. Chem*. **2003**, *681*, 91-97.

(91) Mori, A.; Takahisa, E.; Yamamura, Y.; Kato, T.; Mudalige, A. P.; Kajiro, H.; Hirabayashi, K.; Nishihara, Y.; Hiyama, T. *Organometallics* **2004**, *23*, 1755-1765.

(92) Arico, C. S.; Cox, L. R. *Org. Biomol. Chem*. **2004**, *2*, 2558-2562.

(93) Alauzun, J.; Mehdi, A.; Reye, C.; Corriu, R. *Chem. Mater*. **2007**, *19*, 6373-6375.

(94) Sabourault, N.; Mignani, G.; Wagner, A.; Mioskowski, C. *Org. Lett*. **2002**, *4*, 2117-

2119.

(95) Lewis, L. N.; Lewis, N. *J. Am. Chem. Soc*. **1986**, *108*, 7228-7231.

(96) Nobrega, C.; Vazquez, J. T. *Tetrahedron: Asymmetry* **2003**, *14*, 2793-2801.

(97) Soli, E. D.; Manoso A. S.; Patterson, M. C.; DeShong, P.; Favor, D. A.; Hirschmann, R.; Smith, A. B. *J. Org. Chem.* **1996**, *64*, 3171-3177.

(98) Vo-Dinh. T. *Nanotechnology in Biology and Medicine: Method, Device, and Applications*; CRC press, New York, 2007.

(99) Klostranes, J. M.; Chan, W. C. W. *Adv. Mater.* **2006**, *18*, 1953-1963.

(100) Brunker, S. E.; Cederquist, K. B.; Keating, C. D. *Nanomedicine* **2007**, *2*, 695-710.

(101) Jun, Y.-W.; Seo, J.-W.; Cheon, J. *Acc. Chem. Res*. **2008**, *41*, 179-189.

(102) Rosi, N. L.; Mirkin, C. A. *Chem. Rev*. **2005**, *105*, 1547-1562.

(103) Daniel, M. C.; Astruc, D. *Chem. Rev*. **2004**, *104*, 293-346.

(104) Frens, G. *Nature Phys. Sci*. **1973**, *241*, 20-22.

(105) Brust, M.; Walker, M.; Bethell, D.; Schiffrin, D. J.; Whyman, R. J. *J. Chem. Soc., Chem. Commun.* **1994**, 801-802.

(106) Connor, E. E.; Mwamuka, J.; Gole, A.; Murphy, C. J.; Wyatt, M. D. *Small* **2005**, *1*, 325-327.

(107) Willets, K. A.; Van Duyne, R. P. *Annu. Rev. Phys. Chem*. **2007**, *58*, 267-297.

(108) Eustis, S.; El-Sayed, M. A. *Chem. Soc. Rev*. **2006**, *35*, 209-217.

(109) Murphy, C. J.; Gole, A. M.; Hunyadi, S. E.; Stone, J. W.; Sisco, P. N.; Alkilany, A.; Kinard, B. E.; Hankins, P. *Chem. Commun*. **2008**, 544-557.

(110) Huang, X.; Jain, P. K.; El-Sayed, I. H.; El-Sayed, M. A. *Nanomedicine* **2007**, *2*, 681-693.

(111) Han, G.; Ghosh, P.; Rotello, V. M. *Nanomedicine* **2007**, *2*, 113-123.

(112) Katz, E.; Willner, I. *Angew. Chem., Int. Ed.* **2004**, *33*, 6042-6108.

(113) de la Fuente, J. M.; Barrientos, A. G.; Rojas, T. C.; Rojo, J. Canada, J.; Fernandez, A.; Penades, S. *Angew. Chem., Int. Ed.* **2001**, *40*, 2257-2261.

(114) Barrientos, A. G.; de la Fuente, J. M.; Rojas, T. C.; Fernandez, A.; Penades, S. *Chem. Eur. J.* **2003**, *9*, 1909-1921.

(115) de la Fuente, J. M.; Alcantara, D.; Eaton, P.; Crespo, P.; Rojas, T. C.; Fernandez, A.; Hernando, A.; Penades, S. *J. Phys. Chem. B.* **2006**, *110*, 13021-13028.

(116) de la Fuente, J. M.; Eaton, P.; Barrientos, A. G.; Menendez, M.; Penades, S. *J. Am. Chem. Soc.* **2005**, *127*, 6192-6197.

(117) Bucior, I.; Burger, M. M. *Curr. Opin. Struct. Biol*. **2004**, *14*, 631-637.

(118) Rojo, J.; Diaz, V.; de la Fuente, J. M.; Segura, I.; Barrientos, A. G.; Riese, H. H.; Bernad, A.; Penades, S. *ChemBioChem* **2004**, *5*, 291-297.

(119) Lin, C.-C.; Yeh, Y.-C.; Yang, C.-Y.; Chen, C.-L.; Chen, G.-F.; Chen, C.-C.; Wu, Y.-C. *J. Am. Chem. Soc*. **2002**, *124*, 3508-3509.

(120) Chen, Y.-J.; Chen, S.-H.; Chien, Y.-Y.; Chang, Y.-W.; Liao, H.-K.; Chang, C.-Y.; Jan, M.-D.; Wang, K.-T.; Lin, C.-C. *ChemBioChem* **2005**, *6*, 1169-1173.

(121) Nolting, B.; Yu, J.-J.; Liu, G.; Cho, S.-J.; Kauzlarich, S.; Gervay-Hague, J. *Langmuir* **2003**, *19*, 6465-6473.

(122) Svarovsky, S. A.; Szekely, Z.; Barchi, Jr. J. J. *Tetrahedron: Asymmetry* **2005**, *16*, 587-598.

(123) Otsuka, H.; Akiyama, Y.; Nagasaki, Y.; Kataoka, K. *J. Am. Chem. Soc*. **2001**, *123*, 8226-8230.

(124) Reynolds, A. J.; Haines, A. H.; Russell, D. A. *Langmuir* **2006**, *22*, 1156-1163.

(125) Schofield, C. L.; Field, R. A.; Russell, D. A. *Anal. Chem*. **2007**, *79*, 1356-1361.

(126) Podsiadlo, P.; Sinani, V. A.; Bahng, J. H.; Kam, N. W. S.; Lee, J.; Kotov, N. A. *Langmuir* **2008**, *24*, 568-574.

(127) Hostetler, M. J.; Wingate, J. E.; Zhong, C. J.; Harris, J. E.; Vachet, R. W.; Clark, M. R.; Londono, J. D.; Green, S. J.; Stokes, J. J.; Wignall, G. D.; Glish, G. L.; Porter, M. D.; Evans, N. D.; Murray, R. W. *Langmuir* **1998**, *14*, 17-30.

(128) Alvarez, M. M.; Khoury, J. T.; Schaaff, T. G.; Shafigullin, M. N.; Vezmar, I.; Whetten, R. L. *J. Phys. Chem. B* **1997**, *101*, 3706-3712.

(129) Brown, L. O.; Hutchison, J. E. *J. Am. Chem. Soc*. **1999**, *121*, 882-883.

(130) Castner, D. G. *Langmuir* **1996**, *12*, 5083-5086.

(131) Liu, X.; Atwater, M.; Wang, J.; Huo, Q. *Colloids Surf. B* **2007**, *58*, 3-7.

(132) Brown, K. R.; Walter, D. G.; Natan, M. J. *Chem. Mater*. **2000**, *12*, 306-313.

(133) Sharon, N.; Lis, H. *Science* **1989**, *246*, 227-234.

(134) Lis, H.; Sharon, N. *Chem. Rev*. **1998**, *98*, 637-674.

(135) Goldstein, I. J.; Hollerman, C. E.; Smith, E. E. *Biochemistry* **1965**, *4*, 876–883.

(136) Bhattacharyya, L.; Koenig, S. H.; Brown III, R. D.; Brewer, C. F. *J. Biol. Chem*. **1991**, *266*, 9835-9840.

(137) Lotan, R.; Skutelsky, E.; Danon, D.; Sharon, N. *J. Biol. Chem*. **1975**, *250*, 8518-8523.

(138) Neurohr, K. J.; Young, N. M.; Mantsch, H. H. *J. Biol. Chem*. **1980**, *255*, 9205-9209.

(139) Loris, R.; Hamelryck, T.; Bouckaert, J. Wyns, L. *Biochim. Biophys. Acta*. **1998**, *1383*, 9-36.

(140) Banerjee, R.; Das, K.; Ravishankar, R.; Suguna, K.; Surolia, A.; Vijayan, M. *J. Mol. Biol*. **1996**, *259*, 281-296.

(141) Decastel, M.; Boeck, H. D.; Goussault, Y.; De Bruyne, C. K.; Loontiens, F. G.; Frenoy, J.-P. *Arch. Biochem. Biophys*. **1985**, *240*, 811-819.

(142) Hone, D. C.; Haines, A. H.; Russell, D. A. *Langmuir* **2003**, *19*, 7141-7144.

(143) Weare, W. W.; Reed, S. M.; Warner, M. G.; Hutchison, J. E. *J. Am. Chem. Soc.* **2000**, *122*, 12890-12891.

(144) Cairo, C. W.; Gestwicki, J. E.; Kanai, M.; Kiessling, L. L. *J. Am. Chem. Soc*. **2002**, *124*, 1615-1619.

(145) Miller, R. L. *Anal. Biochem*. **1983**, *131*, 438-446.

(146) Bangham, A. D.; Standish, M. M.; Watkins, J. C. *J. Mol. Biol*. **1965**, *13*, 238-252.

(147) Allen, T. M.; Moase, E. H. *Adv. Drug Deliv. Rev.* **1996**, *21*, 117-133.

(148) Zhou, W.; Yuan, X.; Wilson, A.; Yang, L.; Mokotoff, M.; Pitt, B.; Li, S. *Bioconjugate Chem.* **2002**, *13*, 1220-1225.

(149) Yang, L.; Li, J.; Zhou, W.; Yuan, X.; Li, S. *J. Controlled Release* **2004**, *95*, 321-331.

(150) Dubey, P. K.; Mishra, V.; Jain, S.; Mahor, S.; Vyas, S. P. *J. Drug Target*. **2004**, *12*, 257-264.

(151) Guo, X.; Szoka, F. C. *Acc. Chem. Res.* **2003**, *36*, 335-341.

(152) Abraham, S. A.; Waterhouse,D. N.; Mayer, L. D.; Cullis, P. R. *Methods Enzymol*. **2005**, *391*, 71-97.

(153) Xiang, T.-X.; Chen, J.; Anderson, B. D. *J. Membrane Biol*. **2000**, *177*, 137-148.

(154) Apel-Paz, M.; Doncel, G. F.; Vanderlick, T. K. *Langmuir* **2005**, *21*, 9843-9849.

(155) Ishida, A.; Otsuka, C.; Tani, H.; Kamidate, T. *Anal. Biochem*. **2005**, *342*, 338-340.

(156) Kaler, E. W.; Murthy, A. K.; Rodriguez, B. E.; Zasadzinski, J. A. N. *Science* **1989**, *245*, 1371-1374.

(157) Kaler, E. W.; Herrington, K. L.; Murthy, A. K. *J. Phys. Chem*. **1992**, *96*, 6698-6707.

(158) Koehler, R. D.; Raghavan, S. R.; Kaler, E. W. *J. Phys. Chem. B* **2000**, *104*, 11035-11044.

(159) Tondre, C.; Caillet, C. *Adv. Colloid Interface Sci.* **2001**, *93*, 115-134.

(160) Lee, J.-H.; Gustin, J. P.; Chen, T.; Payne, G. F.; Raghavan, S. R. *Langmuir* **2005**, *21*, 26-33.

(161) Wang, X.; Danoff, E. J.; Sinkov, N. A.; Lee, J.-H.; Raghavan, S. R.; English, D. S. *Langmuir* **2006**, *22*, 6461-6464.

(162) Walker, S. A.; Zasadzinski, J. A. *Langmuir* **1997**, *13*, 5076-5081.

(163) Danoff, E. J.; Wang, X.; Tung, S.-H.; Sinkov, N. A.; Kemme, A. M.; Raghavan, S. R.; English, D. S. *Langmuir* **2007**, *23*, 8965-8971.

(164) Hentze, H.-P.; Raghavan, S. R.; McKelvey, C. A.; Kaler, E. W. *Langmuir* **2003**, *19*, 1069-1074.

(165) Deuticke, B. In *Red Cell Membrane Transport in Health and Disease*; Bernhardt, I., Ellory, J. C., Eds.; Springer: New York, 2003; Chapter 2, pp 43-44.

(166) DuBois, M.; Gilles, K. A.; Hamilton, J. K. ; Rebers, P. A. ; Smith, F. *Anal. Chem*. **1956**, *28*, 350-356.

(167) Luzardo, M. D. C.; Lanio, M. E.; Alvarez, C.; Pazos, I. F.; Figueroa, S.; Verez, V.; Disalvo, E. A. *Colloids Surf. B* **2002**, *26*, 281-289.

(168) Sundler, R. *FEBS Lett*. **1982**, *141*, 11-13.

(169) Guo, C. X.; Boullanger, P.; Liu, T.; Jiang, L. *J. Phys. Chem. B* **2005**, *109*, 18765-

18771.

(170) Bakowsky, U.; Rettig, W.; Bendas, G.; Vogel, J.; Bakowsky, H.; Harnagea, C.; Rothe, U. *Phys. Chem. Chem. Phys.* **2000**, *2*, 4609-4614.

(171) Kuo, J. H. S.; Jan, M.-S.; Chang, C.-H.; Chiu, H.-W.; Li, C.-T. *Colloids Surf. B* **2005**, *41*, 189-196.